

Mörlin, Joel  
Melhuus, Victor  
Mørk, Oscar

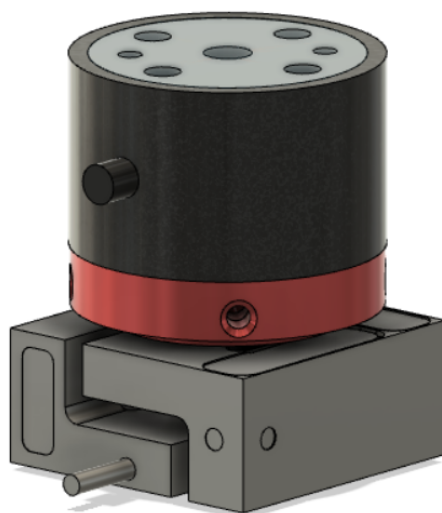
## Intrinsic Force-Torque Sensor System for a Next Generation Snake Robot

Essensielt Kraft-Dreiemoment Sensorsystem for  
en Neste Generasjons Slangerobot

Bachelor's project in Electrical Engineering, Automation and  
Instrumentation

Supervisor: Mathisen, Pål

Co-supervisor: Løwer, Jostein







Mörlin, Joel  
Melhuus, Victor  
Mørk, Oscar

## **Intrinsic Force-Torque Sensor System for a Next Generation Snake Robot**

Essensielt Kraft-Dreiemoment Sensorsystem for en  
Neste Generasjons Slangrobot

Bachelor's project in Electrical Engineering, Automation and  
Instrumentation

Supervisor: Mathisen, Pål

Co-supervisor: Løwer, Jostein

May 2021

Norwegian University of Science and Technology  
Faculty of Information Technology and Electrical Engineering  
Department of Engineering Cybernetics



Kunnskap for en bedre verden



## Summary

A new snake robot is to be developed at NTNU/ITK. It will be an intended test-platform for Hybrid Obstacle Aided Locomotion (HOAL) with snake robotics. HOAL, within snake robotics, is the concept of artificial impersonation of how biological snakes achieve propulsion in an unstructured environment, pushing up against objects in the terrain. The robot needs an advanced intrinsic force-torque sensor system that produces reliable and accurate measurements to achieve this.

The force-torque sensor system presented is based on commercially available sensor technology and combines a 3-axis force sensor and a 1-axis torque sensor. Tests conducted on the sensor system demonstrate that it out-performed and surpassed the project's expectations. Achieving high accuracy, minimal voltage drift, low time delay, high sensitivity, and most importantly, producing a reliable measurement signal. Moreover, by comparing the presented sensor system to the results of the sensor system in the Mamba snake-robot, the improvements are notable.

Firstly, this paper covers the underlying theory regarding HOAL, importance, and intended usage of force-torque measurements within snake robots. Next, it covers basic theory regarding the traditional workings of strain-gauge-based force and torque transducers. Finally, covering sensor solutions from previous snake-robot research.

Secondly, it deeply covers the research process of finding a suitable force-torque sensor system based on commercially available solutions. It presents suggested specifications and requirements for such a system to be applicable as an intrinsic sensor solution within snake robotics. It introduces some alternative solutions and research, apart from commercial strain-gauge-based transducers. Then it presents four commercially available sensor solutions that meet the set physical requirements and how the project concluded that a combined sensor solution was the most beneficial.

Thirdly, it deeply covers the steps taken to test and assess the combined sensor solution—furthermore, testing and design of suggested measurement electronics as projected by previous research. The sensor system was then tested in realistic conditions, and its performance was assessed. Finally, its performance was compared to previous tests conducted on the most current snake-robot at ITK; Mamba.

Lastly, the paper covers the intentional use of the sensor system and presents suggested improvements regarding the measurement electronics based on the project's experiences.

## Sammendrag

En ny slangerobot skal utvikles av NTNU/IKT som en testplattform for HOAB (Hybrid Obstruksjons Assistert Bevegelse). HOAB bygger på kunstig etterligning av hvordan biologiske slanger beveger seg i terreng ved å presse seg mot hindringer. Slangrobotikken er derfor tungt avhengig av et iboende kraft-dreiemoment system som kan gi ut presise og pålitelige målinger.

Det presenterte kraft-dreiemoment sensorsystemet er basert på kommersielt tilgjengelig sensorteknologi. Løsningen kombinerer en 3-akset kraftsensor med en 1-akset dreiemomentsensor. Tester gjennomført på systemet viser at det imøtekommer og overgår kravene satt av prosjektet og oppdragsgiver. Det har høy nøyaktighet, minimalt med spenningsdrift, lite tidsforsinkelse, høy sensitivitet og produserer pålitelige målinger. Sammenlignet med det tidligere sensorsystemet i slangeroboten Mamba, så presterer det bedre på mange områder.

Den første delen av denne prosjektrapporten dekker den underliggende teorien bak HOAB, samt betydningen av presise kraft-dreiemoment målinger til bruk i slangerobotikk. Videre dekker den også grunnleggende teori, som ligger til grunn for den tradisjonelle virkemåten til strekkklappbasert kraft- og dreiemoment sensorteknikk. Til slutt dekker delen sensorsystemer fra tidligere forskning på slangeroboter ved NTNU og internasjonalt.

Andre delen av prosjektrapporten går i detalj på prosessen bak jakten på kommersielt tilgjengelige sensorløsninger. Krav og spesifikasjonslister er presentert, og knyttes opp mot behovene til en gitt slangerobot. Videre er det presentert forskning og andre alternative løsninger som baserer seg på å bygge et spesialisert sensorsystem fra bunnen av. Fire potensielle kommersielt tilgjengelige løsninger, som møter prosjektets krav er presentert, etterfulgt av prosjektets endelige løsning, som var å kombinere to kommersielle sensorer som oppfølger de ønskede kravene.

Tredje del dekker prosessen bak testing og vurdering av det kombinerte sensorsystemet. Den går dypt inn i prosessen bak design og implementering av måleelektronikk, samt testtriggen, opp mot sensorsystemet. Videre går den inn i hvordan sensorsystemet ble testet under realistiske omstendigheter for å vurdere systemets ytelse. Resultatene blir sammenlignet med tidligere forskning på et eldre målesystem, i en tidligere slangerobot. Konklusjonen var at det nye kraft- dreiemoment-målesystemet, funnet av prosjektet, presterer klart bedre enn det tidligere spesialiserte målesystemet.

Til slutt går rapporten dypt inn i hvordan dette målesystemet vil kunne brukes i praksis og trekker frem forbedringspotensialer vedrørende måleelektronikk, design og produksjon av fysiske deler.

## Preface

This project report is written in the spring of 2021 for the Department of Engineering Cybernetics at the Norwegian University of Science and Technology. The report marks the end of the 6th and last semester of the 3-year study: Bachelor in Electrical Engineering.

We want to thank Jostein Løwer for his guidance and support. Pål Mathisen for continued guidance and feedback. Moreover, the machine workshop at ITK for their help in machining vital components.

- Victor Melhuus, Joel Mörlin and Oscar Mørk, May 20, 2021

## Tilleggsinformasjon

<b>Graddering:</b> Åpen	<b>Prosjektnummer:</b> 26
<b>Antall sider/bilag:</b> 119	<b>Innleveringsdato:</b> 20.05.2021
<b>Studieretning:</b> Automatiseringsteknikk Instrumenteringsteknikk	
<b>Gruppedeltakere:</b> Joel Mörlin, joeltem@stud.ntnu.no Victor Melhuus, victorme@stud.ntnu.no Oscar Mørk, oscarbm@stud.ntnu.no	
<b>Oppdragsgiver:</b> NTNU-ITK	
<b>Kontaktpersoner hos oppdragsgiver:</b> Øyvind Stavdahl, oivind.stavdahl@ntnu.no Jostein Løwer, jostein.lower@ntnu.no	
<b>Veileder internt:</b> Pål Holthe Mathisen, pal.mathisen@ntnu.no	
<b>Stikkord:</b> Slangrobot Kraft-dreiemoment sensorsystem Kombinert løsning	<b>Keywords:</b> Snake robot Force-torque sensor system Combined solution

# Contents

<b>Summary</b>	i
<b>Preface</b>	iii
<b>Tilleggsinformasjon</b>	iii
<b>Contents</b>	iv
<b>List of figures</b>	vii
<b>List of tables</b>	xi
<b>Nomenclature/glossary</b>	xii
<b>1 Introduction</b>	1
1.1 Motivation	2
1.2 The thesis assignment	3
<b>2 Background and theory</b>	4
2.1 HOAL - Hybrid Obstacle Aided Locomotion	4
2.1.1 The importance of multi-axis force measurement in HOAL	5
2.1.2 The importance of torque measurement in HOAL	6
2.1.3 2D configuration example	6
2.2 Torque	7
2.2.1 Measuring torque	8
2.3 Strain gauges and force measurement	9
2.3.1 Resistance Strain Gauges	9
2.3.2 Measuring the change in resistance with a Wheatstone bridge	11
2.4 Kulko - Force measurement on a spherical bowl	12
2.5 Mamba - Resistance Strain Gauge system	13
2.5.1 Issues with the Mamba force-torque measurement system	14
<b>3 Finding a commercially available force-torque sensor solution suitable for a novel snake robot</b>	17
3.1 Method	17
3.2 Specifications for an intrinsic force-torque measurement system for a next generation snake robot	18
3.2.1 Measurement capabilities	20
3.2.2 Temperature tolerance	21
3.2.3 Design, length and width limitations	21
3.2.4 Cost and accessibility	22
3.2.5 Summary of specifications for an intrinsic F/T sensor solution for a next generation snake robot	23
3.3 A brief introduction to the market for force- and torque sensors	24
3.4 Strain Measurement with Fiber Bragg Grating(FBG)	25
3.5 Tokyo Institute of Technology - Position Sensitive Detectors(PSD)	27

3.6	3D printed Low-Cost Force-Torque sensors	27
3.7	Futek	29
3.7.1	QMA142 - 6 axis force-torque sensor	29
3.8	ATI - Industrial Automation	32
3.8.1	Mini40 - 6 axis force-torque sensor	32
3.9	ME-mefsysteme	34
3.9.1	K6D40 - 6-axis force-torque sensor	34
3.9.2	K3D40 - 3-axis force sensor	36
3.10	Transducer Techniques	37
3.10.1	TRT-series	37
3.11	3-axis force- and 1 axis torque transducer combined solution (Sandwich Solution)	39
3.12	Discussion and conclusion	41
3.12.1	Findings regarding the market for F/T-transducers with relevance to the needs of a next generation snake robot at NTNU	41
3.12.2	Coherence in industrial sensor-system-solutions regarding multi-axis force measurements and degree of "how industrially produced"	41
3.12.3	Comparing the different sensors to each other	42
3.12.4	Deciding what F/T transducer solution to test and assess	43
<b>4</b>	<b>Designing the sensor system for testing purposes</b>	<b>44</b>
4.1	Designing the linkage	44
4.1.1	K3D40 requirements	44
4.1.2	TRT-50 requirements	45
4.1.3	3D-design	46
4.2	Designing the test bench	48
4.3	Designing the power supply circuit	49
4.4	Designing the amplifier circuit	50
4.4.1	Comparing Amplifiers	51
4.4.2	Digital potentiometers	52
4.4.3	Noise reduction	53
4.5	Headers Selection and substitution	54
4.5.1	Issues	54
4.6	Amplifier offset voltage	55
4.7	Microcontroller	56
<b>5</b>	<b>Implementing the sensor system for testing purposes</b>	<b>57</b>
5.1	Sensor assembly	57
5.2	Test-bench assembly	58
5.3	The sensor system and test-accessories	60
5.4	Preparing the measurement electronics	62
5.5	Preparational testing of the power supply circuit	64
5.6	Preparational testing of the amplifier circuit	65
5.7	Preparational testing of the 3-axis force sensor with the amplifier circuit and a multi-functional DAQ	67

5.8	Preparational testing of the microcontroller with the amplifier circuit and the 3 axis force sensor	69
<b>6</b>	<b>Testing the sensor system</b>	<b>70</b>
6.1	Testing equipment	70
6.2	Experiment 1: Periodically applied force and torque	74
6.2.1	Results: Periodic force experiments on the x-axis	74
6.2.2	Results: Periodic force experiments on the y-axis	75
6.2.3	Result: Periodic torque experiment	76
6.3	Experiment 2: Crosstalk analysis	77
6.3.1	Results: Applying torque	77
6.3.2	Results: Applying force (X-axis)	78
6.3.3	Results: Applying force (Y-axis)	78
6.4	Experiment 3: Shaking the sensor system	79
6.5	Experiment 4: Heating the sensor system	80
<b>7</b>	<b>Discussion</b>	<b>81</b>
7.1	Experiment 1: Periodically applied force and torque	81
7.2	Experiment 2: Crosstalk analysis	85
7.3	Experiment 3: Shaking the sensor system	86
7.4	Experiment 4: Heating the sensor system	86
<b>8</b>	<b>Conclusion</b>	<b>88</b>
8.1	The market for suitable commercially available force-torque sensors	88
8.2	Performance of the selected sensor system	88
<b>9</b>	<b>Future work</b>	<b>89</b>
9.1	Linkage, issues, and possible improvements	89
9.2	Implementing the Sandwich Solution within a robotic joint	89
9.3	Suggested electronic improvements	90
9.3.1	Switching amplifiers	90
9.3.2	Replacement of the digital potentiometer	90
9.3.3	Redesigning the integrated offset	91
9.3.4	Noise reduction improvements	91
9.3.5	Header and terminal replacement	92
<b>A</b>	<b>Appendices</b>	<b>94</b>
A.1	Poster	95
A.2	Sensor research Excel sheet	96
A.3	Ordering the Sandwich Solution	97
A.4	Component list with description	99
A.5	Arduino code	105
A.6	Matlab code: Plotting periodic experiment	108
A.7	Matlab code: Crossfeed analysis	112
A.8	Matlab code: Plotting shaketest	113
A.9	Matlab code: Plotting temperature experiment	114
	<b>References</b>	<b>116</b>



## List of Figures

2.1	3D illustrations of <i>Hybrid Obstacle Aided Locomotion</i> with snake robotics	4	2.12	A graph from <i>Veshum's</i> experiments, showcasing the noise, inaccuracy, unpredictability, and hysteresis over time, estimated with a linear- and second-order polynomial regression. The experiment was force measurement on the x-axis. Courtesy of [2]	15
2.2	Forces and torques applied on a 2-jointed 2D-snake pushing up against an object.	5	2.13	Results of <i>Liljebäck's</i> experiments on the <i>Mamba</i> sensor system analysing sensor drift/hysteresis. Courtesy of [10]	16
2.3	Simplified example of HOAL on a 2D-surface. The snake is illustrated by the black line. The gray dots represents obstacles. The red arrows represents the external force vectors, and the blue arrow represents torque generated by the motor in each joint.	6	3.1	Configuration example of a snake robot intended to operate on a flat 2D-surface.	19
2.4	Sum of the external force vectors from Figure 2.3	7	3.2	The different topics of specifications in prioritized order. It was a helpful tool in the research process, as it helped evaluate different sensors to each other with regards to the projects priorities.	19
2.5	Illustration of relation between force and torque. Courtesy of [7]	7	3.3	Examples of common applications of 1-axis torque sensors	24
2.6	Illustration of the functionality of a prony break sensor	8	3.4	Examples of common applications of 6-axis force-torque sensors	25
2.7	Strain gauge examples	10	3.5	Principle of of a fiber bragg grating strain sensor. Courtesy of [16]	26
2.8	The <i>Kulko</i> snake robot, and its sensor system	12	3.6	A fiber bragg grating strain gauge sensor system produced by FBGS. Courtesy of [17]	26
2.9	The <i>Mamba</i> snake robot, courtesy of [2]	13			
2.10	The strain gauge sensor system in the <i>Mamba</i> snake robot	13			
2.11	The analog potentiometer calibration of the <i>Mamba</i> sensor system. Courtesy of [2]	14			

3.7	The concept behind a 3DOF force sensor developed by the <i>Tokyo Institute of Technology</i> . Courtesy of [19]	27	3.18	Size comparison of the three different implementation examples	43
3.8	3D printed low-cost force- and tactile sensing sensors. Courtesy of [20].	27	4.1	Instructions for mounting of the <i>K3D40</i> 3-axis sensor system. Courtesy of [32]	45
3.9	Table of 3D printed sensors and their estimated cost. Courtesy of [20].	28	4.2	Schematic drawing of the TRT reaction torque sensor. Couresy of [11]	45
3.10	The QMA142 sensor system, and an example of implementation exploiting the through hole design	29	4.3	3D-model of the linkage components that connects the different sensors together. Shown here is <i>LinkageType4</i> , it has the benefits of being one continuous part, but it had mounting difficulties that would result in the part being tall	46
3.11	Examples of ATI force transducers	32	4.4	3D model of <i>LinkageType7</i> . It has two parts that are mounted to each sensor. The two parts can then be locked together through screw holes on the side.	46
3.12	The K6D40 multi-axial force-torque sensor system, with it's two cable configuration variants. Courtesy of [28]	34	4.5	3D model of <i>LinkageType7</i> assembled.	47
3.13	Implementation example with the K6D40	35	4.6	Linkage (black) mounted on the 3-axis force sensor.	47
3.14	Picture of the <i>K3D40</i> 3-axis force-sensor by <i>Me-meßsysteme</i> . Courtesy of [29]	36	4.7	A sketched 3D-model of the test bench	48
3.15	A picture of the TRT-50 reaction torque transducer by <i>Transducer Techniques</i> . Courtesy of [11]	38	4.8	A 3D model of the torque shaft	48
3.16	The 3-axis force sensor and 1-axis torque combined "sandwich" solution	39	4.9	Power supply circuit schematic	49
3.17	Comparing the presented sensor system solutions in terms of price, temperature range, and size	42	4.10	Power supply circuit	49

4.11	The completed amplification circuit <i>THE BLOCC</i> . Designed as a testing circuit, little focus was put on size regulation causing the <i>block</i> like appearance	50	5.5	The sandwich solution mounted with different accessories for testing	60
4.12	Headroom for the INA122 in single and dual supply mode [33]	51	5.6	The force-sensor mounted to the test-bench for tests without the torque sensor	61
4.13	Comparison of rail to rail performance between the INA126 and INA849	52	5.7	Example of proper placement when pouring solder into the terminals. The soldering iron stops tin from leaking into the header connector.	62
4.14	Gain and load values comparison	53	5.8	The external Wheatstone full-bridge used for initial testing of the sensor system	63
4.15	Size comparison between the ZH and XH terminals	54	5.9	Voltageregulator fluctuation test	64
4.16	The headers connected to the amplifier via the XH series connector. Note the melted insulation on the green and orange cable and the sharp angle caused by twisting on the purple cable	54	5.10	Voltageregulator consistency test	65
4.17	The offset circuit fully connected to the final system through a proto-board	55	5.11	Amplifier test schematic	66
4.18	Adafruit microcontroller	56	5.12	Frequency analysis of a stationary signal (Sampling frequency = $1000Hz$ ), measured with a DAQ. Comparing a signal digitally filtered with moving average ( $n = 50$ ) to the raw signal (Time in seconds)	68
4.19	Adafruit microcontroller pin layout, Courtesy of [40]	56	5.13	Test schematic of circuitry used during microcontroller test. (The offset pins were provided 1.65V through the protoboard shown in 4.6).	69
5.1	The K3D40 linkage-part mounted on the K3D40	57	6.1	Different configurations for the different experiments using the test bench clamped to a table while applying a static force/torque using weights.	71
5.2	Full implementation of the linkage mount	58			
5.3	The test-bench	59			
5.4	The mounting of the Sandwich Solution to the test-bench	60			

6.2	Circuitry used during experiments with the sensor. The connections from the Adafruit microcontroller (to the right), are not seen in this picture. The remaining connections can be referenced in Figure 6.3.	72	6.9	Result of applying $343Nmm$ of torque around the z-axis (with the torque-shaft unsupported, therefore showing $F_x \approx -8.6N$ ).	77
6.3	Schematic of circuitry used during experiments with the sensor. The ISEN $\pm$ inputs on the amplifier circuit are the outputs from the force and torque sensors.	72	6.10	Result of applying $-8.6N$ of force on the x-axis	78
6.4	Result from the experiment of applying a periodic force in the positive x-direction on the force sensor.	74	6.11	Result of applying $-8.6N$ of force on the y-axis	78
6.5	Result from the experiment of applying a periodic force in the negative x-direction on the force sensor.	75	6.12	Results of shaking the sensor system for a long period of time.	79
6.6	Result from the experiment of applying a periodic force in the positive y-direction on the force sensor.	75	6.13	Result of the temperature experiment conducted on the sensor system. It shows the measurement value as the sensor system was heated for a period of time	80
6.7	Result from the experiment of applying a periodic force in the negative y-direction on the force sensor	76	7.1	Average measurement drift in each iteration (referenced to the first iteration), compared between the 4 different periodic force tests. Formula seen in (7.5)	83
6.8	Result from the experiment of applying a periodic torque on the torque-sensor	76	7.2	Average torque measurement drift in each iteration referenced to the first iteration	84
			7.3	Linear regression of each measurement value from experiment 4. Analyzing measurement drift as the sensor system was heated	87

## List of Tables

3.1	Measurement capabilities	20	3.10	Specifications for the TRT-50 reaction torque transducer by <i>Transducer Techniques</i> . Courtesy of [11]	38
3.2	Specified temperature range. <i>Operational</i> meaning the range in which the manufacturers can ensure that the sensor works as intended. <i>Maximum</i> meaning the range in which the sensor can operate without being damaged	21	3.11	Theorized specifications for the <i>Sandwich Solution</i> (combining the limits of the K3D40 3-axis force transducer and the TRT-50 torque transducer and adding a linkage)	40
3.3	Specifications regarding the physical design of the sensor system	21	5.1	The complete list of parts needed to assemble one sensor	57
3.4	Early estimated sensor budget	22	7.1	Average measured value within the time-span of the sensor being strained. Calculated for 6 iteration for the 5 different tests, with the intention of accurately identifying any measurement drift.	82
3.5	Summary of specifications for an intrinsic force-torque sensor system in a next generation novel snake robot	23	7.2	Measured and calculated crosstalk between axis in percent. (The z-axis is not included due to it not being part of the testing)	85
3.6	Specifications for the QMA142 6-axis force-torque transducer	30	7.3	Average measurement values before shaking, and after shaking the sensor system	86
3.7	ATI Mini 40 SI-40-2 specifications	33			
3.8	Specifications for the K6D40-50N/5Nm variant	35			
3.9	Specification sheet of the K3D40-50N	37			

## Nomenclature/Glossary

<b>ITK</b>	Department of Engineering Cybernetics
<b>HOAL</b>	Hybrid Obstacle Aided Locomotion
<b>Force</b>	An interaction that, when unopposed, will change the motion of an object.
<b>Torque</b>	A force that causes an object to rotate (a rotational force)
<b>OEM</b>	Original Equipment Manufacturer
<b>Transducer</b>	Any device converting one form of energy to another, preferably electrical energy.
<b>F/T transducers</b>	Force-torque transducers capable of measuring both force and torque.
<b>ADC</b>	Analog-to-digital converter
<b>LSB</b>	Least Significant Bit. The smallest digitally definable value in an ADC
$m$	Mass
$a$	Acceleration
$\tau_n$	Symbol for torque applied on the $n$ 'th joint
$h_n$	Symbol for the constraint force vector applied on the $n$ 'th joint
$f_{ext}$	Symbol for external forces vector
$F_R$	Symbol for friction force vector
$F_x, F_y, F_z$	Symbols for axial forces
$M_x, M_y, M_z$	Symbols for axial torques

# 1 Introduction

The science of mimicking biological systems, or *biomimetics*, is an essential theme in robotics. By utilizing natural selection and millions of years of trial and error progression, humans can swiftly solve complex design problems. Flight and aerodynamics are the two fields where this emulation is the most transparent. The earliest flying machines took heavy inspiration from their biological brethren. *Otto Lilienthal* was arguably the pioneer within this field and produced sleek and elegant glider designs with noticeable bird-like construction. Modern aviation is still heavily inspired by nature, from the crane-like "neck" on the *Sukhoi* fighter-jets to the falcon-like cross section of the *B-2* bomber. Thus it is clear that nature is an essential source of inspiration. Perhaps the most remarkable example of biomimetics in aviation is the *Horton* brothers *Ho 229*. As gliding enthusiasts, the brothers created the world's first proper flying wing by copying the natural vertical stability occurring in birds' body shapes. Perhaps a fascinating aspect was the plane's imperviousness to radar. The Hortons had unknowingly minimized the plane's radar cross-section by utilizing natural lines and absorbent materials like wood. They granted the then deeply struggling Nazi regime a stealth aircraft 30 years before any of their adversaries.

The field of robotics is also embossed with biological inspiration. Although the earliest examples strived to mimic human behavior and movement, the focus has shifted towards animals. Recent developments like Boston dynamics robot dog and NTNU's snake robot program have proved the concepts of practical usage and paved the way towards an automated future.

The work on snake-like robots started in the 1970s at the Tokyo Institute of Technology and has progressed to where multiple universities have taken an interest. As the technology is still in its infancy, there is no concrete and standardized solution for the required sensor system. As a result, all new research on snake robots has developed unique systems that differ widely, pertained to their theory and research interests. Some of the more notable ones include the snake robots from *Carnegie Mellon University*, who utilize a mechanical gear that compares the actual angle to the commanded angle. The aforementioned, TIT, still sticks to their original Position-Sensitive Detector (PSD) design.

NTNU, along with SINTEF, started their work on snake robots in the early 2000s and are currently on the 6th iteration named *Mamba*. *Mamba* is unique in the world of snake robots for implementing a force-torque sensor system based on strain gauges.

## 1.1 Motivation

In the time of writing this report, the *Mamba* snake robot developed by *Pål Liljebäck* in 2011 [1], have reached an age of 10 years, making it old in a technological perspective. Thus, the development of a 7th generation snake robot at NTNU was initiated. The next generation snake robot aims to demonstrate *Hybrid Obstacle Aided Locomotion* (HOAL) and autonomous navigation in rugged and cluttered terrain. To achieve autonomous HOAL, the robot needs an advanced sensor system that, through snake slithering, and movement can gather sufficient data from the environment to plan, calculate and predict the path of locomotion.

The most crucial part of this sensor system is multi-axis force-torque measurement. The HOAL team decided that the next generation snake robot shall be developed upon the sensor system, illustrating its importance in HOAL. One of the advancements in the previous generation, *Mamba*, was the new force-torque sensor system. In terms of measurement, it has imperfections and is considered inadequate for use in the next generation [2].

Thus, the target of this project was to find a more suitable solution for force- and torque measurement. The project's participants expected that the market for such technology had advanced since the original iteration of the *Mamba* snake robot. Therefore it was desired that the solution works upon commercially available sensor technology. The success of finding a suitable commercial sensor would result in a streamlined and simplified upgrade, build- and repair process, and provide measurements of industrial grade.



## 1.2 The thesis assignment

<b>Navn bedrift:</b> NTNU ITK		<b>Kontaktperson:</b> Øyvind Stavdahl <b>Epost:</b> oivind.stavdahl@ntnu.no		
<b>Tittel på oppgave:</b> Intrinsic force-torque sensor system for a next generation snake robot				
<b>Hvilken studieretning passer oppgaven for? (kryss av for alle aktuelle retninger):</b>	Automatisering  X	Elektronikk	Elkraftteknikk	Instrumentering  X
<p><b>Short description:</b></p> <p>The assignment revolves around the subject of snake robots. Snake robots are hyper-redundant robots intended to mimic biological snakes. The HOAL project (where HOAL means Hybrid Obstacle Aided Locomotion) aims to make snake robots autonomously navigate in rugged and cluttered terrain. In the HOAL project the robot seeks to use the fixed obstacles that it encounters in its path to aid propulsion. To achieve this goal, though, there is the need for an advanced sensor system that lets the snake robot gather sufficient information about its environment, information that will then be used to decide how to move. The core part of this sensor system is then the ability to continuously and precisely sense the forces and torques acting on each joint. This assignment focuses then on the development of an improved force-torque measurement system to be implemented in the next generation of snake robots.</p> <p><b>Expected key tasks (all of them in collaboration with the HOAL-team):</b></p> <ul style="list-style-type: none"> <li>• Get acquainted with the Mamba robot, and with the previous research on snake robots from the Department of Engineering Cybernetics.</li> <li>• Develop a specification for a force/torque measurement system for a novel snake robot.</li> <li>• Investigate the market for commercially available force-torque sensors and identify which ones are suitable for a novel snake robot.</li> <li>• Build a test model for the force/torque sensor system, test it in real-life conditions, and assess its performance</li> </ul>				

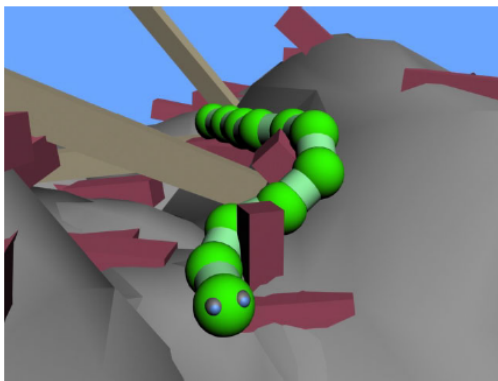
As presented in the course document "*Bacheloroppgaver 2021*"

## 2 Background and theory

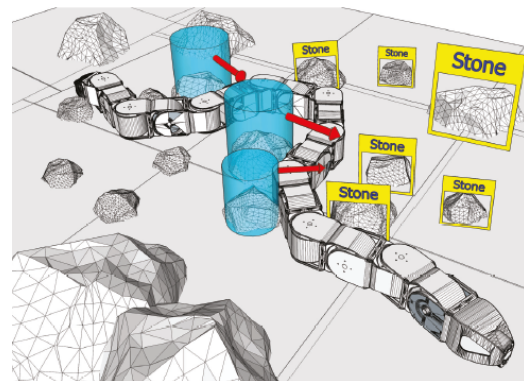
This chapter covers the fundamental theoretical aspects of the report. It digs deep into the motivation and purpose of the sensor system with apropos to snake robots and HOAL. Moreover, it introduces elementary physics knowledge and formulas to explain the workings of a classic force-torque sensor system. Lastly, it briefly presents previous research and solutions regarding force and torque measurement with snake robotics.

### 2.1 HOAL - Hybrid Obstacle Aided Locomotion

The main appeal of building an artificial snake is the real life counterpart's ability to exploit rough terrain. Snakes move by using friction, where the friction is created using the scales and scutes on its belly. These scales and scutes are asymmetrically shaped to only provide friction in a single direction. If this single direction friction were to be made omnidirectional or removed altogether, the snake would be unable to propel itself (as demonstrated [3]). Therefore, snakes heavily exploit the ruggedness in the terrain to locomote. This is called *Obstacle Aided Locomotion* and revolves around using the body to put pressure on irregularities in the landscape to propel itself in its desired direction [4]. Because snakes can achieve locomotion entirely without relying on friction, it is the most efficient way a serpent can move.



(a) Snake robot locomotion in an unstructured environment. Courtesy of Pål Liljebäck 2011 [1]



(b) The concept of perception-driven obstacle-aided locomotion. It illustrates how the snake robot may use sensor data to navigate the environment, push up against objects and propel itself. Courtesy of [5]

Figure 2.1: 3D illustrations of *Hybrid Obstacle Aided Locomotion* with snake robotics

The concept of HOAL is crucial regarding snake robotics, as it is a necessity with regards to the final goal of fully autonomous snake robots that mimic their biological counterparts. An essential aspect of HOAL is for the snake robot to be able to measure and analyze the external forces ( $f_{ext}$ ) applied on each joint (visualized by the red arrows in Figure 2.1b). By summarizing all the external force vectors, the snake robot can calculate, predict and manipulate the desired path of locomotion.

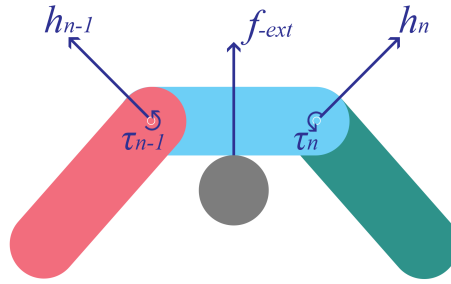


Figure 2.2: Forces and torques applied on a 2-jointed 2D-snake pushing up against an object.

### 2.1.1 The importance of multi-axis force measurement in HOAL

The challenge and aim of the thesis is through measurement of torque and constraint forces on each axis, provide the necessary values to calculate the directional external force vector on each joint. A simplified physical model is derived from Newton's second law (2.2) applied on the 3-jointed snake robot in Figure 2.2. It relies on the assumptions that mass( $m$ ) is known, acceleration( $a$ ) is measured through an accelerometer, and the environment is frictionless.

$$F_R \approx 0$$

$$\Sigma F = ma \quad (2.1)$$

$$f_{ext} = ma - h_n - h_{n-1} \quad (2.2)$$

The force vector  $h_n$  will be acquired from the multi-axis force-sensor in the joint pushing up against an object. The force sensor provides a measurement of the magnitude of force upon each axis within the joints reference frame, respectively  $F_{xn}, F_{yn}, F_{zn}$  (2.3). Together those three measurements will form a 3-dimensional force vector with a scalar length and two directional components.

$$h_n = [F_{xn}, F_{yn}, F_{zn}] \quad (2.3) \quad |h_n| = \sqrt{F_{xn}^2 + F_{yn}^2 + F_{zn}^2} \quad (2.5)$$

$$\alpha = \arctan\left(\frac{F_{xn}}{F_{yn}}\right) \quad (2.4) \quad \beta = \arcsin\left(\frac{F_{zn}}{|h_n|}\right) \quad (2.6)$$

The  $h_{n-1}$  force vector measurement will be acquired from the sensor in the previous joint. By referring  $h_{n-1}, h_n$  as well as the acceleration vector to the same reference frame, Newton's second- and third law can be applied, and the external force vector  $f_{ext}$  can be calculated.  $f_{ext}$ , being a vector, has both an angular and a magnitude component, and by comparing all the external force vectors, a direction- and acceleration of locomotion can be calculated.

### 2.1.2 The importance of torque measurement in HOAL

Torque measurement around the motor shaft axis (defined as the  $z$ -axis) is needed to accurately control, measure, and predict the motor output. Moreover, it can also be referred to the external force vectors, along with joint angle and position to predict and observe how each motor will influence the snake robot's propulsion and direction of locomotion by performing said action.

In a 3D environment, torque measured around the  $x$ - and the  $y$ -axis is also of great relevance. For example, it would provide the robot with information regarding rotational strain on each joint, as each joint's  $z$ -axis may be placed perpendicular to each other in the robot's reference frame. Also, as each motor actively attempts to maintain a specified angle, the robot is relatively stiff. Therefore, the torque produced by a motor in a single joint may affect other joints.

$$\tau_n = [\tau_{xn}, \tau_{yn}, \tau_{zn}] \quad (2.7)$$

One thing to note is the importance of accurate torque measurements, as explained by Christian Holden and Øyvind Stavdahl [6]. Given a set of external contact points and a desired total propulsive force, the article shows which motor torques are necessary to achieve a satisfactory result. The problem typically presents an infinite number of solutions and is therefore solved by minimizing the consumed energy (using motor torque as a proxy).

### 2.1.3 2D configuration example

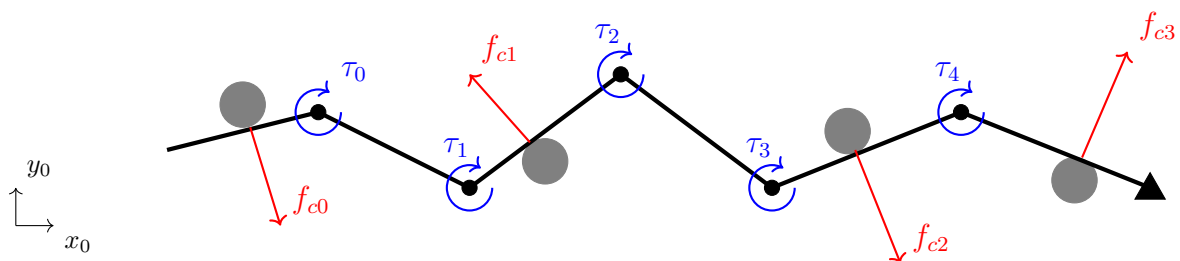


Figure 2.3: Simplified example of HOAL on a 2D-surface. The snake is illustrated by the black line. The gray dots represents obstacles. The red arrows represents the external force vectors, and the blue arrow represents torque generated by the motor in each joint.

[4] As shown in Figure 2.3 and 2.4, by summarizing the external force vectors (referred to the same frame), the snake can calculate the real-time path of locomotion ( $f_{sum}$ ), being the direction of force and thereby the direction of acceleration. Moreover, by using the torque measurement as feedback, each motor torque output can be regulated to manipulate both the length and direction of each external force vector. Therefore, by careful coordination and cooperation between each joint, a desired path of locomotion can be planned and executed.

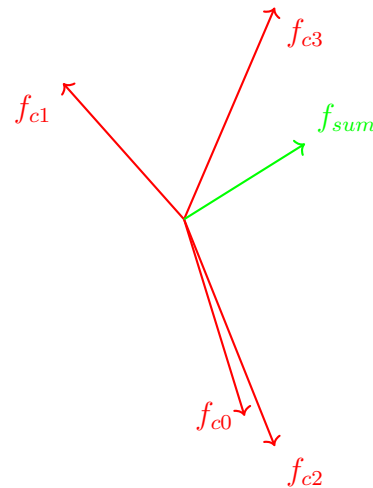


Figure 2.4: Sum of the external force vectors from Figure 2.3

A goal with HOAL is to digitally command the direction and size of the sum-of-external-forces-vector ( $f_{sum}$ ), being the direction of travel. And through advanced software and regulation of motor torque, direct and proportionate each external force vector so that they in total resemble the commanded direction of travel. This illustrates the importance of accurate force and torque measurement, as a small amount of noise or measurement inaccuracy will amplify into imprecise and unreliable movement.

## 2.2 Torque

[8] Torque is a measurement of the force causing an object to change its angular momentum. Torque is measured in either Newton-meters or foot-pounds. It is most commonly referenced in the automotive industry, where it describes the available twisting force an engine can generate when it exerts itself.

Torque ( $\tau$ ) is the time derivative of angular momentum ( $L$ ) (2.8). The angular momentum of a rigid body can be written in terms of its moment of inertia ( $J$ ) and its angular velocity ( $\omega$ ) (2.10). If the inertia is constant for a body, its torque is given by equation 2.9. By measuring torque, the angular velocity can be calculated (2.11).

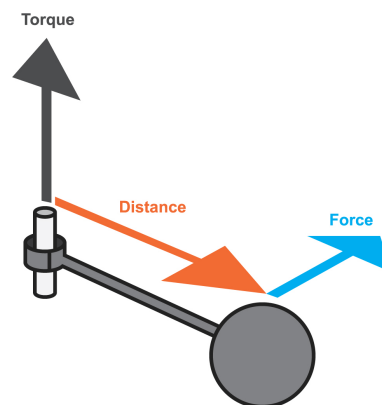


Figure 2.5: Illustration of relation between force and torque. Courtesy of [7]

$$\tau = \frac{dL}{dt} \quad (2.8) \quad L = J\omega \quad (2.10)$$

$$\Sigma\tau = J\dot{\omega} = J\alpha \quad (2.9) \quad \dot{\omega} = \frac{\Sigma\tau}{J} \quad (2.11)$$

### 2.2.1 Measuring torque

There are several different techniques to measure torque within the scope of the two types of torque, static and dynamic. Static torque is the torque applied when the torque is in equilibrium with a countering external torque/forces and therefore is virtually stationary in terms of rotation. Dynamic torque is the torque applied to the object when the force applied is larger than the countering torque/forces and therefore is accelerating and has an angular momentum that could be measured.

Static- and dynamic torque, in terms of the measurement technique, is drastically different, and both can't usually be measured with the same sensor.

Different types of torque sensors: [8]

#### Absorption type:

Introduces a countering force/torque to a rotating shaft, measures it, and thereby torque can be calculated based on the size of the force, and distance from the axis of rotation. Examples are frictional absorption, hydraulic absorption, electromagnetic absorption, and prony break (Figure 2.6). These sensors usually measure dynamic torque.

#### Transmission type dynamometer:

Measures the shear stress a shaft applies to a surface and thereby measures static torque. The relation between torque and the parameters of a solid cylindrical shaft under shear stress is given by (2.12).

$$\tau = \frac{G\pi r^4 \phi}{2l} \quad (2.12)$$

where  $G$  is the modulus rigidity of the shaft material.

$r$  is the radius of the shaft.

$\phi$  is the angle of deflection.

$l$  is the length of the shaft.

The torque is measured by either measuring the deflection angle  $\phi$  caused by a twisting force or by detecting the effect of this deflection on transducers like strain gauges. The Mamba robot uses the strain gauge measurement system shown in Figure 2.10.

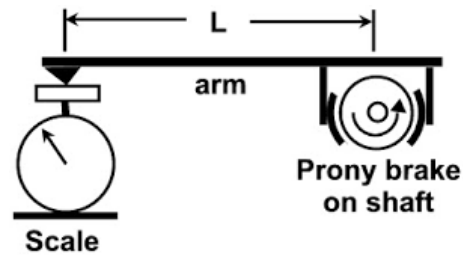


Figure 2.6: Illustration of the functionality of a prony break sensor

## 2.3 Strain gauges and force measurement

[8] Most commercial force- and torque transducers are based on strain gauges. When a force is applied to a solid object at rest, it gets mechanically deformed. Depending on the material being used and force applied, this could be bending in micrometers or contract in millimeters. Strain gauges exploit this property of materials by measuring the length of deformation. The applied force can then be calculated by referring the measurement to known material properties and their elastic constants.

$$\sigma_a = \frac{F}{A} \quad (2.13)$$

Where  $\sigma_a$  is the material stress  
 $F$  is the force applied  
 $A$  is the the area the force is applied on

$$\varepsilon_L = \frac{\Delta L}{L} \quad (2.14)$$

$\varepsilon_L$  is the relative longitudinal strain.  
 $\Delta L$  is the change in length  
 $L$  is the original length

$$\varepsilon_D = \frac{\Delta D}{D} \quad (2.15)$$

$\varepsilon_D$  is the relative lateral strain  
 $\Delta D$  is the change in diameter  
 $D$  is the original diameter

If the relation between  $\varepsilon_L$  and  $\sigma_a$  is linear, Hook's law is applied (2.16), where  $E_m$  is the *Young's modulus* (elasticity modulus).

$$\sigma_a = E_m \varepsilon_L \quad (2.16)$$

The French mathematician, geometer, and physicist *Siméon Poisson* showed that the ratio between lateral strain (2.15) and longitudinal strain (2.14) is constant for a material. Shown in equation 2.17, denoted by  $v$  as Poisson's ratio.

$$v = -\frac{\varepsilon_D}{\varepsilon_L} = -\frac{\frac{\Delta D}{D}}{\frac{\Delta L}{L}} \quad (2.17)$$

### 2.3.1 Resistance Strain Gauges

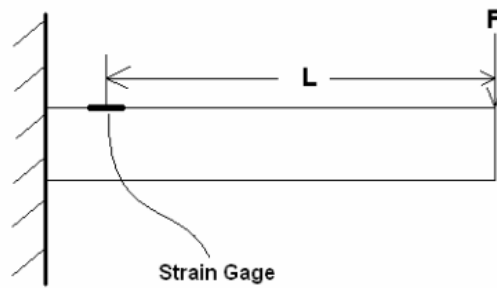
Resistance strain gauges changes resistance as it is bent or flexed. It usually contains a series of conductive wires mounted on a thin elastic plate (shown in figure 2.7b). When the wire is held under tension, its length increases slightly, and as a consequence, the cross-sectional area is reduced.

As shown in equation 2.18, the nominal resistance of a strain gauge  $R$  is directly proportional to the resistivity  $\rho$ , and the ratio between the length of the conductor  $L$  and the

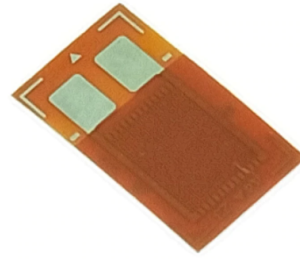
cross-sectional area  $A$ . The relation in equation 2.18 is relevant for common metals and many nonmetals at room temperature when subject to direct or low-frequency currents. When the sensor is strained, the change in resistance can be expressed by equation 2.19.

$$R = \rho \frac{L}{A} \quad (2.18)$$

$$\Delta R = \rho \frac{L}{A} - (\rho + \Delta\rho) \frac{L + \Delta L}{A + \Delta A} \quad (2.19)$$



(a) Strain gauge mounted on a cantilever



(b) A resistance strain gauge

Figure 2.7: Strain gauge examples

$$\frac{\Delta R}{R} = \frac{\Delta L}{L} - \frac{\Delta A}{A} + \frac{\Delta\rho}{\rho} \quad (2.20)$$

$$\frac{\Delta A}{A} = 2 \frac{\Delta D}{D} \quad (2.21)$$

$$G_m = \frac{\frac{\Delta R}{R}}{\varepsilon_L} = 1 + 2\nu + \frac{1}{\varepsilon_L} \frac{\Delta\rho}{\rho} \quad (2.22)$$

The relation between relative change in resistance (2.20) and relative change in area (2.21) is shown in equation 2.22.  $G_m$  is called *gauge-factor* and describes the sensitivity. The relative change in resistance given by the *gauge-factor* and the relative longitudinal strain is shown in equation 2.23.

$$\frac{\Delta R}{R} = G_m \varepsilon_L \quad (2.23)$$

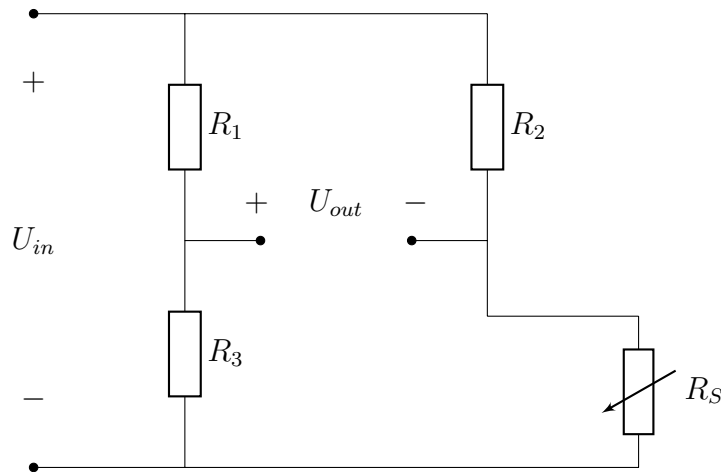
$$\Delta R = R \frac{G_m}{E_m} \sigma_a = R \frac{G_m}{E_m A} F \quad (2.24)$$

By solving (2.23) for resistance change,  $\Delta R$ , adding the equation for the relative longitudinal strain  $\varepsilon_L$  (2.14), and adding the formula for material stress  $\sigma_a$  (2.13), the resulting equation (2.24) gives the relation between resistance change and applied force  $F$ .



### 2.3.2 Measuring the change in resistance with a Wheatstone bridge

A Wheatstone bridge is commonly used to detect the measurement signal from strain gauge sensors, as they are particularly good at measuring changes in resistance. It works by balancing resistances on two sides of a bridge circuit, where one or more of the resistors are strain gauges. When one of the resistors changes value, a current will flow from one side to the other. It is then possible through mathematics shown in 2.25, 2.26, 2.27 and 2.28 to deduce the resistance change. 6 of them can be found in each joint of the *Mamba* snake robot. The example shown in this section is a Wheatstone Quarter-bridge.



- $U_{in}$  Supply voltage
- $U_{out}$  Measurement voltage
- $R_S$  Variable resistance (resistance strain gauge sensor)
- $R_{1,2,3}$  Resistors, preferably equal

$$U_{out} = U_{in} \left( \frac{R_3}{R_1 + R_3} - \frac{R_S}{R_2 + R_S} \right) \quad (2.25)$$

Assuming  $R_1 = R_2 = R_3 = R$  so the bridge is in balance. When in balance, and there is no change in resistance from the strain gauge ( $R_S$ ), the output voltage will be  $U_{out} = 0V$ .

$$U_{out} = U_{in} \left( \frac{R}{R + R} - \frac{R + \Delta R}{R + R + \Delta R} \right) = -U_{in} \left( \frac{\Delta R}{4R + 2\Delta R} \right) \quad (2.26)$$

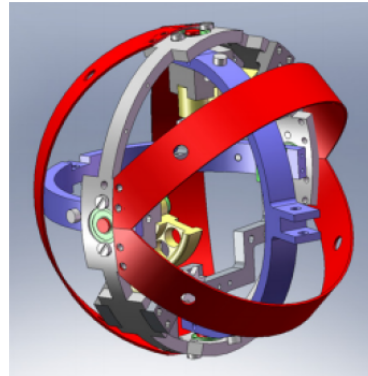
In equation 2.26, assuming  $R \gg \Delta R$ , (2.27) is the approximated relationship between the input and output voltage. By inserting the equation for  $\Delta R$  in strain gauges (2.24), you can approximate the relationship between input- and output voltage as a function of force in equation 2.28.

$$U_{out} \approx -U_{in} \left( \frac{\Delta R}{4R} \right) \quad (2.27) \qquad U_{out} \approx -\frac{U_{in} G_m}{4E_m A} F \quad (2.28)$$

## 2.4 Kulko - Force measurement on a spherical bowl



(a) Kulko. Courtesy of [9]



(b) The sensor system in Kulko. Courtesy of [9]

Figure 2.8: The *Kulko* snake robot, and its sensor system

*Kulko* is the third generation of snake robots developed by the Norwegian University of Science and Technology (NTNU). *Kulko* was developed to test a new idea for a snake robotics environment sensing system using force sensing resistors (FSR). The force sensing resistors would be implemented as shown in figure 2.8b, where the FSR would be placed alongside the red aluminum plates.

### FSR: Force sensing resistors

An FSR or force-sensing resistors are sensor components that use the piezoresistive effect to perceive forces that interact with it. When the resistor is exposed to a force of any kind, the resistor will change its shape and, due to the piezoresistive effect, change its resistance output. In this fashion, it's possible to measure the amount of force that affects the sensor as the change in the resistance output equals the amount of force it is affected with. *Kulko* would use the information from the FSR to determine where it made contact with obstacles and the floor and could, through the use of this information, propel itself forward.

### Issues with *Kulko*

The theoretical aspect of the system was promising. However, during real-world tests, the system proved to have some major flaws. The system was prone to inaccurate as well as nonlinear measurements. This inaccuracy proved it hard to maneuver the robot since the control system relies on accurate data. Secondly, the system was fragile, which proved a challenge as the snake robot would be under much stress during use. *Kulko* was deemed unsuitable, with relation to HOAL, and NTNU proceeded with the development of a new snake robot.

## 2.5 Mamba - Resistance Strain Gauge system

[2]

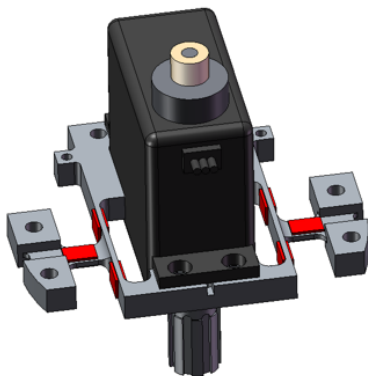
*Mamba* is the 6th generation snake robot at the Norwegian University of Science and Technology, shown in Figure 2.9. NTNU used the snake robot for robotic testing on both ground and in water. One of the main differences between *Mamba* and previous generations was the new intrinsic force/torque sensor system.



Figure 2.9: The Mamba snake robot, courtesy of [2]

### Strain gauges:

The force/torque measurement system in the *Mamba* robot is based on strain gauges. As shown in Figure 2.10, the strain gauges are mounted on an aluminum frame perpendicular to each other, enabling it to measure force and torque on three axes, making it a 6-axis/multi-axis force torque transducer. Figure 2.10a and Figure 2.10b presents two different versions of the sensor system, as there have been several attempts to improve the system and its issues.



(a) 3D-model of an older version(v0) of the force-torque measurement system



(b) The strain gauge sensor system (v3) mounted on the amplifier circuit board

Figure 2.10: The strain gauge sensor system in the *Mamba* snake robot

The strain gauges are mounted on each side of the aluminum frame, wrapping around a servo, making it space-efficient. There are two identical strain gauge configurations on each side of the motor because the sensor system is offset from the center point, and to distinguish between strain caused by a linear force and strain caused by a rotating force (torque).

### Measurement electronics:

The strain gauges are mounted in pairs for each axis of measurement and amplified through a Wheatstone bridge, forming a Wheatstone Half-Bridge. This is relatively similar to the Wheatstone Quarter-bridge covered in 2.3.2, the difference being that the resistance  $R_2$

is replaced with an active strain gauge. The Wheatstone Half-Bridge has measurement benefits in terms of temperature compensation.

### 2.5.1 Issues with the Mamba force-torque measurement system

*Fredrik Veslum* conducted several experiments on the *Mamba* sensor system in the fall of 2020. *Veslum's* report [2], sheds light on many of the issues with the sensor system. His findings were important for this project regarding determining the specifications and needed improvement for the sensor system in a next generation snake robot.

#### Calibration:

As described in almost every article or report regarding the *Mamba* robot, the calibration of the sensor system is a tedious and difficult process. Shown in Figure 2.11, the calibration system consists of a matrix of analog potentiometers. Each measurement signal has an adjustable gain, range, and offset influencing the output of each amplified signal. There are six signals, resulting in a total of 18 potentiometers per joint. Each signal on each joint has to be manually calibrated by adjusting the potentiometers, making calibration a tedious and lengthy process. Adding to the tediousness, when a new joint is mounted, or another one is removed, every signal may need to be readjusted or re-calibrated. Closing the housing with the plastic plate after calibrating has sometimes shown to provide an error in the measurements (making the calibration useless).

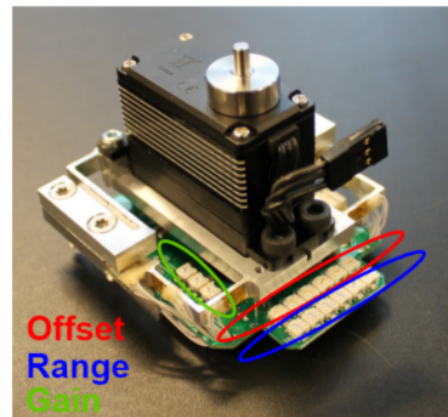


Figure 2.11: The analog potentiometer calibration of the Mamba sensor system. Courtesy of [2]

#### Temperature tolerance:

The servos in the *Mamba* robot are prone to produce a lot of heat over a period of time, as they have a high current draw. Moreover, the motor is placed, along with the sensor system, in an isolated plastic housing intended to be waterproof. As a result, each joint quickly warms up, and the sensor system would be exposed to heat substantially above room temperature. Experiments showed that heat greatly reduces the measurement accuracy and increases hysteresis (Figure 2.13b). Several attempts have been made to improve upon the robot's ability to dissipate heat, but with limited results.

#### Noise:

As shown in Figure 2.12, the measured signal is overwhelmed by noise. The noise being unwanted oscillations in the measurement signal. *Veslum* [2] conducted frequency analysis on the different measurements, which showed noise on three different frequencies. One of the frequencies was determined to likely be a disturbance from the motor shaking, and the other two are unknown. Other noise sources also seem to relate to the slightly bendable

plastic shell and motor bracket. Moreover, the impact of noise and disturbance seems to vary from the different axis of measurement of both force and torque, some axis being less impacted than others.

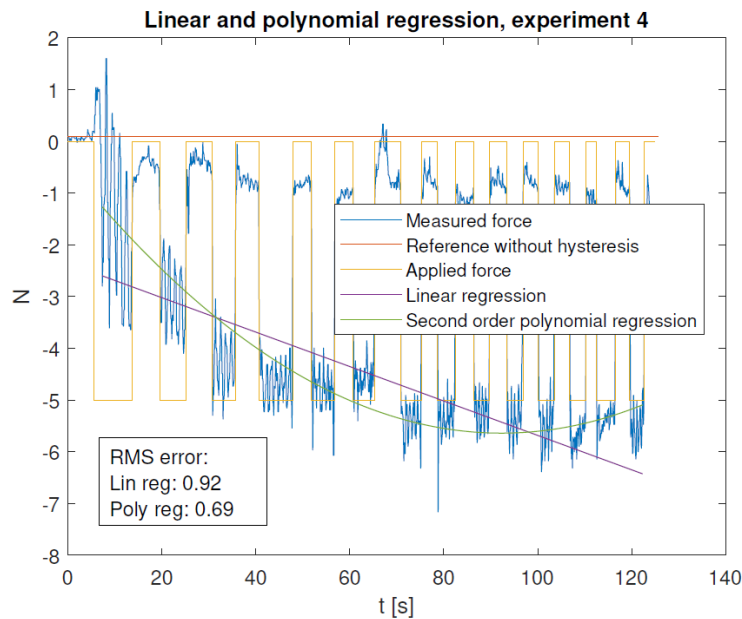


Figure 2.12: A graph from *Veslum*'s experiments, showcasing the noise, inaccuracy, unpredictability, and hysteresis over time, estimated with a linear- and second-order polynomial regression. The experiment was force measurement on the x-axis. Courtesy of [2]

### Inaccuracy:

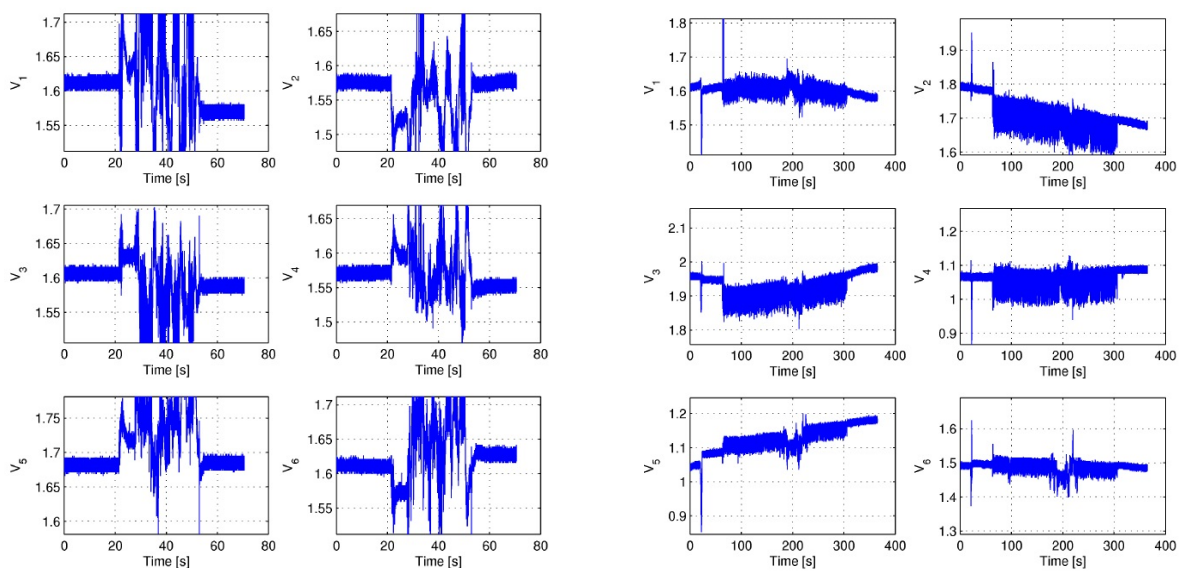
One of *Veslum*'s findings was a substantial measurement error/inaccuracy varying greatly between the different axis. The one with the most error being force and torque measurement around the x-axis. The experiment of force measurement on the x-axis can be seen in Figure 2.12.

### Hysteresis:

As shown in figure 2.12, when the sensor is extruded to a periodic and equal force over a period of time, the measurement signal is not reproducible. It changes its stationary measurement value between each iteration, even with the same force being applied. A linear regression of the presented experiment shows a negative trend over time; this is called hysteresis. In many cases, the hysteresis is systematic, can be predicted and thereby attenuated. However, some of the sources of the hysteresis could originate from the sensor's material properties, being different in every sensor. Thus reducing the problem effectively and efficiently is difficult. *Pål Liljebäck*'s experiments on the sensor systems also showed that all sensors are unique and behave differently. This is likely linked to inaccuracy and differences in the assembly process of said sensor.

### Conclusion

The *Mamba* sensor system has several flaws. Many of them are related to the constructional design and the inaccuracy of the self-built sensor system. All of these issues combined make the sensor system practically unusable in relation to the goal of proving *HOAL*, which requires accurate and reliable force-torque measurement.



(a) Voltage drift when the module was shaken for a while

(b) Voltage drift when the temperature inside the robot was increased.

Figure 2.13: Results of *Liljebäck's* experiments on the *Mamba* sensor system analysing sensor drift/hysteresis. Courtesy of [10]

### 3 Finding a commercially available force-torque sensor solution suitable for a novel snake robot

This chapter deeply covers the process of researching different force-torque sensor solutions. First, it presents suggested specifications for an intrinsic force-torque measurement solution for a next generation snake robot intended as a test platform for HOAL. Moreover, it introduces the current market for viable commercial solutions and discusses a few different possibilities the project considered in the selection process. Moreover, it highlights different commercially available products in different price ranges that the project has deemed viable solutions. Finally, it presents the project's solution and gives reasoning to the project's decisions.

#### 3.1 Method

This subsection contains a summary of the steps taken and methods used to research possibilities for an intrinsic force-torque sensor system for a next generation snake robot.

##### **Determining and prioritizing specifications:**

To begin the process of finding a fitting sensor, the project developed a specifications sheet. The specification sheet laid the groundwork for further research, narrowed down the number of sensors, and was an important tool to reference when deciding what solution to proceed with. The prioritized specification sheet can be seen in figure 3.2, along with a more detailed description in section 3.2, and a summary of all specifications topics with values in table 3.5.

##### **Researching different F/T transducers and possible solutions:**

Step two in the process of finding the sensor was searching the internet for possible F/T transducers and solutions. Google was the main resource for locating different products, manufacturers, and second-hand retailers.

##### **Creating a list over possible F/T transducers and solutions:**

After the specification sheet was developed, and while researching different solutions, possible solutions were gathered in an excel sheet. Moreover, each transducer was color-coded as to how well they met each topic of specification. The resulting Excel sheet is found in attachment A.2.

##### **3D-model evaluation:**

The majority of the sensor manufacturers openly provide 3D models of force-torque transducers. By downloading the *STEP*-file with accurate measurements of each transducer, *Fusion 360* was used to compare the different sensors to each other. Seeing the sensor in a digital 3D environment was helpful, as it gave a clearer picture of the design than comparing sensors only by a simple picture and datasheet. Using the 3D model, the project attempted to 3D-visualize and designed rough examples of implementation. This was useful to further analyze the possibilities and limitations of each sensor design.



**Discussion:**

Finally, the most relevant sensors and solutions were discussed and evaluated based on the defined specifications.

**Method criticism and uncertainties:**

There are several uncertainties in the method of finding and determining the best commercially available sensor solution, the most prominent being the Google algorithm, as it was the search engine of choice to find the sensors. There might exist more viable sensor system solutions on the market that are left untouched by this project due to the search engine only displaying what itself deemed the most relevant in relation to the inputted search words. Moreover, with regards to the slim market, many of said manufacturers have old and outdated websites. The same goes for the small second-hand retailers. As a result, a few sensor systems might have been left out.

### 3.2 Specifications for an intrinsic force-torque measurement system for a next generation snake robot

Prior to determining a sensor system, developing a set of specifications was important. This chapter presents the project's opinion regarding specifications for an intrinsic F/T sensor system for a next generation snake robot, with emphasis on the HOAL-team's aspirations. Moreover, it presents each relevant topic and gives reasoning to the project's decisions.

Information and specifications regarding the next generation snake robot at NTNU were gathered through meetings and conversations with *Jostein Løwer* and previous research from the HOAL-team. The design approach is to first develop the sensor system and then design the snake robot upon the sensor system.

**A brief introduction to the next generation snake robot at NTNU:**

The appeal of the next generation snake robot is to prove *HOAL* with snake robots. The HOAL-team has decided that the next generation snake robot will be an intended test-platform for demonstrating HOAL, primarily on a flat 2D plane (Figur 3.1). Therefore only requiring two axis of force measurement ( $F_x$  and  $F_y$ ), and one axis of torque ( $M_z$ ). This enables more solutions regarding the sensor system, as it decreases the minimum amount of measurement-axis required and possibly different combinations of sensors.

**Prioritizing different topics of specifications:**

*Hysteresis* was of utmost importance as it was one of the main issues with the previous sensor system in the Mamba snake robot (as discussed in 2.5.1). As stated by the HOAL-team, having an accurate and reliable measurement system is the most important factor. Moreover, hysteresis related to temperature tolerance is one of the main sources of inaccuracy and unreliability in strain-gauge measurement systems due to temperature's effect on electric resistance.



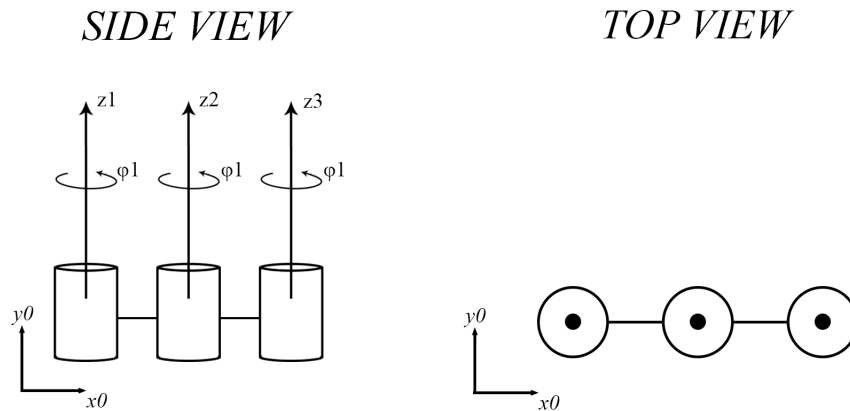


Figure 3.1: Configuration example of a snake robot intended to operate on a flat 2D-surface.

## SENSOR

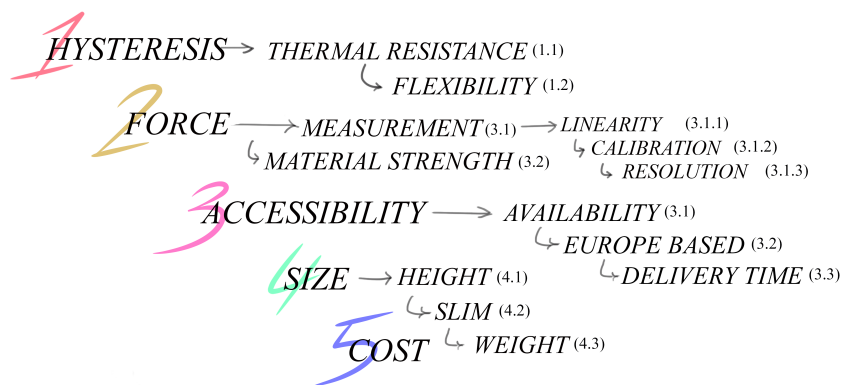


Figure 3.2: The different topics of specifications in prioritized order. It was a helpful tool in the research process, as it helped evaluate different sensors to each other with regards to the projects priorities.

*Force* was bullet point number two. The chosen sensor must have enough axis of force and torque measurement, high linearity with regards to applied force/torque, an efficient and reliable method of calibration in the measurement electronics, and high resolution with regards to the ADC capabilities and measurement amplification.

*Accessibility* is the subject of delivery and production time. The project had time constraints. Therefore, it was vital that the components used for the system could arrive within a certain time frame. Moreover, it was beneficial that a said replacement (in future projects) could be reordered swiftly if any problems arose.

*Size* is the subject of physical dimensions and weight. For an intrinsic force-torque measurement system, it was considered preferable to keep the sensor system as small as

possible to not limit the future design process and cause complications in terms of robotic capabilities.

*Cost* is self explanatory. It was considered the least important subject but proved to be the most limiting factor when deciding what sensor to proceed with.

### 3.2.1 Measurement capabilities

Measurement range	
$F_x, F_y (F_z)$	ca. $\pm 20$ N
$M_x(M_y, M_z)$	ca. $\pm 3$ Nm

Bending moments and forces	
$F_x, F_y, F_z$	$> 20$ N
$M_x, M_y, M_z$	$> 3$ Nm

Table 3.1: Measurement capabilities

For the sensor to be of use, it needs to be able to measure the necessary forces, measure them accurately, and be able to withstand said forces. From *Veslum's, Liljebäck's* reports, as well as conversations with *Jostein Løwer*, some maximum limitations in terms of force and torque measurement and durability was set. These limitations are shown in table 3.1.

Comparatively to temperature specifications, these were considered the realistically feasible limitations with regards to the size requirements. However, as high measurement range and limits as possible were favored.

It's preferable that each sensor has a relatively high bending moment (Table 3.1). For reference, the servo used in the *Mamba* snake robot (HSR-5990TG) produces a maximum torque of 2.95Nm. It's also obviously preferable that the system won't self-destruct under rare but expected load. Therefore it is important that the sensor has a higher maximum bending moment specification than the motor with a comfortable margin. Because the sensor is being chosen before the motor, and the motor will be chosen upon the sensor's specifications, this subject is relatively open, but the project has decided to use *Mamba's* servo as a reference to not halt or limit the future design process.

The sensor system needs to be able to measure the necessary forces and torques required. For the system to work as intended, the sensor must, at a bare minimum, be able to measure torque on the z-axis ( $M_z$ ) and force on the x- and y-axis ( $F_x, F_y$ ). Thus, being the necessary axis to achieve HOAL on a flat 2D configuration. If desired, the robot could be able to lift itself off the ground, providing 3-dimensional travel, but would require a third axis of force measurement ( $F_z$ ).  $F_z$  in 2D configuration is considered redundant with apropos to HOAL, but including it could provide information regarding strain along the length of the snake (depending on the way the sensor system is configured).

In addition to these limitations, the sensor also needs to be able to measure accurately and have as little hysteresis and measurement creep as possible. These properties are usually given as a certain percentage of maximum measurement output. The project did not specify specific numbers, but they were compared between the different suitable sensors.

### 3.2.2 Temperature tolerance

The servo-motor used with Mamba has a high current draw, which results in a lot of heat being produced. Combined with the fact that the housing is waterproof and made of plastic, each joint is prone to reach high temperatures. This posed major problems and was one of the main reasons the system needed reconstruction. Heat dissipation between the housing and the environment will therefore be an important subject in the development of the next generation snake robot. Regardless, it's preferable that the chosen force-torque transducer can operate in a wide range of temperatures.

Operational	0°C to 60°C *
Maximum	-10 °C to 80°C *

Table 3.2: Specified temperature range. *Operational* meaning the range in which the manufacturers can ensure that the sensor works as intended. *Maximum* meaning the range in which the sensor can operate without being damaged

\* Realistically, but preferable as high temperature tolerance as possible

### 3.2.3 Design, length and width limitations

Design is a crucial aspect for specifying an intrinsic force-torque transducer in a snake robot. A key part is trying to keep the sensor system as small as possible without influencing other equally important aspects, such as measurement range and accuracy. The transducer is to fit inside a small space, inside the robotic joint, along with a motor and other electronic components. The size of the transducer will then greatly influence the size and design of each robotic joint. For example, having a too wide transducer may increase the distance between each joint, which may increase the number of joints required to comfortably achieve autonomous HOAL with a snake robot.

Most of the force-torque transducers on the market have a cylindrical shape, much like the robotic joints in the Mamba snake robot. Therefore, the width and diameter limitation is based on the Mamba robotic joint design. However, as stated by Løwer, the next generation snake robot will likely be significantly larger.

Height	< 40 mm
Diameter(Ø)/width	< 60 mm
Weight	As light weight as possible

Table 3.3: Specifications regarding the physical design of the sensor system

Weight is also an important aspect of the design as the sensor is likely to be offset from each joint's center of volume. Therefore, having a too heavy sensor may offset the center of mass from the center of volume if not compensated for. Moreover, it would increase the motor-torque requirement.

The last important aspect of the design is the implement-ability, meaning how suitable it is for implementation in a compact environment and what type of electronics is required. Moreover, what alterations and additions may be needed for it to be usable.

### 3.2.4 Cost and accessibility

The cost was an important factor when it came to specifying a new sensor system. The main appeal was to stay within the given budget, with room to spare, without affecting the result. The project was early in the process informed of an approximate value of around 20000 Kr per sensor. This value ended up being used as an estimated value for the specification sheet. However, it was more vital to the client that the sensor system worked rather than its cost, which is why the last point in the specification sheet was cost. The estimation used for early design is shown in table 3.4.

**Early estimated budget for the HOAL transducer purchase:**

Price per sensor	Number of sensors	Total
20 000	40	800 000 NOK

Table 3.4: Early estimated sensor budget

The third point in the specification sheet is accessibility. This revolves around factors like production- and delivery time. The time from ordering the product until reception had to fit within the timespan of the bachelor thesis, giving enough time for implementation, testing, and assessment of the sensor system.

**Production- and delivery time:** < 4 weeks

### 3.2.5 Summary of specifications for an intrinsic F/T sensor solution for a next generation snake robot

This section contains a summary of the specifications set and discussed in this section, collected in a single table (Table 3.5)

#### Specifications for a F/T sensor in a novel snake robot

Subject	Value	
Height	<40mm	
Diameter	<60 mm	
Weight	As light as possible	
Measurements	$F_x, F_y, F_z$	$M_z$
Capacity	ca. $\pm 20N$	ca. $\pm 3Nm$
Safe overload	$> 20N$	$> 3Nm$
Operational temp. range	$0^\circ C$ to $60^\circ C$	
Price	<20 000 NOK	
Delivery time	< 4 weeks	

Table 3.5: Summary of specifications for an intrinsic force-torque sensor system in a next generation novel snake robot

### 3.3 A brief introduction to the market for force- and torque sensors

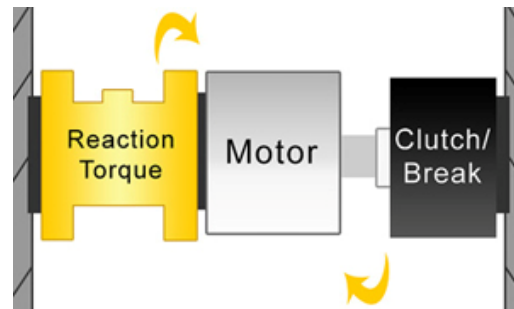
The market for force and torque transducers is mainly specialized within a narrow field of industries. The sensors are classified by their axis of measurement. This section briefly introduces the market for the different sensors and presents some of the project's experiences.

#### 1-axis static torque transducers:

The 1-axis torque transducers most relevant for the project are static torque transducers, most commonly referred to as *reaction torque* transducers. As the name suggests, they measure torque on 1-axis. The most common applications of these sensors are in the calibration of various hardware, such as accurately calibrating the torque produced by hand-held drills or measuring the tightening of screws and bolts (Figure 3.3a). Another common usage is torque measurement of various motors (Figure 3.3b).



(a) Example of use with a *TRT* reaction torque sensor, in this example it's used to calibrate a manual wrench. Courtesy of [11]



(b) Illustration of use with a reaction torque sensor to measure torque produced by a motor. Courtesy of [12]

Figure 3.3: Examples of common applications of 1-axis torque sensors

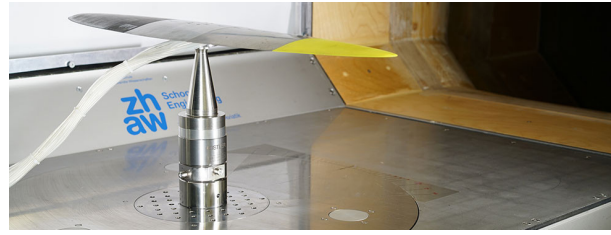
Most of the reaction torque transducers on the market are based on resistance strain gauges. The market for these sensors is fairly versatile, as they are available in a wide variety of sizes and specifications.

#### 6-axis force-torque transducers:

The 6-axis force-torque transducers/sensors, also known as multi-axis force-torque sensors, are mainly used in the robotic industry, where the accuracy of touch and placement is important (Figure 3.4a). Moreover, they are also used in various fields of scientific research, such as aerodynamic experiments in wind tunnels (Figure 3.4b). They are hyper-sensitive transducers that can measure forces and torques applied to an object in 3-dimensions. They can be used to calculate a force-vector in the XYZ-plane ( $F_x$ ,  $F_y$ ,  $F_z$ ) and simultaneously distinguish torque/momentum around the x-, y-, and z-axis ( $M_x$ ,  $M_y$ ,  $M_z$ ). They are most commonly based on strain-gauges (covered in 2.3), placed in pairs of 4 to each axis and coupled in a Wheatstone Full-Bridge configuration.



(a) 6-axis force-torque sensor mounted on a robotic wrist. Courtesy of [13]



(b) 6-axis force torque sensor used in a wind tunnel to gather data in aerodynamic research, to study the effects of air moving past solid objects. Courtesy of [14]

Figure 3.4: Examples of common applications of 6-axis force-torque sensors

The available sensors differ widely in terms of range and size. However, the market for small sensors suitable for the implementation inside a snake robot is slim, but the project was able to localize a few of them. The one main similarity between all multi-axial force-torque sensors is that they are costly, ranging between 20 000 and 100 000 NOK.

### Crosstalk:

An important subject regarding multi-axial force-torque measurement is crosstalk. It is the issue that when for instance, a torque is applied on the z-axis, it would also affect the force measurement on x- and y-axis. To counteract this, some manufacturers also provide *calibration matrices*, that through tests and linear- and nonlinear regression determine the correlation between the different outputs. By, for example implementing the matrices through algorithms, the crosstalk can be reduced digitally.

### 3-axis force transducers:

6-axis force-torque transducers are inherently expensive. This led to the idea of utilizing the 3-axis force transducers, most commonly referred to as *3-axis load cells*. The relevant areas in industry and science are roughly the same as with the 6-axis force-torque sensors. However, they only measure force on 3-axis ( $F_x$ ,  $F_y$ ,  $F_z$ ). The exclusion of torque measurement makes them a cheaper alternative, but given the specifications and need for torque measurement, it would have to be combined with a 1-axis torque transducer.

## 3.4 Strain Measurement with Fiber Bragg Grating(FBG)

*Fiber Bragg grating* was first demonstrated by *Ken Hill* in 1978 [15]. [16] It is a method to measure strain by utilizing single-mode fiber-optic cables and a light signal instead of the commonly used resistance strain gauges. They are produced by exposing a portion of a fiber-optic cable to intense light, making a permanent periodic increase in the refractive index in the fiber's core (visualized by the dotted lines on the cable in Figure 3.5b). The result is a fixed index modulation according to the exposed pattern. The fixed index modulation is called a *grating*. As a result of the gratings, when light is transmitted through the cable, certain wavelengths of light will be reflected back (Figure 3.5a). These wavelengths are known as *bragg wavelengths*. The central wavelength of the reflected portion of light is satisfied by *the Bragg relation*  $\lambda_{Brag}$  (equation in Figure 3.5b). The

parameters  $n$  (index of refraction) and  $\Lambda$  (the period of the index refraction of the FBG) are temperature and strain dependant. Therefore, by straining the FBG, a strain can be measured as a function of change in *bragg wavelengths* and a by referring strain to material constants (similarly to the method used with resistant strain gauges), the force that causes the strain can be calculated and measured.

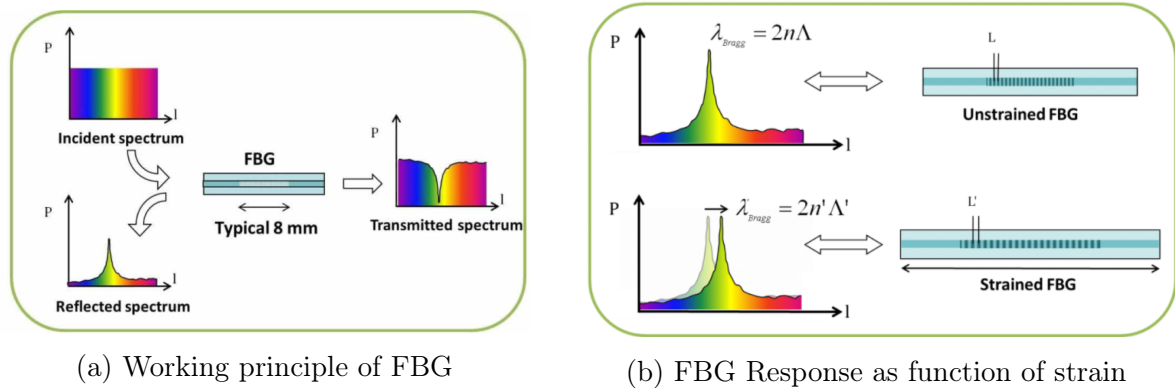


Figure 3.5: Principle of a fiber bragg grating strain sensor. Courtesy of [16]

### The future of FBG sensors technology and relevancy:

A whole paper could be written on this subject alone; the possibilities for FBG in the future are vast. A subject this report would highlight is the possibility of contact force measurement along surfaces. The technology enables several different series of gratings to be placed along the same fiber and distinguish between forces at each different grating. In the future, this could, for example, be utilized to give the robot the feeling of touch along each contact surface. And by, for example coupling these fibers in a mesh of wanted resolution, the robot would be able to gather more information about the environment and accurately pinpoint the location and size of external forces ( $f_{ext}$  in Figure 2.2). Moreover, the technology could be used to produce a multi-axis F/T sensor, using only a single cable with multiple gratings.

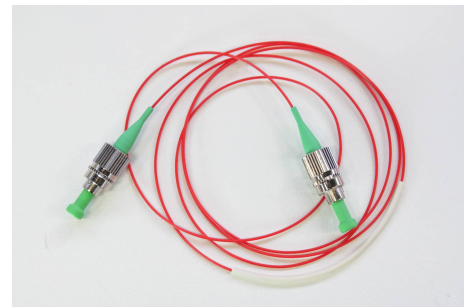


Figure 3.6: A fiber bragg grating strain gauge sensor system produced by FBGS. Courtesy of [17]

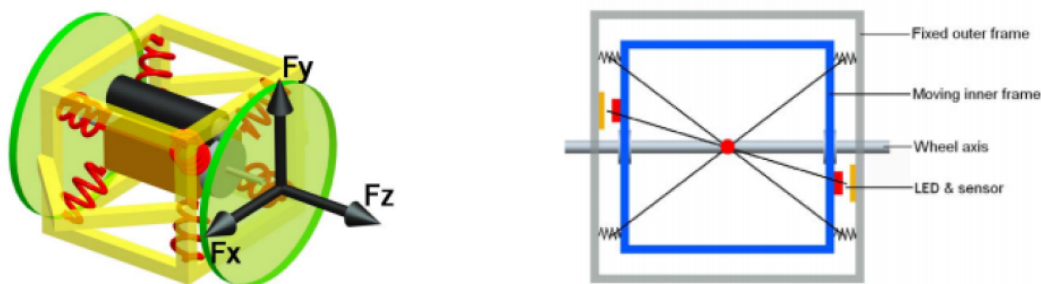
### Conclusion:

In summary, FBG-sensors are the optical-fiber equivalent of resistance strain gauge sensors. The technology seems promising, might be hyper-relevant in the future and is a worthy successor of the regular strain gauge sensor system. However, they are out of the scope of this project as there are no production-built multi-axis solutions available on the market at the time of writing (except for *sub-millimetric 3-DOF force sensors* [18]). It would be equivalent to buying regular strain gauges (an example is shown in Figure 3.6) and designing a multi-axis force-torque sensor from the bottom, which was not the project's intention. Moreover, the technology is still premature with regards to the currently available solutions on the market, and the required electronics are large in size and unsuitable to be implemented inside a snake robot.



### 3.5 Tokyo Institute of Technology - Position Sensitive Detectors(PSD)

[19] The snake robot researchers at *Tokyo Institute of Technology* have developed a specialized Position-Sensitive Detector system used in their snake robot intended to examine damage inside Fukushima's reactors. The system utilizes a moving inner frame, supported by springs inside a fixed outer frame. LEDs and light sensors are placed between the inner and outer frame, on all sides. They measure the internal frame's position relative to the outer frame, and by referring it to properties of the spring-loaded system, force may be calculated on three axes. The intended use is to put the wheel axis, or the motor of the robotic joint inside the moving housing. *TIT* claims it has measurement benefits, such as resistance to temperature and aging, as well as a low measurement inaccuracy.



(a) Schematic inner segment with driven wheel axis. Courtesy of [19]

(b) Positions of PSDs and flexible parts. Courtesy of [19]

Figure 3.7: The concept behind a 3DOF force sensor developed by the *Tokyo Institute of Technology*. Courtesy of [19]

### 3.6 3D printed Low-Cost Force-Torque sensors

Researchers at the University of Hamburgs Informatics Department have developed and researched 3D printed multi-axis force-torque sensors [20]. The article presents several different force-torque sensor solutions intended to mimic industrial counterparts, but at a substantially lower cost, using ABS print filament, optical proximity sensors, and microcontrollers. Moreover, it emphasizes the agility of 3D prints, being able to produce flexible shapes and spring-loaded parts with ease. The designs do have some setbacks, such as their small payload size  $N, Nm$ . The range of the presented prototypes maxes out in the 20 Newton range, which is on the low side for use with a snake robot. Including this, during a test print of the adjustable-FT (shown in



Figure 3.8: 3D printed low-cost force- and tactile sensing sensors. Courtesy of [20].

figure 3.9), it was shown to be slightly wider than other available sensors. However, it introduces the concept of designing a sensor system specialized to the needs of a novel snake robot using 3D-printable parts. This would allow for extensive and cheap prototyping. Moreover, measurement range and limits could be adjusted by changing the design (i.e., increasing the stiffness by increasing the thickness of said bendable object).

In conclusion, the paper introduces an interesting concept that should be further investigated. The possibility of designing and creating a specialized force-torque sensor system through the use of 3D prints would be of great interest if practically possible, as well as providing a major cost reduction. However, as previously mentioned, it is not without flaws. An excerpt of their researched prototypes is shown in figure 3.9.









	Sensor	DOF	Size [x,y,z] [mm]	Payload [N, Nm]	Sensors number, type	ADC channels, bits	Parts microcontroller	Qty	Cost	Sum
	Foot-Sensor	4x1	50, 10, 5	50 N	1x reflex	4x13	Teensy 3.2 ITR 8307	1 4	24 \$ 50 €	26 \$
	Pushing-FT	2	50, 50, 12	0.05 N	2x fork	2x10	Arduino Nano (clone) Vishay 1103	1 2	5 \$ 1 \$	7 \$
	Screwdriver handle tool mount	6x2 5	5, 13, 50 $\phi$ 50, $h$ 17	20 N 3 Nm	12x reflex 5x reflex	muxed 6x2 5	Nano 33 IOT (WiFi) ITR 8307 ITR 8307	1 12 5	30 \$ 50 € 50 €	39 \$
	Spacemouse (fork, thin hat)	6	$\phi$ 42, $h$ 35	2 N	6x fork	6x13	Teensy 3.2 Vishay 1103	1 6	24 \$ 1 \$	30 \$
	Spacemouse (reflex, thick hat)	6	$\phi$ 42, $h$ 50	4 N	6x reflex	6x13	Teensy 3.2 ITR 9904	1 6	24 \$ 1 \$	30 \$
	Adjustable-FT	6	$\phi$ 104, $h$ 42	20 N	8x fork	8x10	Arduino Nano (clone) Vishay 1103	1 8	5 \$ 1 \$	13 \$
	Block-FT	6	56, 56, 36	11 N	8x reflex	8x10	Arduino Nano (clone) ITR 8307	1 8	5 \$ 50 €	9 \$
	Bottle-FT (ring-type)	6	$\phi$ 114, $h$ 25 $\phi$ inner 70	10 N	8x fork	8x10	Arduino Mini (clone) Vishay 1103	1 8	5 \$ 1 \$	13 \$
	ATI Nano-17	6	$\phi$ 17, $h$ 15	12 N	6x strain-gauge	external	-	1		5000 \$
	Sunrise M3207	6	$\phi$ 74, $h$ 17	500 N	6x strain-gauge	external	-	1		4000 \$

Figure 3.9: Table of 3D printed sensors and their estimated cost. Courtesy of [20].

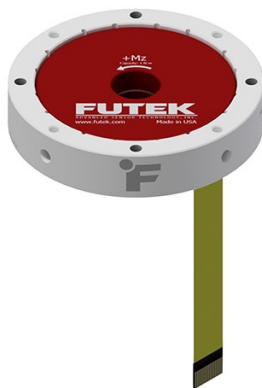
### 3.7 Futek

This section briefly introduces Futek as an industrial sensor system manufacturer and thoroughly covers and assesses one of their sensors considered relevant in the selection process.

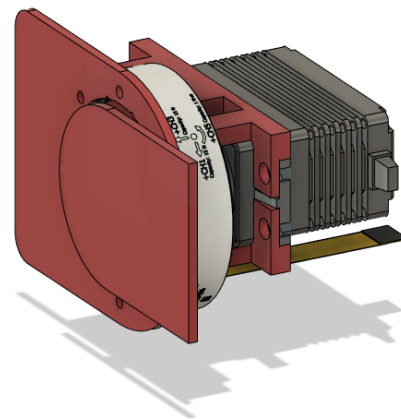


*Futek* [21] is one of the leading designers and manufacturers of sensor systems for force and torque measurement. Futek's multi-axis sensors became apparent to the project early in the research process. They seem to be one of very few innovative sensor system manufacturers on the market. Moreover, their expertise and experience seem unmatched in relevancy to the needs of the project. For example, they've produced multi-axis sensors for NASA's Mars lunar rover and currently have 2 sensors on Mars, which illustrates their capabilities. Futek and its production is located in the US, but they are represented in Scandinavia through *Load Indicator Systems AB* [22].

#### 3.7.1 QMA142 - 6 axis force-torque sensor



(a) 3D model. Courtesy of [23]



(b) Implementation example

Figure 3.10: The QMA142 sensor system, and an example of implementation exploiting the through hole design

Futek has listed several manufacturable models on their website. The QMA142 [23] is highly relevant in terms of its design, range, and features.

**Futek QMA142 specifications**

Subject	Value			
Height	9.5 mm			
Diameter	50 mm			
Weight	40 g			
Material	Aluminum 2024-T4			
Measurements	$F_{xy}$	$F_z$	$M_{xy}$	$M_z$
Capacity	15N	15N	1Nm	1Nm
Overload	100N	100N	4Nm	4Nm
Compensated temperature range	16 to 71 °C			
Operating temperature range	-51 to 93 °C			
Cable	15 Pin FFC , 0.5mm Pitch , 2 in. (5.08cm) Long			
Price	Ordered on quota, early estimate 75 000 SEK			

Table 3.6: Specifications for the QMA142 6-axis force-torque transducer

**Design:**

Regarding the design, it has many advantages. Firstly, the casing is one of the slimmest available. It measures only 9.5mm thick and 50 mm in diameter, advantageous for implementation inside a snake joint, where space is limited. Including this, the sensor only weighs 40g. Moreover, it has a through-hole, as seen in figure 3.10, which enables the rotating shaft to be mounted through, something that could help make a final snake-joint design even slimmer. An example solution shown in figure 3.10b showcases this. Furthermore, the project has a hypothesis that such a solution has measurement benefits. This is because a strain gauge transducer relies on the twisting and bending of the sensor itself. Placing the sensor as close to the shaft and mount as possible, keeping the least length of material between them along the axis of rotation, will likely reduce the amount of twist and flex lost through the components linking it to the sensor. For example, measuring the torque and/or force applied to a servo, mounting the sensor on the bottom would have a higher amount of loss in measurement to the servo's shaft and casing twisting along itself. If very stiff materials are used, this would likely not have a large effect on loss.

**Cable:**

Many of the sensors available on the market utilize large and old cable mounting adapters for use with large amplifiers and analog to digital converters usually provided by the sensor manufacturer. This is far from ideal in a snake robot, as the cable would have to be manually modified to be fitted on a circuit board, or the project would have to request design alterations to the manufacturer. However, the QMA142 already has this solved by utilizing a 15-pin FFC cable, which eases the implementation on a circuit board by just having to add a small compatible 15-pin mount.

**Measurement capacity:**

The range of measurement and measurement limits are well within the set specifications (Table 3.5). It can safely withstand up to 100N of force, equivalent to trying to lift roughly 10kg.

**Temperature range:**

As stated in chapter 3.2, it's important that the sensor system is able to withstand heat, as the motor, being placed in the same housing as the sensor, has a tendency to reach high temperatures. Therefore, the QMA142 is quite fitting, boasting one of the highest temperature ranges on the market, with an operation range between -51 to 93 °C.

**Availability:**

One of the main issues with this sensor is its unavailability. To order, one would have to apply for a quota of production, and the pricing is then dependent on the size of the quota and material cost. In addition, the time it takes to order and for the product to arrive is also highly unpredictable, and there were concerns that it could take several months. This was considered problematic for the Bachelor Thesis regarding the final aspect of testing and assessing a sensor system.

**Price:**

Price may be a deeming factor for this sensor. *LISAB* (Futek's Scandinavian representative) gave the project an early price estimate of 75 000 SEK per sensor, as it is a custom build and requires an engineering budget. Regarding the fact that one would need to order roughly 40 of these sensors, the total expense is staggering.

**Conclusion:**

It was clear that *QMA142* sensor was far too expensive for the project. Ordering 40 of these would total around 3 000 000 SEK, excluding all other costs. Moreover, the project is not too comfortable handling a sensor costing 75 000 a piece, with the slight risk of destroying it. However, the sensor is covered here because the project considers it as one of the most ideal sensors available on the market, excluding the price. Moreover, if a future project gets sufficient funding, the QAM142 could be an interesting consideration.

### 3.8 ATI - Industrial Automation

This section briefly introduces ATI as an industrial sensor system manufacturer and thoroughly covers and assesses one of their sensors considered relevant in the selection process.



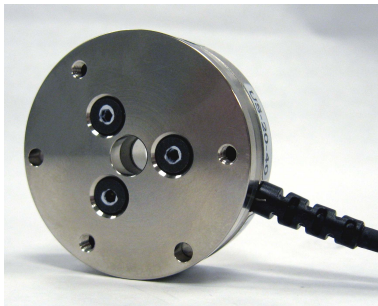
ATI is a North-America-based manufacturer of robotic accessories and robot arm tooling. They specialize in robotic end-effector accessories ranging from electric grippers to sensor systems and measurement electronics. They can be seen as a direct and competent competitor to Futek.

#### Sales representatives

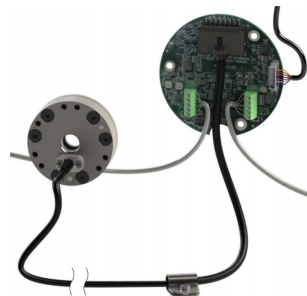
Similar to Futek, ATI does not have a webshop but retails through second-hand industrial retailers where sales representatives can be contacted. All of their listed representatives are listed in either North- or South America. Information regarding price and possible inquiry was gathered through Thomasnet [24] and one of ATI's sales representatives.

#### 3.8.1 Mini40 - 6 axis force-torque sensor

This section thoroughly assesses the Mini40 transducer from ATI Industrial Automation with regards to the set specifications and available information and discussions with the manufacturer. [25]



(a) The ATI Mini 40. Courtesy of [25]



(b) One of ATI's F/T transducers configured with the NETCANOEM-board, with ADC and components for CAN-bus serial communication. Courtesy of [26].

Figure 3.11: Examples of ATI force transducers

#### Design:

In terms of design, the Mini40 has many of the same advantages as the QMA142. It has a slim, compact design that meets the set specifications with a comfortable margin.

#### Measurement:

The Mini40 has measurement advantages compared to the QMA142. With a higher measurement capacity and strong overload protection, with a claimed maximum of 4.2 to 18.9 times rated capacities.

ATI Mini 40 SI-40-2 specifications

Subject	Value			
Height	12.2 mm			
Diameter	40 mm			
Weight	49.9 g			
Material	Stainless steel			
Measurements	$F_x, F_y$	$F_z$	$M_x, M_y$	$M_z$
Capacity	40N	120N	2Nm	2Nm
Safe overload	$\pm 810N$	$\pm 2400N$	$\pm 19Nm$	$\pm 20Nm$
Temperature range	approx. $\pm 25^\circ C$ from room temperature			
Cable				
Price	\$6500 to \$8000 (53 773 to 66 182 NOK)			

Table 3.7: ATI Mini 40 SI-40-2 specifications

It uses silicon strain gauges, and ATI claims it has a signal-to-noise ratio up to 75 times stronger than conventional foil gauges. The amplified signal is said to have a "near-zero noise distortion".

#### Temperature tolerance:

The given temperature range was considered slim compared to other sensors. However, tests would have to be performed to assess this topic accurately and determine if it is viable.

#### Electronics:

ATI excels in terms of OEM measurement electronics applicable for an intrinsic force-torque sensor system solution. As shown in Figure 3.11b, the Mini 40 can be configured with a NETCANOEM-board supplied by the OEM(ATI). The board has built-in measurement electronics and enables high-speed RS-485 communication to swiftly enable F/T data in a selected interface.

#### Conclusion:

The Mini40 force-torque transducer is considered a highly viable solution for an intrinsic force-torque sensor system for the next generation snake robot. With its small and compact design and preferable measurement capabilities, along with OEM measurement electronics. It is an all-in-one solution. However, given the high price estimate, it was considered too expensive to proceed with.

### 3.9 ME-meßsysteme



This section briefly introduces ME-meßsysteme as an industrial sensor system manufacturer and thoroughly covers and assesses two of their sensors that were considered relevant in the selection process.

[27] *Me-meßsysteme* has more than 20 years of industry experience regarding sensor systems and measurement electronics. Their production is based in Germany. They specialize in sensors and transducers for force, strain, and torque measurement, as well as amplifiers for said sensors.

#### 3.9.1 K6D40 - 6-axis force-torque sensor



(a) MP11 cable variant



(b) Cable gland (CG) variant

Figure 3.12: The K6D40 multi-axial force-torque sensor system, with its two cable configuration variants. Courtesy of [28]

#### Design:

The *K6D40* has an acceptable design, with a small diameter of 60 mm and 40 mm thickness making it one of the slimmest on the market. However, it would add more than 40mm to the design in comparison with Futeks QMA142, which makes it slightly less suited. Exploring the 3D model and assessing its implementation possibilities (shown in figure 3.13), shows that each joint would have to be more than 90mm in z-axial length (z being the motor rotation axis). This is, of course, dependent on the chosen motor and the linkage design, but size certainly reduces the possibilities. However, in a 2-axial (flat plane) snake robot solution, the length is less of a problem.

#### Cable:

There are two variants of the sensor system, the difference being the cable system (shown in figure 3.12). The cable gland (CG) variant in figure 3.12b has a fixed cable mounted to it, and the MP11 variant in figure 3.12a has an MP11 cable port. Neither is preferable, as the cable would, either way, have to be modified to fit on a circuit board.



**K6D40 Specifications [28]**

Subject	Value			
Height	40 mm			
Diameter	60 mm			
Weight	160g			
Material	Aluminum alloy, stainless steel			
Measurements	$F_x, F_y$	$F_z$	$M_x, M_y$	$M_z$
Capacity	50N	200N	5Nm	5Nm
Safe overload	200N	800N	20Nm	20Nm
Rated temperature range	-10 to 70 °C			
Operating temperature range	-10 to 85 °C			
Environmental protection	IP65			
Cable	MP11 24-pole plug, or cable gland (CG)			
Base price	1 650 EUR(+430 EUR calibration)(17 192 NOK feb. 2021)			
Full price est.	27 018 NOK (march 2021, with shipping and taxes)			
Availability	3-4 weeks delivery time			

Table 3.8: Specifications for the K6D40-50N/5Nm variant

**Measurement:**

The measurement range is considered decent. Moreover, it is able to withstand more force and torque than the *Futek QMA142* counterpart. The sensors are internally coupled in a Wheatstone Full-bridge configuration, which enables an output in  $mV/V$ .

**Price:**

This product stands out regarding the price because it is cheaper than the *Futek* counterpart. Moreover, it is the cheapest 6-axis solution that meets the requirements of a sensor system in a snake robot.

**Availability:**

*Me-meßsysteme* states that it has 3-4 week delivery time on the product. This is excluding eventual hold time in Norwegian customs. This short delivery time is considered an advantage.

**Conclusion:**

The *K6D40* was a highly viable option, as it is one of the cheapest 6-axis alternatives on the market that meets all requirements in an intrinsic solution. However, by adding tax and import fees, the project found it to stretch just outside the available budget. Putting the price in perspective with all possible solutions, it is placed in the medium range.

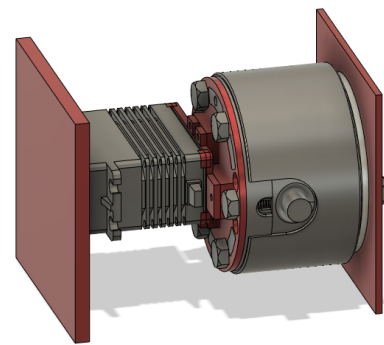


Figure 3.13: Implementation example with the K6D40

### 3.9.2 K3D40 - 3-axis force sensor

The K3D40 is one of the 3-axis force-transducers considered by the project.

#### Design:

The *K3D40* sensor has a few weaknesses in terms of design, but it is overall acceptable. Firstly, the square design is not preferable in an intrinsic solution, as robotic joints are preferably cylindrical. Although a width ( $w$ ) and length ( $l$ ) of 40 mm seems slim, by using simple *Pythagoras* (3.1) it shows that a cylindrical joint housing would have to have a minimum inner diameter of roughly 57mm to fit the sensor. This is barely within the desired specifications defined in section 3.2, but was not considered a problem overall.



Figure 3.14: Picture of the *K3D40* 3-axis force-sensor by *Me-meßsysteme*. Courtesy of [29]

$$ld = 2\sqrt{\left(\frac{l}{2}\right)^2 + \left(\frac{w}{2}\right)^2} = 2\sqrt{2\left(\frac{40\text{mm}}{2}\right)^2} \approx 57\text{mm} \quad (3.1)$$

Secondly, the sensor has a center mounting point, as seen in Figure 3.14, where the 4 screw holes are. Inevitably, the sensor would have to be mounted in a confined space with objects above and below it with adapter-mounting components between the sensor, motor, and housing. It is expected that the sensor will flex a certain amount. The exact amount is undisclosed by the manufacturer. The sensor center mounting point introduces the need for a certain amount of space between the edge of the sensor and the edge of the adapter so that the adapter doesn't collide with the edge of the sensor when extruded with force, and thereby cutting the measurement. *Me-meßsysteme* states that the minimum amount of space required is 1mm. This subject, regarding the bending of the sensor and what effects this may have on the rest of the system, was further investigated during testing and implementation. It is not considered an issue but something to be aware of. Moreover, a center mounting point centralizes the strain area, further increasing the strength requirement for the chosen adapter material.

#### Cable connection:

The *K3D40* is shipped with a 3 meter long, 12-core *MESC-12x0061-PUR* cable and doesn't come with a standard cable connector configuration. Regardless, the cable would have to be cut open and each core manually extracted to be implemented on a circuit board. It has an outer diameter of 3.1 mm and a cable extraction on the side. If, for example, the chosen housing has the minimum inner diameter of 57mm, the cable has about 8.5mm of space to bend, which was considered plentiful.

#### Measurement:

The *K3D40* measures force in 3-axis ( $F_x, F_y, F_z$ ). The sensor comes in four different variants with different measurement ranges ( $\pm 2N, \pm 10N, \pm 20N, \pm 50N$ ). The project chose the  $\pm 50N$  as it seems to serve the purpose with relation to measurement range

according to the specifications 3.2. Moreover, according to the *K3D40-±50N data sheet* [30], it has good accuracy, a high temperature tolerance, and a high enough force- and torque bending limit. As the *K3D40* only measures force, it would have to be combined with a torque-sensor to meet the necessary measurement requirements.

### Price and availability:

Price was one of the main reasons why this sensor was considered, because if combined with a 1-axis torque sensor, the whole solution would be a couple of thousand NOK cheaper. In terms of availability, it ships from *Me-meßsysteme*'s factory in Germany and has a 3-4 weeks delivery time, including production time.

**K3D40-50N specifications [29]**

Subject	Value
Height	20 mm
Width	40x40 mm
Weight	85g
Material	Aluminum alloy, stainless steel housing
Measurements	$F_x, F_y, F_z$
Rated force	$\pm 50N$
Safe overload	200% FS ( $\pm 100N$ )
Bending moment limit	$5Nm$
Rated temperature range	-20 to 60 °C
Operating temperature range	-20 to 70 °C
Cable	12-core (MESC-12x0061-PUR). Outer diameter: 3.1mm
Base price	EUR 880
Full price est.	11 953 NOK (mar. 2021) /w shipping and taxes

Table 3.9: Specification sheet of the K3D40-50N

## 3.10 Transducer Techniques

This section briefly introduces Transducer Techniques as an industrial sensor system manufacturer and thoroughly covers and assesses one of their sensors considered relevant in the selection process.

*Transducer Techniques* is a designer and manufacturer of force and torque sensor systems. They are based in California, USA.

### 3.10.1 TRT-series

*"The TRT Series reaction torque sensors offer long-term reliability due to non-moving parts and state-of-the-art bonded foil strain gages. Whenever possible, the best approach for precision torque measurements is via reaction torque-sensing, eliminating high maintenance and high cost of slip rings, bearings and brushes."*

- *Transducer Techniques* [11]



Figure 3.15: A picture of the TRT-50 reaction torque transducer by *Transducer Techniques*. Courtesy of [11]

**TRT-50 specifications**

Subject	Value
Height	1 inch (25.4mm)
Diameter( $\emptyset$ )	1.630 inches (41.4mm)
Measurements	1-axis of torque ( $M_z$ )
Rated torque	50 lb-in (5.65 Nm)
Bending moment limit	50 lb-in (5.65 Nm)
Compensated temperature range	60° to 160° F (15.6° to 71° C)
Safe temperature range	-65° to 200° F (-54° to 93° C)
Cable	AMX-4 10ft mating cable (4-core) [31]
Base price	\$675 (est. 8 918 NOK (mar. 2021) /w shipping and taxes)
Full price est.	est. 8 918 NOK (mar. 2021) /w shipping and taxes
Availability	est. 14 days delivery time

Table 3.10: Specifications for the TRT-50 reaction torque transducer by *Transducer Techniques*. Courtesy of [11]

### Design:

Assessing the design of the *TRT-50* was difficult, as the *Transducer Techniques* does not have a 3D model of that specific transducer. Therefore, the project may only assess the design by judging the picture, specifications, and the schematic drawing. However, the project roughly constructed a 3D model with the available data and imagery.

Overall, the design is considered to suit the project's specifications. It has a relatively small diameter and is not too tall. In conclusion, it is suitable for an intrinsic sensor solution.

### Measurement:

The *TRT-50* has an acceptable measurement range within the desired specifications. By only measuring 1-axis of torque, it is not a stand-alone solution and would have to be combined with a 3- or 2-axis force transducer to meet the project specifications.

### Cable connection:

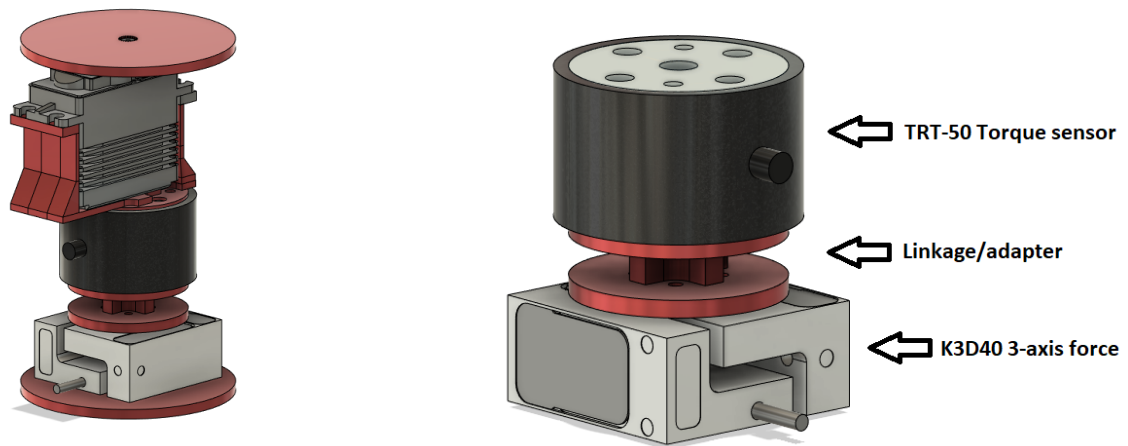
The *TRT-50* has a *AMX* connector on the side for connection with an *AMX* cable. There are different types of *AMX* connector cables available on *Transducer Techniques*-website, the most interesting ones being the *AMX-410-90* which has a 90° connector head.

However, a standard *AMX-4* 10ft connector cable is included with each sensor but has a straight connector head.

#### Price and availability:

In terms of price, the *TRT-50* was considered well within the desired price range. However, it is among the more expensive torque-transducers on the market due to its compact design. The availability is also fairly good, as *Transducer Techniques* states that it has a 14-day delivery time.

### 3.11 3-axis force- and 1 axis torque transducer combined solution (Sandwich Solution)



(a) Example of implementation with the *TRT-50* torque sensor (black) and the *K3D40* 3-axis force sensor (bottom)

(b) Combining the *TRT-50* reaction torque sensor, with the *K3D40* 3-axis force sensor through a linkage/adaptor

Figure 3.16: The 3-axis force sensor and 1-axis torque combined "sandwich" solution

In addition to 6-axis force-torque sensors that measure every axis in a combined solution, the project was also asked to investigate the possibility of combining different sensors that in total meets the minimum requirement of measurement axis and provides an acceptable range of measurement. That is the basis of combining a 3-axis force sensor and 1-axis torque sensor shown in Figure 3.16. For simplicity, this solution is referred to as the *sandwich solution*.

#### Design:

Compared to the other solutions presented in this section, the *sandwich solution* takes up more space than the counterparts. One of the reasons being that it needs some sort of linkage between the different sensors. As both the *TRT-50* and the *K3D40* have specified connection points on the top and bottom, and taking the need for space for screw mounting into account, makes the linkage design intricate and difficult. The height of the linking component will vary according to the required material thickness and the length of the different screws.

### Sandwich Solution specifications

Subject	Value	
Height	58.4 mm (width the final linkage design)	
Diameter/diagonal width	57mm	
Measurements	$F_x, F_y, F_z$	$M_z$
Capacity	$\pm 50N$	$5Nm$
Safe overload	$\pm 100N$	$7.5Nm$
Rated temperature range	15.6°C to 60°C	
Operating temperature range	-20°C to 70°C	
Cable	12-core (MESC-12x0061-PUR) and 4-core (AMX-4)	
Price estimate	20 871 NOK (march 2021) /w shipping and taxes	

Table 3.11: Theorized specifications for the *Sandwich Solution* (combining the limits of the K3D40 3-axis force transducer and the TRT-50 torque transducer and adding a linkage)

One of the benefits of the 2-sensor solution is that it can be configured in several different ways. For instance, the force sensor could be placed in between the joints of the snake robot.

#### Measurement:

In total, *TRT-50* and the *K3D40* meets the specified requirements regarding axis of measurement and range. However, it's theorized that it has certain measurement disadvantages.

Firstly, as the system is taller than its counterparts and there is a need for material between the sensors, it's imminent that the sensor will have a higher and more unpredictable strain loss. This would have to be accounted for. Secondly, there will certainly be measurement *crossstalk* between the different sensors and measuring signals. To counteract this, each sample of the *sandwich solution* would have to be put through vigorous test with special equipment to estimate a calibration matrix.

#### Temperature range:

It has the slimmest temperature range of the solutions presented in this section, with the lowest maximum and the highest minimum operating temperature. However, it was considered to be within the required limits.

#### Price:

One of the main advantages of the Sandwich Solution is that it was within the specified budget of the project, making the acquirement of a prototype feasible.

### 3.12 Discussion and conclusion

This section summarizes the findings in the research process. Moreover, it compares the different sensor solutions uncovered in the research process and gives reason to why the project decided to proceed with the Sandwich Solution.

#### 3.12.1 Findings regarding the market for F/T-transducers with relevance to the needs of a next generation snake robot at NTNU

The project used extensive time researching different possibilities regarding possible F/T-transducer sensor solutions for a next generation snake robot. At the time of writing, the overall conclusion is that the market is slim, and the options are few. Moreover, the most relevant are based on old strain gauge technology. Lastly, suitable sensors for an intrinsic solution regarding size and accuracy are costly, ranging from 20 000 NOK to 100 000 NOK.

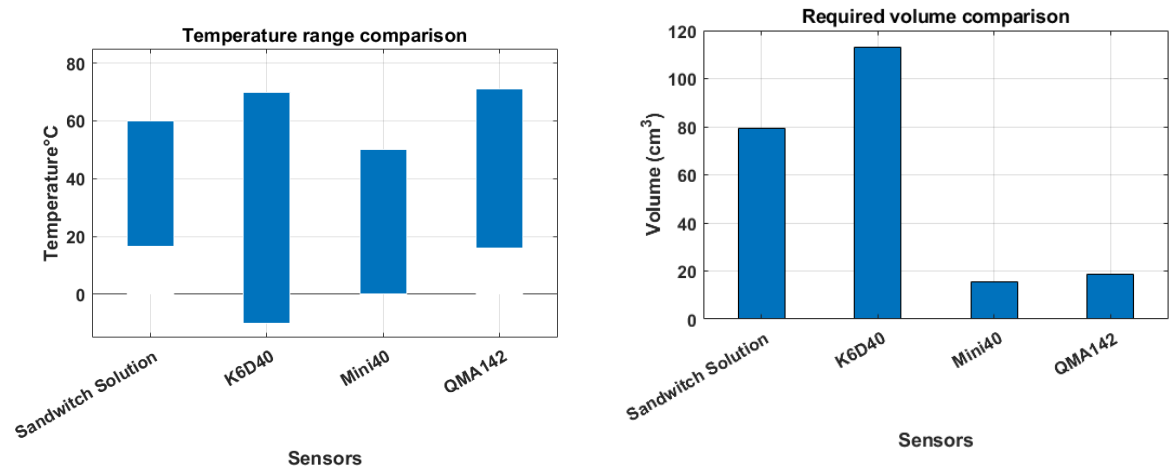
#### 3.12.2 Coherence in industrial sensor-system-solutions regarding multi-axis force measurements and degree of "how industrially produced"

The whole basis of this project was to investigate the possibilities and different solutions from different commercial sensor manufacturers. The manufacturers usually have years of experience concerning the production of said multi-axis sensors. Secondly, they have expensive equipment that helps them reduce inaccuracy factors in production. This lays the foundation for the important subject of how much better and how much more efficient in terms of cost and result. Moreover, industrial manufacturers will produce said systems better than us, regarding the inaccuracies in the hand-built *Mamba sensor-system*.

Taking the 6-axis force/torque sensor as an example, it is considered the highest degree of "industrially produced", because all required axis is included and manufactured in a single combined solution. Choosing a 3-axis force-sensor would mean a step down in degree of "industrially produced" because torque measurement is needed and would have to be added in as a second sensor system that would require custom parts to be produced to accommodate these two sensors. Producing those custom parts, and aligning the sensors, could be sources of measurement inaccuracies. Moreover, the calibration matrices would have to be manually estimated and produced. Referring it to a low degree of "industrially produced", like the *Mamba sensor system* or a solution with multiple torsion bars, introduces several possible sources of inaccuracy in measurement and alignment.

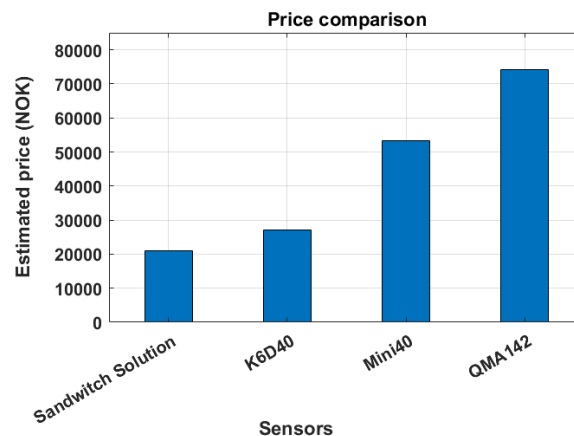
In summary, the report theorizes that a low degree of "industrially produced" will have greater inaccuracy but may have major deceiving cost benefits. The issue at hand was finding an accurate measurement system solution that meets the requirements, and at the same time, was affordable given the limited budget.

### 3.12.3 Comparing the different sensors to each other



(a) Comparing the different sensor's temperature range

(b) A bar graph comparing the different sensors in terms of required space. Calculated based on specified dimensions.



(c) A bar graph comparing the different sensors in terms of price

Figure 3.17: Comparing the presented sensor system solutions in terms of price, temperature range, and size

With regards to the set specifications, all of the 4 solutions covered fit the desired requirements for an intrinsic sensor system. However, they differ in terms of specified temperature range, price, and size (Figure 3.17).

In terms of rated/compensated temperature range (Figure 3.17a), the 6-axis F/T-transducer, K6D40, was seemingly the winner. However, it has the same maximum rated temperature range as the QMA142. Comparing the sensors in terms of the specified temperature range can not be deemed accurate because the different manufacturers use different definitions and likely different methods. Nevertheless, it is a good measurement of the manufacturer's confidence in the sensor's ability to operate at varying temperatures.



Space is a highly limited commodity concerning an intrinsic robotic joint F/T-transducer solution. Therefore, comparing size is also important. Figure 3.17b shows a bar graph comparing the different sensors in terms of the minimum volume each sensor would consume (side-by-side 3D models can also be seen in Figure 3.18). The QMA142 and the Mini40 take up significantly less amount of space than the two other sensors. By the looks of the graph, the K6D40 seems to be a clear loser by having the highest volume. However, by comparing the K6D40 to the Sandwich Solution in terms of height, the K6D40 is shorter, which is considered an advantage.

Price was initially deemed the least important aspect of specification but proved to be a crucial subject. As it is budgeted to purchase about 40 sensors, a small price difference between sensors would be greatly amplified. Moreover, the sensors presented here are costly and vary widely in terms of price (Figure 3.17c).

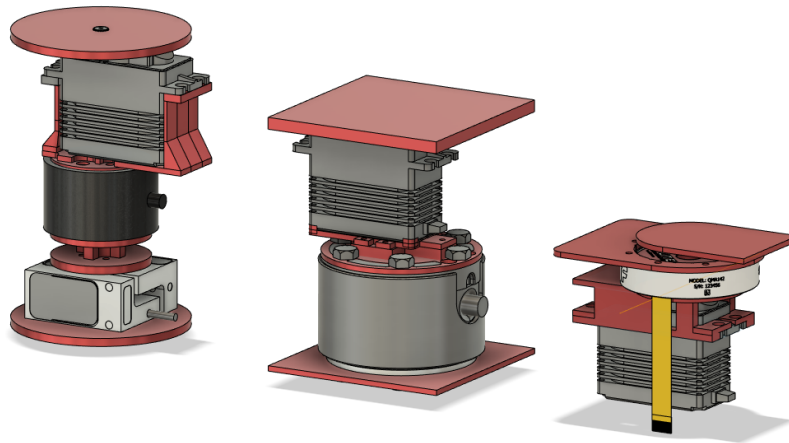


Figure 3.18: Size comparison of the three different implementation examples

### 3.12.4 Deciding what F/T transducer solution to test and assess

Due to the "limited" budget of roughly 20 000 NOK per sensor, the project decided to proceed with the combined sensor solution covered in section 3.11. It meets the criteria of being based on commercially available solutions and fulfills all specifications regarding axis of measurement and range of measurement. However, compared to the 6-axis F/T transducer solutions presented, it falls short in terms of size. Moreover, requiring a custom-designed and manufactured part that links the different sensors is considered a disadvantage due to the probable resulting inaccuracies in strain-loss and alignment. In conclusion, all covered sensor systems are considered viable and functional solutions. However, the *Sandwich Solution* is the only financially realizable solution that is affordable given the project's budget. Disregarding the budget, all the covered 6-axis F/T transducers are considered better solutions.

## 4 Designing the sensor system for testing purposes

According to the given task, the chosen sensor system was to be tested and assessed in realistic conditions. This chapter thoroughly covers the design process of the sensor system, test bench, and required measurement electronics.

For the sensor system to be operational, the system needs to be provided with supportive electronics in the form of power supply circuits and amplifier circuits. The power supply circuit makes sure the system receives the correct voltage and current, while the amplifier circuit amplifies the signal from the wheatstone bridges for each measurement axis in the sensor.

### 4.1 Designing the linkage

This section thoroughly covers the design process of the linking/adapter component, called the linkage, required between the 3-axis force sensor (*K3D40*) and the reaction torque sensor (*TRT-50*). The purpose of the linkage is to transfer strain between the two sensors and ensure accurate positioning between the sensors for accurate measurement. To assure the best result, mounting instructions and requirements provided by each manufacturer were taken into account.

#### 4.1.1 K3D40 requirements

*Mounting instructions for 3-axis sensors* [32]

##### Requirements for mounting surface:

- The distance between sensor body and fastening elements must be 1 mm.
- Screw depth for thread min. 1.0 up to 1.5 x  $\emptyset$ .
- Scew depth in the live end / dead end should be 5-7 mm.
- High stiffness of the mounting surface, no deformation under load.
- Flatness of mounting surface 0.05 to 0.1mm.
- Quality of the mounting surface Rz6.3 $\emptyset$ .

##### Screws

- **Position:** 1 and 2 (seen in Figure 4.1).
- **Type:** Cylindrical head screws DIN EN ISO 4762 M3 (requires 3mm hole)
- **Material:** Aluminium alloy
- **Tightening torque:** 1 Nm

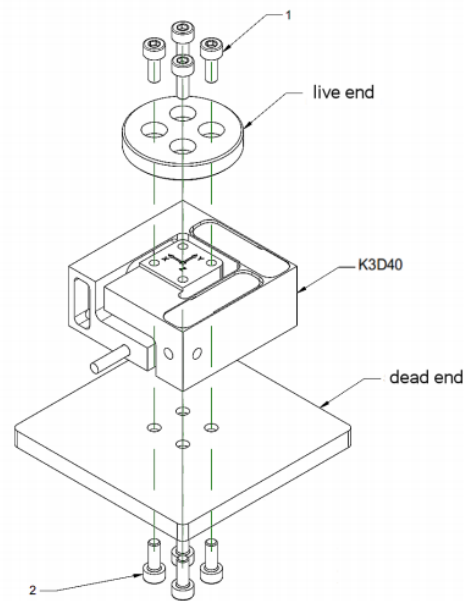


Figure 4.1: Instructions for mounting of the *K3D40* 3-axis sensor system. Courtesy of [32]

#### 4.1.2 TRT-50 requirements

*Transducer Techniques* does not provide any information on how to mount this sensor. They had to be estimated with regards to the given dimensions and compared to the mounting techniques used with socket adapters provided by the same manufacturer.

##### Dimensions in Inches, TRT-25 through 500

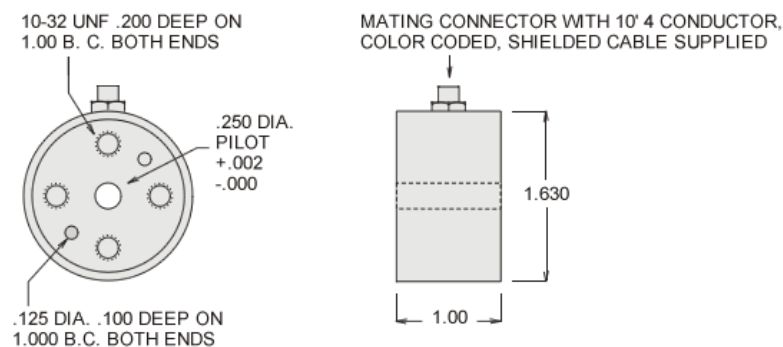


Figure 4.2: Schematic drawing of the TRT reaction torque sensor. Couresy of [11]

#### Mounting:

- **Screws:** 8 x 10-32 UNF .200 inches deep (5.1mm)
- **Postions:** 4 points on each side (spiked circles in Figure 4.2)
- **Thru-hole:** .250 DIA PILOT thru-hole in the middle. May be utilized to stabilize the sensor.

Firstly, since the TRT-50 sensor is American, it needs imperial machine screws. Moreover, Transducer Techniques does not ship the sensor with screws. The 10-32 UNF is fairly similar to the M5 screw, but they are not completely interchangeable. Thus, custom imperial machine screws had to be ordered from England.

### 4.1.3 3D-design

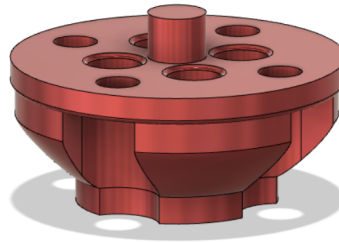


Figure 4.3: 3D-model of the linkage components that connects the different sensors together. Shown here is *LinkageType4*, it has the benefits of being one continuous part, but it had mounting difficulties that would result in the part being tall

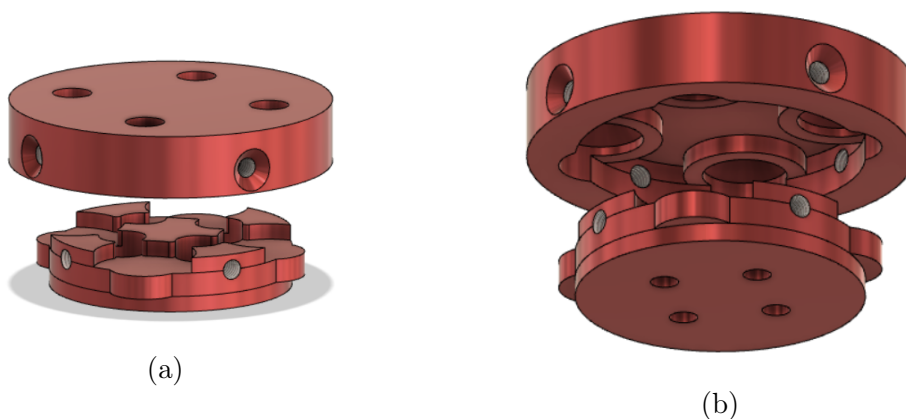


Figure 4.4: 3D model of *LinkageType7*. It has two parts that are mounted to each sensor. The two parts can then be locked together through screw holes on the side.

Several linkage prototypes were designed in Autodesk Fusion 360 (Figure 4.3 and Figure 4.4).

#### Mounting plates

Each mounting plate (the surfaces in direct contact with the sensors) was designed using the given sensor specifications and mounting requirements. The project assumed that 3mm thickness would provide enough material stiffness.

#### Spacer/link

The purpose of this component is to provide the necessary stiffness between the two sensor-mounting plates. Moreover, to add enough space between the mounting plates so that it is possible to access the screw holes with screws and mount them sufficiently. The chosen shape for *LinkageType4* was a type of cylinder with a length of 10mm. Access

holes were cut out to enable the mounting of screws. Lastly, the edges were rounded using the "fillet"-tool.

*LinkageType7* (Figure 4.4) was designed with another approach in mind. *LinkageType4* and other iterations had to be fairly tall to accommodate the mounting of screws. Therefore, creating two objects that are mounted to each sensor, then locking the two objects together through the side-mounted screws would have benefits in terms of height and assembly. As seen, the object is fairly intricate and complex with grooves to accommodate for the mounting and collision of screws and has grooves to stabilize the two parts together.

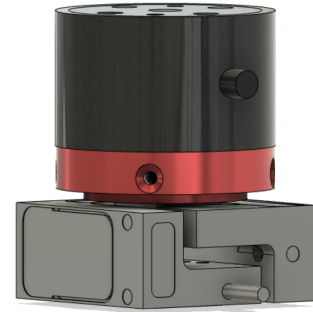


Figure 4.5: 3D model of *LinkageType7* assembled.

### 3D-printed prototype

Using the available PrusaSlicer at the *Mamba Workshop*, a prototype was printed using ASA filament. Moreover, the project conducted tests to determine whether a plastic model is stiff enough to be utilized further.

### Ideal material

Ideally, the linkage needs to be as stiff as possible to ensure the least strain loss between the sensors. For testing purposes, given the budget and time limitations, the project decided to use ASA-plastic-filament as it is lightweight, stiff, and has a fairly high temperature tolerance.

The ideal material for this component would be a type of stiff and lightweight metal, composite or hard plastic. In cooperation with the machine workshop at ITK, a CNC cut prototype was produced using *POM-C* (Figure 4.6), a type of hard plastic with high temperature tolerance and stiffness.

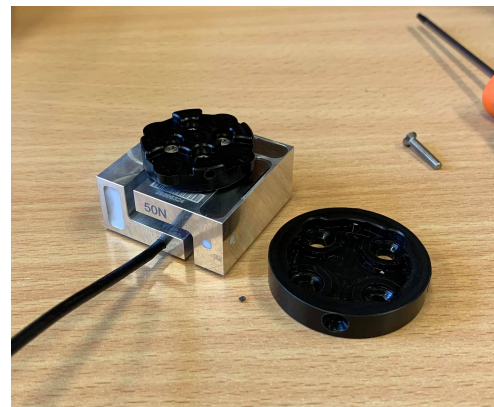


Figure 4.6: Linkage (black) mounted on the 3-axis force sensor.

## 4.2 Designing the test bench

In *Veslum*'s experiments on the Mamba sensor system, he exploited the robotic snake structure and shell, placed a joint on the edge of a table, and applied force using weights. At the time of writing, the next generation snake-robot is just an early stage concept, and the joints are yet to be produced. Therefore, the project had to design and build a test bench that emulates the conditions of a snake robot in realistic environments. Moreover, to reproduce some of the experiments performed by *Veslum* with the new sensor system, so that the results could be compared to each other to some extent.

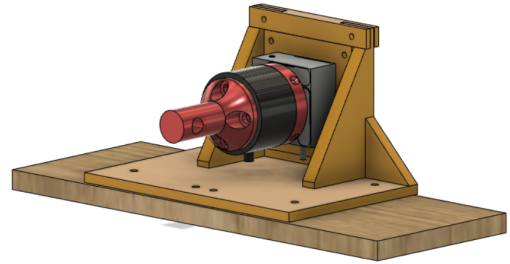


Figure 4.7: A sketched 3D-model of the test bench

Figure 4.7 shows a sketched 3D model of the test bench. It consists of a vertical plate with screw-hole mountings for the sensor system. The vertical plate is supported at 90 degrees by a horizontal plate. The plan was that the horizontal plate could be mounted to a wooden plank that could then be clamped to a table to stabilize the test bench.

To apply known forces and torques, weights could be mounted to the shaft that extends beyond the table. In this design, a force can be tested on 2 axes (x and y) in the positive and negative direction, consequently 4 directions. This is achieved simply by remounting the sensor system 90° to the previous position. To achieve a greater variety of angles that can be tested, the 90° mounting bracket could be mounted to a ball-jointed clamp (available in the HOAL-workshop).

To apply known torques, a 90° L-shaped shaft is used (Figure 4.8). By applying weights offset along the XY-plane, a resulting torque will be generated around the z-axis.

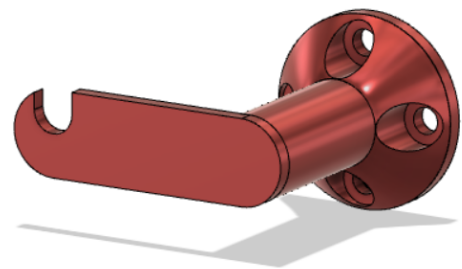


Figure 4.8: A 3D model of the torque shaft

### 4.3 Designing the power supply circuit

The current iteration of Mamba runs off an external power supply distributing 36 Volts across the entire robot. These 36 volts are distributed to each joint through a power supply circuit, transforming down the voltage to a suitable level (7.4 Volts and 3.3 Volts). These voltage levels are used to accommodate the servo motors need for 7.4 Volts, and the microcontrollers need for 3.3 volts. However, due to the designed sensor system, the required voltages are different, therefore the power supply circuit had to be retrofitted. The new power supply circuit (shown in figure 4.9 and 4.10) was inspired by the previous design made by Pål Liljebäck. It contains a switching voltage regulator that reduces the input voltage in the range of 10-36 volts down to 7.4 volts. This is to accommodate the servomotor's need for a high voltage supply. In addition, the switching regulator can deliver up to 6 amperes to the rest of the system, which satisfies the servo's high power consumption. Including the first switching voltage regulator, the circuit also contains an LDO (Low dropout) voltage regulator, which further reduces the voltage down to 5 V with a maximum power consumption of 1 ampere. These five volts are used to power both the sensor and the amplifier circuit. It is also important to note that it was chosen to use two step-down regulators instead of one to reduce signal noise from the power supply circuit, which could interfere with the measurements. For more information about the chosen components, see attached document (Appendix A.4).

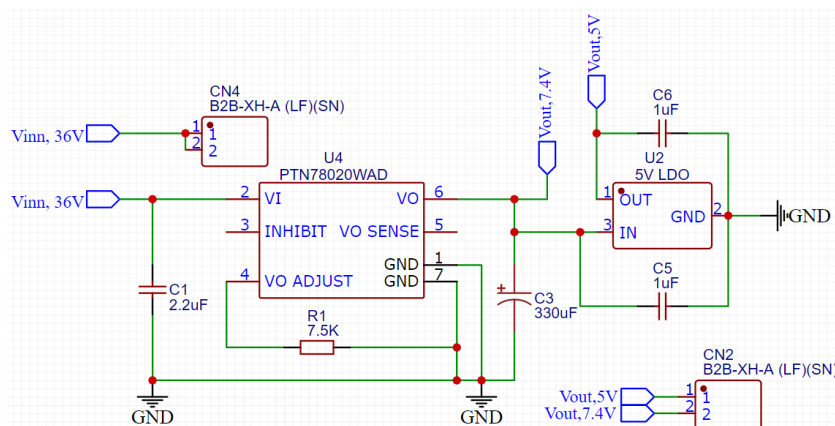


Figure 4.9: Power supply circuit schematic

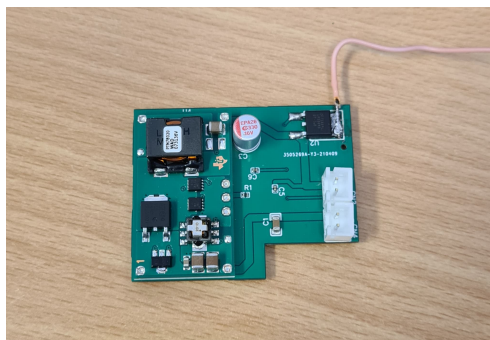


Figure 4.10: Power supply circuit



## 4.4 Designing the amplifier circuit

The sensors that provide torque and force measurements rely on Wheatstone bridges to measure the applied strain (Section 2.3.2). These bridges provide signals in the milli volt-range. Due to their minuscule size, the output signals are below the threshold for usability and require significant upscaling to be successfully implemented in valid applications. An amplifier circuit is therefore required and will aid in increasing the signal amplitude, thus improving readability. This can be done through a simple operational amplifier circuit, but due to the presence of Wheatstone bridges, the optimal choice would be to utilize an instrumentation amplifier instead. Consisting of two amplifiers connected in an input buffer and a differential amplifier creating a single-ended output, the in-amp benefits from high input impedance and easy gain regulation through the changing of a single resistor 4.4.2. Retaining the differential amplifier's common-mode rejection ratio, the in-amp is less versatile but flourishes in operations that require superior characteristics. Therefore although more than capable of fulfilling the task, if possible, the standard op-amp will almost always be neglected in favor of its superior instrumentation brethren. Therefore, choosing the in-amp allows one to fully capitalize on its features and results in a noise-canceling amplifier that more than fulfills the requirements of an amplifier circuit.

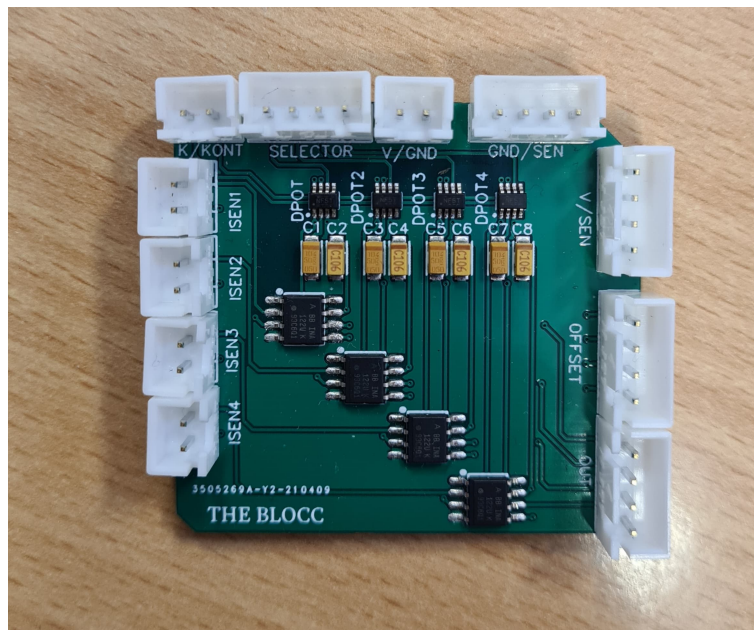


Figure 4.11: The completed amplification circuit *THE BLOCC*. Designed as a testing circuit, little focus was put on size regulation causing the *block* like appearance



#### 4.4.1 Comparing Amplifiers

The original amplification circuit for mamba utilizes a Texas Instruments INA122 instrumentation amplifier supplied by Farnell. The reason for choosing this exact amplifier is not entirely known but may have been chosen due to its easy obtainability in conjunction with its exceptional single supply properties. Commonly op-amps require dual supplies with inverted polarity  $\pm 5V$ . This allows the amp to theoretically boost any signal up to the supply voltage and thrives in amplifying signals that swing around the center axis. Single supply mode connects the negative supply pin to GND and doubles the positive supply voltage. This limits the amplifier to positive signal amplification but allows the system to run off a simple single supply.

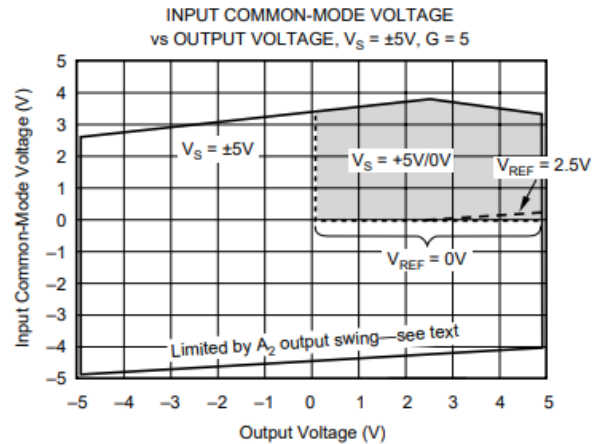
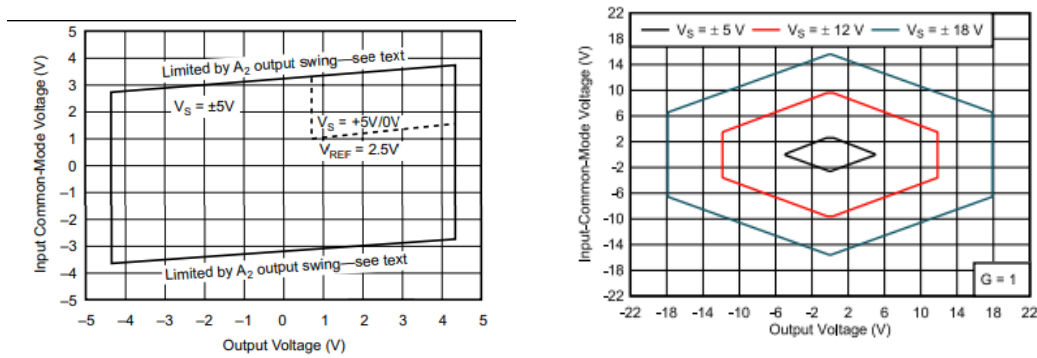


Figure 4.12: Headroom for the INA122 in single and dual supply mode [33]

This ability resides within every op/in-amp but suffers due to Headroom. As can be observed in figure 4.13a the INA126 is not designed for rail to rail supply and therefore suffers a limiting output of 0.6V-4.2V. Comparing the INA126 to the more advanced INA122 pictured in figure 4.12, one can clearly observe the minuscule headroom for both supply variations.

This exceptional rail to rail performance may explain why Pål chose the INA122 for the original mamba. However, the INA122 has the unique distinction of achieving the worst slew rate of any TI instrumentation amplifier currently on the market. Achieving  $0.08V/\mu s$  in a role where reaction time transcends noise reduction, this performance is unsuitable. Finding a replacement for the 20-year-old INA122 is therefore mandatory for achieving sufficient results. Due to time constraints and a lack of documentation denouncing the performance of the INA122, the project did not defer from utilizing it for test purposes. Regarding its replacement, the rapid evolution of in-amps has led to the conclusion that close to all TI in-amps produced after 2010 have sufficient rail to rail and slew rate characteristics. Although up to the next HOAL team, the project strongly recommends that the INA849 is to be used in the next generation mamba. Achieving a slew rate of  $35V/\mu s$  in conjunction with excellent rail to rail characteristics (figure 4.13b), the INA849 triumphs the INA122 on all fronts and will ensure excellent amplifier performance.



(a) Headroom for the INA126 in single and dual supply mode. Courtesy of [34] (b) INA849 Rail to rail performance. Courtesy of [35]

Figure 4.13: Comparison of rail to rail performance between the INA126 and INA849

#### 4.4.2 Digital potentiometers

Successfully capitalizing on the gain regulating possibilities of an 8-pinned in-amp such as the INA122 requires a load to be applied to the *gain setting pin*. Commonly this is done by calculating the desired gain from the formula in the amplifiers datasheet.

$$G = 5 + \frac{200k\Omega}{R_g}$$

The modularity of this system also allows for control via potentiometer. Introducing a variable load allows for complete control of the gain and can be viable in testing environments or systems that require rapid calibration measures. The original Mamba utilized such a system with varied success. Mainly flawed due to analog potentiometers, the original system was prone to repeatability and reliability issues, causing major issues for testing and integrity. These issues arrive from the mechanical design of the potentiometers, as they are prone to interference through shock or vibrations, causing changes to the position of the wiper. This will, in turn, cause load changes, resulting in a gain-induced offset to the measurements. As a direct result of this, the mamba required frequent calibration of every single joint, a tedious and otherwise insufferable process requiring a screwdriver and exceptional patience. Mediating the mechanical-related issues is crucial in achieving a stable and reliable system and can be solved by introducing digital potentiometers. Functionally equal to their mechanical brethren, the introduction of digital control allows for higher reliability and accuracy. Working on a timer synchronization, the user controls the resistance by feeding the d-pot an 8-bit value that controls the position of the wiper. Having 255 total positions and a range of  $0k\Omega$ - $100k\Omega$ , the wiper moves in  $390\Omega$  increments. This causes issues with the accuracy at high gains as the load change required is tiny. The INA122 would, for example, not be able to go beyond 515 times the input ref fig 4.14a whilst the INA849 would have a maximum gain of 15 ref fig 4.14b.

DESIRED GAIN (V/V)	R <sub>G</sub> (Ω)	NEAREST 1% R <sub>G</sub> VALUE	DESIRED GAIN (V/V)	STANDARD 1% R <sub>G</sub> (Ω)
5	NC	NC	1	Not connected
10	40k	40.2k	2	6.04 k
20	13.33k	13.3k	5	1.50 k
50	4444	4420	10	665
100	2105	2100	20	316
200	1026	1020	50	121
500	404	402	100	60.4
1000	201	200	200	30.1
2000	100.3	100	500	12.1
5000	40	40.2	1000	6.04
10000	20	20		

(a) Typical gain and load values for INA 122 [36]

(b) Typical gain and load values for INA 849 [37]

Figure 4.14: Gain and load values comparison

This nonlinearity-related issue resides with the nature of gain adjustable in-amps and will only be solved by utilizing a different dig-pot. Although somewhat limiting the full potential of the in-amp, the project has anticipated that a gain of 500 will be sufficient in amplifying the signals into a readable state. Should the next generation group continue the current usage of dig-pots, it is strongly recommended that a 12- or 16-bit version should replace the current one as it heavily limits the versatility of the system.

#### 4.4.3 Noise reduction

Fully capable of noise reduction, the measures implemented on the power circuit should, in theory, suffice to eliminate most of the transmitted noise in conjunction with any internal sources. Theoretically, this would suffice, but the project decided to implement some extra safety measures through decoupling capacitors. Connected to the power pins of important components and/or complete systems, the decoupling capacitor will mediate power surges in a process called shunting. Both the INA122 and TPL0501 would, under usual circumstances, be suited with capacitors in compliance to their respective datasheets ref [38] and [39]. However, due to spatial issues combined with redundancy fears, the project has decided to only implement decoupling capacitors on the dig-pot. The dig-pot was prioritized as any variation in voltage would heavily affect the in-amps gain. This lack of noise reduction was a poor choice as the system was heavily affected. Further discussed in 9.3.4 the source of this noise is external, but the fact that the circuit lacks recommended noise reduction does not aid the matter.

## 4.5 Headers Selection and substitution

Requiring significant wire to board connection points, the widely used JST connector was chosen due to its status as one of the industry standards. Offering a wide selection of connectors series, the project contemplated utilizing the JST ZH series. Its low profile provides a sleek design with no downsides from its contemporaries, however as the correct dimensioned crimping terminals for the cable were unavailable, the XH series was determined to be a suitable replacement. Measuring 9.8 millimeters tall compared to the 5.6 of the ZH, it is effectively twice the height of its contemporary with equal attributes. This switch to the XH series is, from a research standpoint, no different than if one were to utilize the ZH series. However, due to the mambas complexity, the project cannot afford the additional 4.2 millimeters. Limited space makes stacking PCB chips inside the mambas shell inevitable, and extra height will further complicate the internal design and cause wastage of valuable space. There is also the issue of bending transmission cables, improper positioning inside the shell due to height may force bending that exceeds a cable's maximum bend radius causing interference or damage. Had the project not been under strict time restraints, the missing ZH terminals would have been sourced from a different supplier.

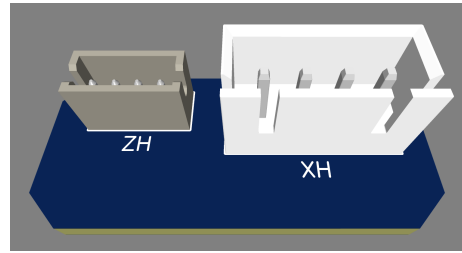


Figure 4.15: Size comparison between the ZH and XH terminals

### 4.5.1 Issues

Apart from the aforementioned spacial issues discussed in 4.5 the replacement headers came with a series of foreseen as well as unforeseen issues. The size difference between the crimping terminals and the sensor wire diameter combined with the failure to locate a correct crimping tool forced the terminals to be manufactured unconventionally. Further discussed in 5.4 the manufacturing process was tedious, long, and produced a subpar result. The process of soldering resulted in the cables being restrained by their exposed strands. Combined with the heat melting the shielding caused brittle terminals with a high risk of the cables tearing off during handling. Additionally, the exposed strands could swing outward and make contact with other strands shorting the cables and ruining measurements. Linking the cables via the strands also comes at the cost of maneuverability. Pictured in 4.16 the purple cable is situated at an unnatural angle. As discussed in 4.5 this may cause a multitude of issues as a result from the strands being twisted. When the terminal is rotated, the strands will retain their original position, generating stress on the strands. In extreme cases, this will cause

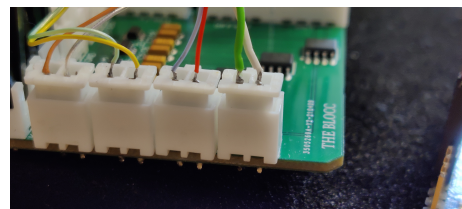


Figure 4.16: The headers connected to the amplifier via the XH series connector. Note the melted insulation on the green and orange cable and the sharp angle caused by twisting on the purple cable

the cables to break or force steep angles generating interference (4.5), neither of which is desired. Although requiring extreme care due to their fragility, the terminals work as intended and, although not ideal, deliver a stable and precise signal.

## 4.6 Amplifier offset voltage

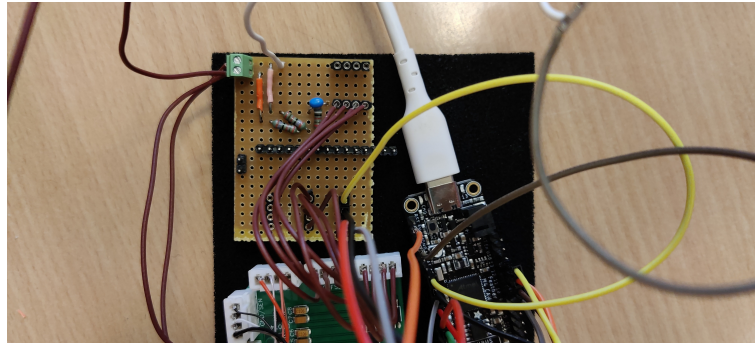


Figure 4.17: The offset circuit fully connected to the final system through a proto-board

With the amplifier running in single supply mode and the sensor bridge centering around  $0V$  the circuit needs to implement a DC offset to be able to measure negative sensor voltage outputs on an ADC. Commonly this will be done by applying the pure DC signal directly to the input. However, as this signal is to be amplified, this measure is unfit for the current system. It is important to note that the INA122 comes prebuilt with a designated *offset* pin. Designated *ref* the pin is commonly grounded but allows for easy offset by applying the desired offset voltage. Originally the offset was to be controlled by the analog pins on the microcontroller, but this quickly fell through due to the raw noise this configuration produced. The project then decided to proceed with a solution enabling fully adjustable offsets, working upon a series of digital potentiometers controlling a voltage divider to provide an accurate and stable offset. Though this was planned, the project had to abandon the idea due to time constraints. Thus a simple voltage divider combined with a lowpass filter to eliminate AC-current was implemented. Pictured in 4.17 the circuit halved the supply voltage of  $3.3V$  down to  $1.65V$  by using two  $27k\Omega$  resistors and then applied a lowpass of  $4Hz$  ( $1\mu f$  and  $39k\Omega$ ) before supplying the signal to the INA122. Crude, as it is unable to supply differing offset to each amplifier, the system will be well-capable as a test bench. Additionally, a microcontroller 4.7 allows for digital adjustment of the data, allowing measurements regardless of tiny offset differences. Although not perfect, picking up some major external noise and causing tiny variations in the individual offsets the system provided enough stability to conduct sufficient testing.



### 4.7 Microcontroller

To make use of the information that the sensor system produces, the signal has to be converted from an analog measurement to a digital value (ADC). For this, the HOAL team has decided to use the Adafruit Feather M4 CAN Express shown in figure 4.18. It is a light and compact microcontroller with many different qualities, including CAN bus communication support and a 12-bit analog-to-digital converter. Including the ADC, the microcontroller is also used to control the digital potentiometers referenced in chapter 4.4.2. This is done by running a program made in Arduino IDE, which is shown in Appendix A.5. Important side note, the internal logic of the microcontroller runs on 3.3 volts which could be problematic when providing the sensors five volts. For more information on the microcontroller, see attached document (Appendix A.4).

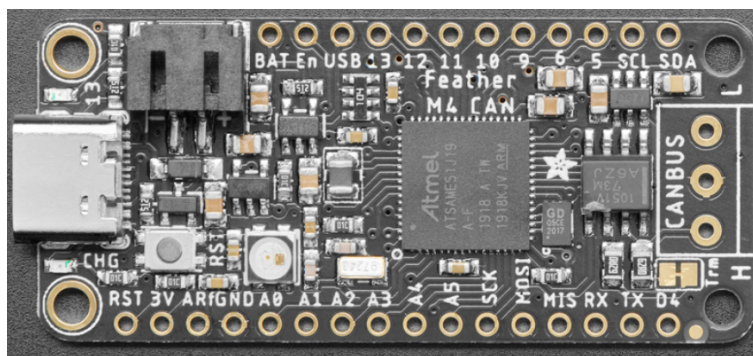


Figure 4.18: Adafruit microcontroller

**On-Board Components**

Component	Pin	Function
QSPI FLASH Memory	PA07	CS
QSPI FLASH Memory	PA08	CS
QSPI FLASH Memory	PA09	CS
QSPI FLASH Memory	PA10	CS
QSPI FLASH Memory	PA11	CS
QSPI FLASH Memory	PA12	CS
QSPI FLASH Memory	PA13	CS
Battery Voltage Divider	PA07	VBAT
Built-In NeoPixel	PA03	LED

**Legend:**

- Power
- GND
- Port Pin
- Interrupt
- Serial<sup>[SERCOM]:[PAD]</sup>
- Timer<sup>[TIMER]:[PAD]</sup>
- Pin Function
- Analog Output
- Control Pin
- IDE
- PWM Pin
- Power Supply

**Notes:**

- ABSOLUTE Max per pin 10mA, 7mA Recommended
- ABSOLUTE Max 130mA for the entire package
- Connected to 5V USB Port
- Connected to Positive Terminal of LiPo Battery
- 3.3V output from regulator

<https://www.adafruit.com/product/3857>

Figure 4.19: Adafruit microcontroller pin layout, Courtesy of [40]

## 5 Implementing the sensor system for testing purposes

After completing the design process, the necessary components were ordered. Reception of the components marked the beginning of the implementation phase. This chapter thoroughly covers the implementation process of the sensor system to prepare it for the experiments and initial tests completed on the circuitry.

### 5.1 Sensor assembly

This section covers how to correctly assemble the Sandwich Solution using *LinkageType7* cut in POM-C (3D-printed ASA-parts were also used).

Parts used for assembly

Part	Dimensions	Quantity	Available
M3x10 Pan head machine screw	3x10mm	4	RS PRO [41]
M3x14 Pan head machine screw	3x14mm	4	Arvid Nilsson [42]
M3x8 Countersunk machine screw	3x8mm	4	RS PRO [43]
10-32 UNF Machine Screws	length: 1/4 inch	4	Spalding Fastners [44]
K3D40 mount	-	1	attachments
TRT-50 mount	-	1	attachments
K3D40 force sensor	-	1	[29]
TRT-50 torque sensor	-	1	[11]

Table 5.1: The complete list of parts needed to assemble one sensor

The project emphasizes using the correct screws with the correct length because of the compact design. Due to time constraints and limited funding, all M3 screws used were manually cut and ground to the correct length from the stock available in the Mamba workshop.

#### 1 - Force sensor linkage mount

The corresponding linkage part was mounted to the live end (live end marked in Figure 4.1) of the K3D40 using 4 M3x10 pan head machine screws, with a length of 10mm [41].



Figure 5.1: The K3D40 linkage-part mounted on the K3D40

## 2 - Torque sensor linkage mount

The corresponding linkage part was mounted to the TRT-50 sensor using four 10-32 UNF machine screws (Figure 5.2a).

## 3 - Lock the sensors together

The sensors were locked together by firstly assembling the two linkage parts, with both sensors mounted to their corresponding linkage part. Secondly, the linkage parts were locked together by inserting and tightening four M3x8 machine screws in the lock holes on the sides of the TRT linkage part.



(a) The TRT-part mounted to the TRT-50 torque sensor



(b) The sensors fully assembled and locked together with *LinkageType7*

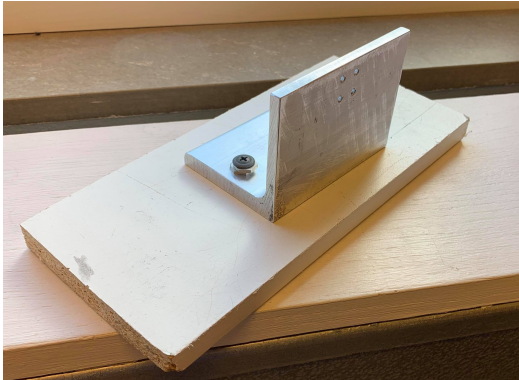
Figure 5.2: Full implementation of the linkage mount

## 5.2 Test-bench assembly

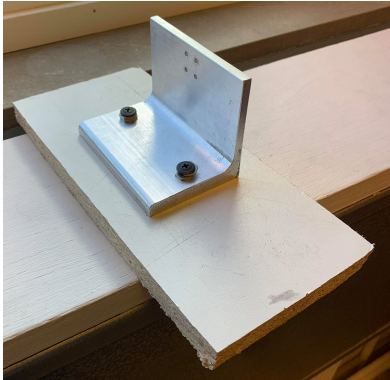
This section covers the building process and assembly of the test bench. As well as the mounting process of the sensor system with different accessories.

The 90° aluminum bracket was cut out in cooperation with the metal workshop at ITK. It is a readily available 65x70mm 90° aluminum bracket, with 4 cut-out M3 holes, spaced 9mm (for the mounting of the K3D40 side of the sensor), and two holes so that the bracket itself can be screwed to a plank or a table. The special aluminum bracket was screwed to a plank (Figure 5.3a and Figure 5.3b). Figure 5.3c shows how the test bench was clamped to a mounting table to enable tests on 1 axis at the time.





(a) Front view



(b) Back view



(c) Clamped to a table

Figure 5.3: The test-bench

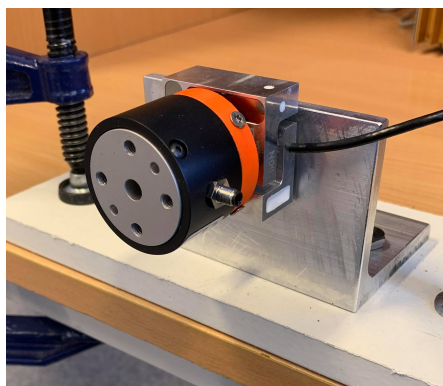
### 5.3 The sensor system and test-accessories

The sensor system was mounted in several different configurations to accurately conduct different experiments to test the sensor system and assess its performance. This section covers the assembly process of the different configurations.

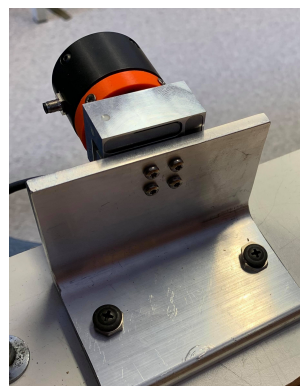
The accessories needed to perform the different experiments were 3D printed using the available PrusaSlicer and Prusament ASA filament.

#### Mounting the sensor system with accessories:

Mounting the sensor system to the test bench was a straightforward process. Mount the K3D40 (force-sensor) side of the Sandwich Solution to the test bench using four M3 machine screws (Figure 5.4).



(a) Viewed from the front

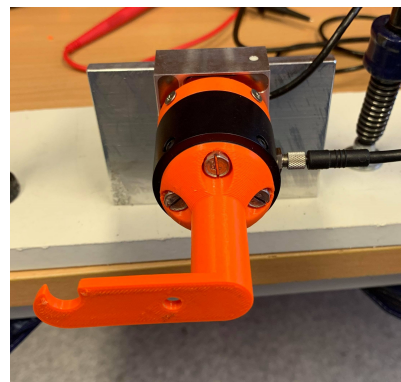


(b) Viewed from the back

Figure 5.4: The mounting of the Sandwich Solution to the test-bench



(a) Mounted with the force-shaft



(b) Mounted with the torque-shaft

Figure 5.5: The sandwich solution mounted with different accessories for testing

**Mounting the force test-shaft without the torque sensor:**

The 10-32 UNF machine screws were severely delayed through Norwegian customs due to new rules following Britain's exit from the European Union. Moreover, they are hard to source within Norway. Therefore, while waiting for the screws that enable the mounting for the TRT torque-sensor, the project decided to assemble the force-shaft directly to the force-sensor to commence the initial testing of the sensor system.



(a) Assembling the force-shaft for mounting, without a torque sensor (b) The force-sensor with the force-shaft, mounted to the test bench

Figure 5.6: The force-sensor mounted to the test-bench for tests without the torque sensor

The assembly process is shown in figure 5.6a. Four M5 screws were inserted and tightened with M5 nuts through the holes initially intended for the mounting of the TRT-sensor. The assembled force test-shaft and TRT mounting bracket were then assembled with the K3D40 and then mounted to the test bench (Figure 5.6b).

## 5.4 Preparing the measurement electronics

Before being able to run any tests, the measurement electronics, just like the test bench, also needs preparation. This chapter therefore covers the necessary steps to make use of the measurement electronics for testing purposes.

### Cable core extraction:

The manufacturer-supplied cable of both the K3D40 force sensor and TRT-50 Torque sensor come pre-stripped from the manufacturer. However, the cables are far too long and need to be cut down before they could be fitted with terminals. This needs to be done with caution as scratches on the strands will cause the metal to become brittle and easily be ripped off. However tempting, the stripping also needs to be done by hand as automatic cable strippers are far too brutal and will directly rip the cables in half. Utilizing a sharp diagonal wire cutter and gently applying force with two fingers whilst rotating the two ends around the diameter of the cable is the optimal solution. One should also refrain from, if possible, cutting down to the strands because the shielding is brittle enough to be cleanly ripped off if damaged. Only cutting the shielding will prevent gouging the strands. Once stripped, the exposed strands should be coated in a thin layer of solder. This will strengthen the cable and, in some instances, ease the soldering process.

### Terminal assembly

Due to the correct crimping terminals being unavailable (4.5), the XH series was deemed a suitable replacement. However, requiring soldering as the sourcing of a suitable crimping tool failed, the process became rather clunky and tedious but sufficient for manufacturing the terminals. Being connected to an aluminum strip, one should refrain from detaching the terminal as the strip provides crucial stability during the manufacturing process. Furthermore, aluminum to aluminum soldering is one of the hardest connections to establish and therefore requires unconventional techniques. Functioning as a heat sink, the temperatures need to be in the 420+ range and combined with quick and accurate solders as the tin quickly cakes due to the flux vaporizing. Firstly, one should attach a generous amount of solder to each terminal. This, combined with the coated ends of the cable, should be sufficient to fully attach the two parts. Importantly the solder pour should be restricted to the "legged" area on the terminal as any solder beyond this area will lock up the header entry and render the terminal useless. The cable should then be pressed into the terminal using the soldering iron and quickly released as the solder melts. If done successfully, this technique should provide a stable and somewhat rugged connection whilst keeping cable and isolation damage to a minimum. The completed terminal should then be attached to the housing. This is done by trimming and bending the "legs" of the terminal to shape and simply sliding

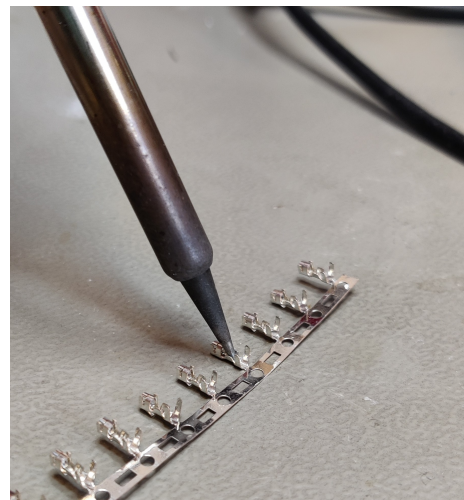


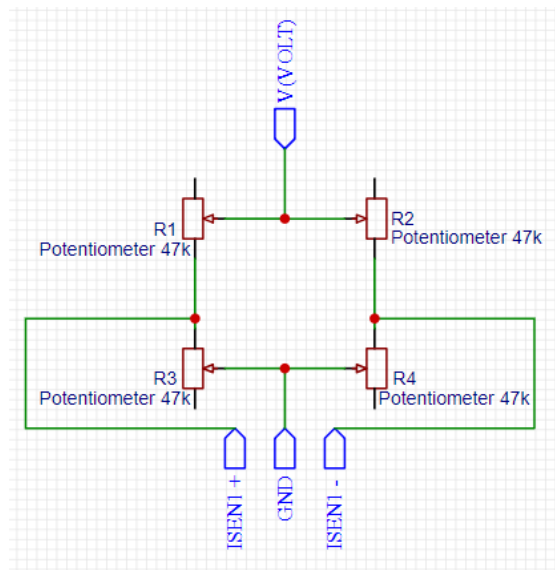
Figure 5.7: Example of proper placement when pouring solder into the terminals. The soldering iron stops tin from leaking into the header connector.



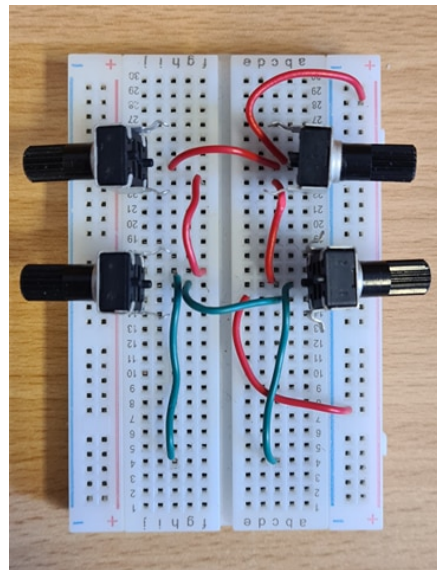
it into the housing until it clicks into place. The terminal is now completed and ready for use. Although a temporary solution, they provide a somewhat stable platform for testing purposes and has served the project well.

### Creating an external Wheatstone bridge

To not risk damaging the sensors during initial testing, the project decided to create an external Wheatstone bridge to simulate the signal created by sensors internal bridges. This external Wheatstone bridge consisted of four analog potentiometers connected to a breadboard. These potentiometers were then connected to form a working full Wheatstone bridge where the output signal of the bridge could be shifted by turning the knobs on the analog potentiometers. The schematic of the external bridge and the working prototype are shown in figure 5.8a and 5.8b respectively.



(a) Schematic



(b) Assembled on a breadboard

Figure 5.8: The external Wheatstone full-bridge used for initial testing of the sensor system

## 5.5 Preparational testing of the power supply circuit

The completed power supply circuit (4.10) requires testing to ensure performance. This subsection describes the tests conducted as well as a step-by-step guide of the methods utilized.

For the power supply circuit to be deemed operational, it has to be able to complete two things. First, it needs to be able to provide a stable output voltage at a set input value over longer periods of time. Secondly, it has to be able to deliver the same output voltage with varying input voltages. This is to make sure the circuit is both stable and is able to reject potential fluctuations that could damage the sensors.

### Method:

To test this, the power supply circuit was exposed to two different tests. The first test consisted of feeding the circuit with a varying amount of input voltage (between 5 and 36 volts) over a short period of time (1 minute). This way, the system gets exposed to fluctuations and will react accordingly if it cannot handle variations. Test two ran a stable input value of 36 volts through the circuit for 10 minutes to see if the output value would deviate from the standard value.

### Results:

The results of the test are shown in the Matlab plots in figure 5.9 and 5.10. As one can deduce from the figures, the power supply circuit seems to be quite stable. NB! These have been produced by manually writing down values over time and then plotted via Matlab. This was due to the lack of an available MyDAQ at the time that would otherwise be used for testing.

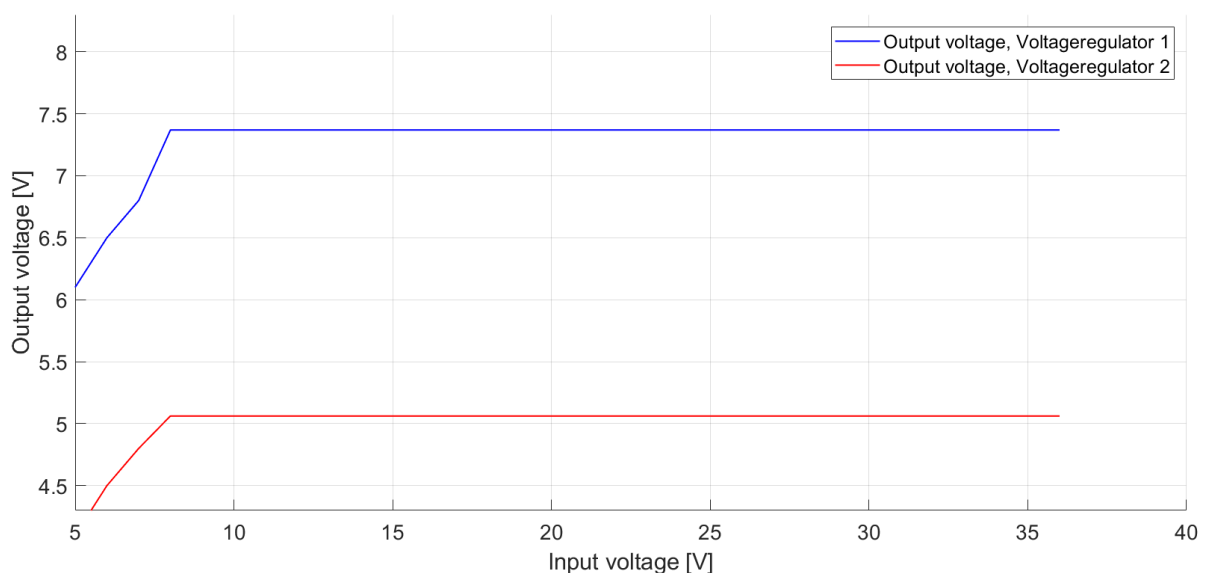


Figure 5.9: Voltageregulator fluctuation test

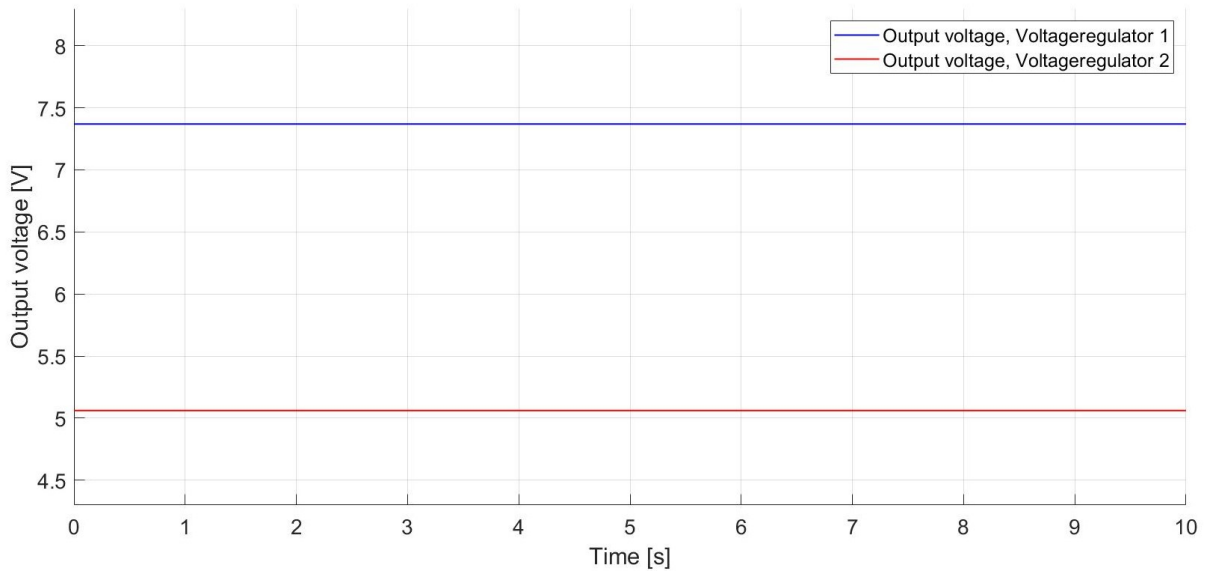


Figure 5.10: Voltageregulator consistency test

## 5.6 Preparational testing of the amplifier circuit

The completed amplifier circuit 4.4 requires testing to ensure its performance. This subsection describes the tests conducted as well as a step-by-step guide of the methods used.

### Method:

To test whether the amplification circuit was operational, two important aspects had to be investigated. Firstly, to test if the instrumentation amplifiers (INA122 UA) could amplify a selected input signal. Secondly, to test whether the gain could be successfully altered utilizing the digital potentiometers. The following is required to conduct the experiments:

- The amplifier circuit shown in figure 4.11.
- The microcontroller shown in figure 4.18.
- A simulation bridge of potentiometers shown in figure 5.8a and 5.8b to simulate the signal from a Wheatstone bridge. (Using an analog signal and ground from the microcontroller does not seem to work due to unknown reasons).
- A multimeter to measure the voltage across the input and output pins of the INA122 UA.
- Arduino IDE program.

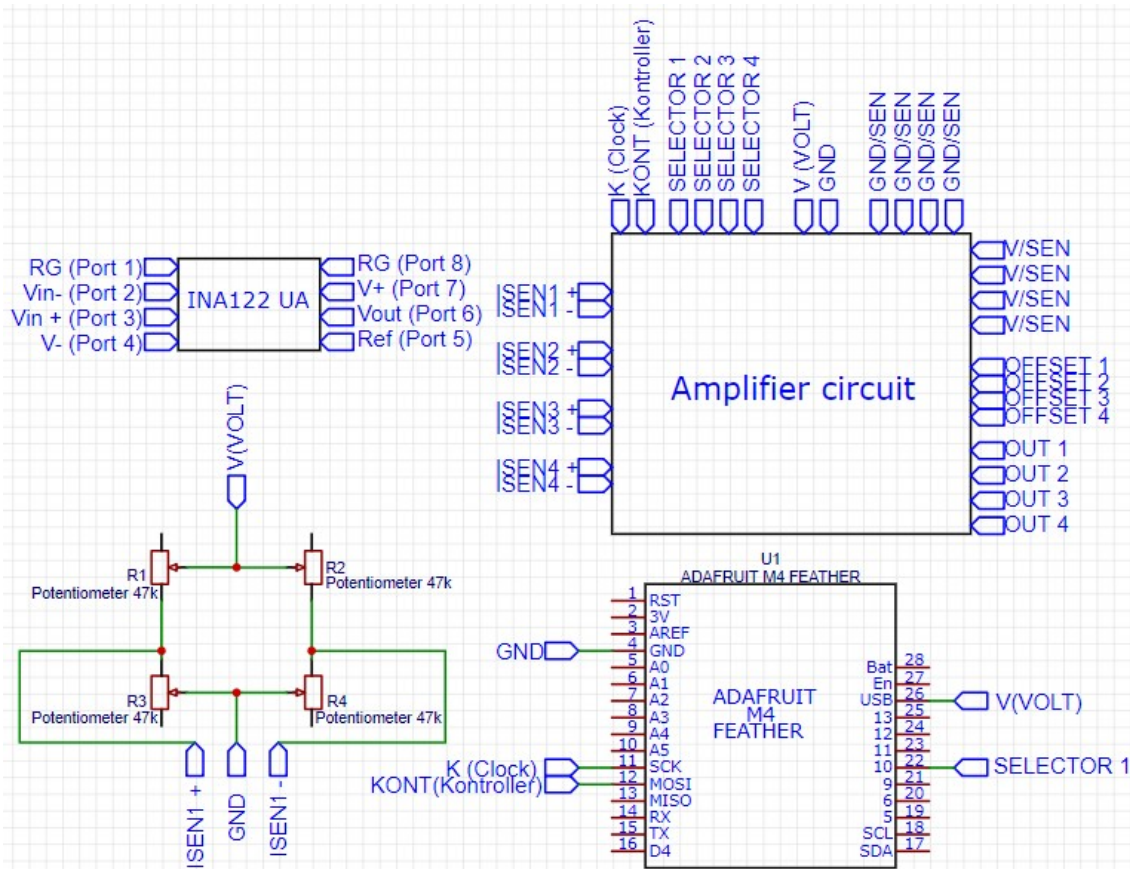


Figure 5.11: Amplifier test schematic

The circuit should be wired, as shown in figure 5.11 to make sure the signal works correctly. (NB! Due to a design error, the label on the header input for V/GND on the amplifier circuit has been flipped. It is, therefore, crucial that the power cable goes into the labeled GND port and ground goes into the labeled V port). For the first test (testing if the INA122 UA produces an amplification), follow these steps:

1. Power up the system by connecting the microcontroller to a computer using a USB-C cable.
2. Set the multimeter in DC mode and read the signal across input terminal 2 and 3 of the INA122 UA shown in the top left of figure 5.11. Record the value for comparison.
3. Use the multimeter again and read the output signal across output terminal 5 and 6, shown in the top left of figure 5.11. Record the value for comparison.
4. If there is a difference between the input and output voltage of the operational amplifier INA122 UA, where the output is around 9 times higher than the input, the INA122 UA works as expected.

For the second test (testing if a program can successfully alter the resistance value of the digital potentiometers and therefore be able to change the gain), follow these steps:



1. Set the multimeter in DC mode and read the signal across input terminal 2 and 3 of the INA122 UA shown in the top left of figure 5.11. Record the value for comparison.
2. Use the multimeter again and read the output signal across output terminal 5 and 6, shown in the top left of figure 5.11. Record the value for comparison.
3. Apply the written code to the system and let it load.
4. Measure the output signal across output terminal 5 and 6 once more and see if the output voltage has changed. If it has changed, the gain has successfully been set.

## Results

After running both tests, the amplifier circuit proves to be able to not only amplify a signal consistently but is also able to change said amplification through the use of digital potentiometers. The amplification circuit will therefore be used in further testing since its functionality has been proven.

## 5.7 Preparational testing of the 3-axis force sensor with the amplifier circuit and a multi-functional DAQ

Since the amplifier circuit was tested and proven to work effectively, it was now possible to test the available 3 axis force sensor. It was chosen to test the 3 axis force sensor with a MyDAQ instead of the microcontroller first. This was due to the MyDAQ being a known quantity and would therefore not introduce any unknown measurement issues.

### Method:

The test consisted of a simple force test where the system was connected to the MyDAQ to record the output data. An unspecified amount of force was then applied to the sensor in different directions and the readings recorded. This was repeated a couple of times until enough data had been gathered.

### Background noise frequency analysis:

Initial testing showed low-power high-frequency noise on all three measured output signals. Frequency analysis was performed on the measured signal (Figure 5.12), but with limited results and appearing as white-noise. It could simply be local electromagnetic background noise inducing current in the wires, a noisy power supply, or related to the DAQ itself. It was difficult to single out any definite source, as no frequency stood out as more prominent than others.

The issue of noise was resolved by digitally implementing a moving average filter that takes the average of a specified amount of previous measurement samples to cut off the unwanted white noise. Its efficiency is shown in Figure 5.12. Using a moving average filter is viewed as taboo in scientific and engineering work because of its simplicity. However, it is highly efficient in terms of results and computing time.

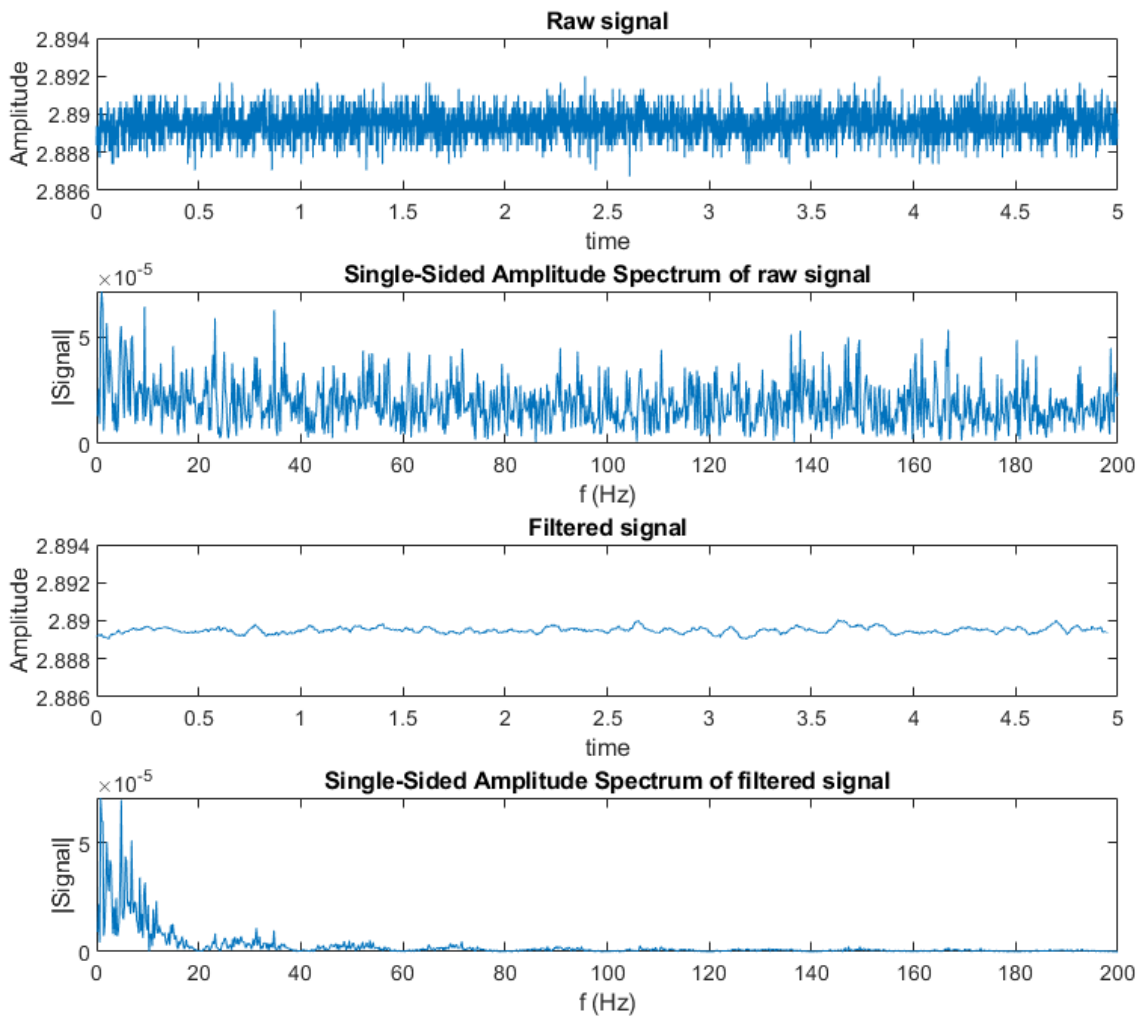


Figure 5.12: Frequency analysis of a stationary signal (Sampling frequency =  $1000\text{Hz}$ ), measured with a DAQ. Comparing a signal digitally filtered with moving average ( $n = 50$ ) to the raw signal (Time in seconds)

## 5.8 Preparational testing of the microcontroller with the amplifier circuit and the 3 axis force sensor

Previous tests showed that the circuitry worked as expected along with the sensors. Therefore, testing was commenced with the Adafruit M4 Feather microcontroller. The tests would check if the microcontroller could provide the same reading capabilities as the MyDAQ, all while still controlling the digital potentiometers.

### Method:

To test the performance with the microcontroller, compared to the MyDAQ, the same test was completed. The system was wired as shown in figure 5.13, but instead of using the external Wheatstone bridge, the actual force sensor was used. This provided the system with three input signals ( $F_x$ ,  $F_y$ ,  $F_z$ ) that needed to be amplified and then read by the microcontroller. The input signals would be altered by applying pressure to the sensor in different directions, and the resulting signal was verified through the Arduino serial monitor. (The test was conducted without the torque sensor attached because the screws that were needed to fasten the sensor had not yet arrived 5.6).

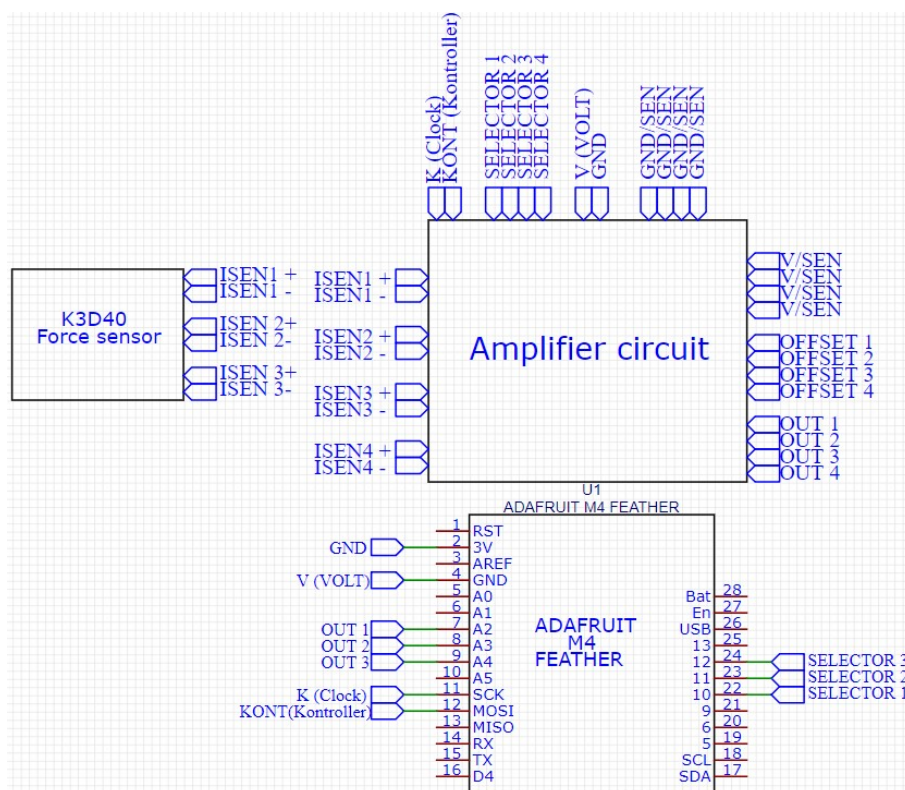


Figure 5.13: Test schematic of circuitry used during microcontroller test. (The offset pins were provided 1.65V through the protoboard shown in 4.6).

### Results:

The microcontroller proved to work as intended for both sending SPI data to the digital potentiometers consistently and recording and printing data from the output ports of the amplifier. The microcontroller could therefore be deemed operational and used for further experiments.

## 6 Testing the sensor system

Essential in the process, the sensor solution needed to be tested in order to assess its performance and control that the complete system met the initial requirements. This section covers the tests performed with the assembled sensor system, electronics, and test bench. The methods for performing the tests are described in detail and assessed for potential shortcomings or issues. Results will be presented but not discussed as that is covered in section 7.

### 6.1 Testing equipment

This section covers the different physical configurations of the sensor system and electronics used to conduct the different tests. Moreover, to produce the different test data to provide enough information to reproduce the given results.

#### **Configuring the F/T sensor system for the experiments:**

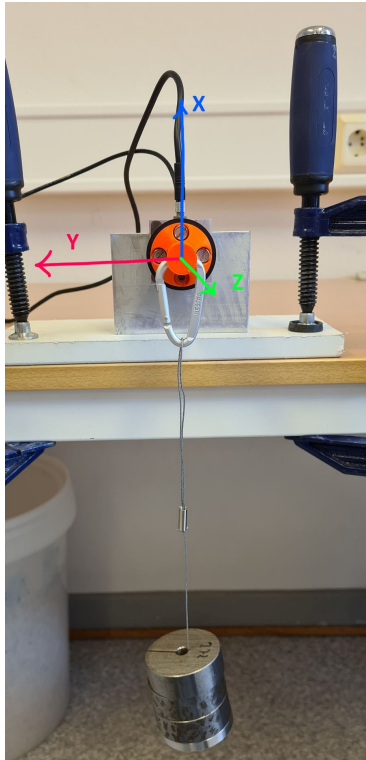
Figure 6.1 shows how the F/T sensor system was mounted to the test bench, with differing test accessories to conduct the different tests. As visible, force and torque were applied using weights mounted to the force- and torque-shaft.

The weight, attached to a metal wire with a Carabiner hook, weighed approximately 875g. In the experiments where force was applied perpendicular to the plane of the other axis, this would translate to a force of approximately  $8.58N$  (6.1).

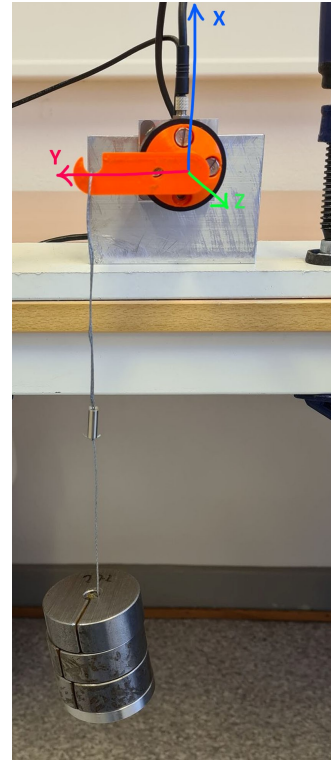
$$F = mg = 0.875kg \times 9.81 \frac{m}{s^2} \approx 8.58N \quad (6.1)$$

The weight mounting point on the torque shaft was offset 40mm from the z-axis. The same weight used in the force test was used. This would result in roughly  $343Nmm$  (6.2) of torque being applied in the experiments testing torque.

$$\tau = F \times d = 8.58N \times 40mm \approx 343Nmm \quad (6.2)$$



(a) The sensor system mounted on the test bench, configured to measure force on the negative x-axis. Force being applied with weights attached to the force-shaft.



(b) The force-shaft was replaced with the torque-shaft for torque testing. Torque was applied by attaching weights to the torque shaft.

Figure 6.1: Different configurations for the different experiments using the test bench clamped to a table while applying a static force/torque using weights.

### Electronics used in the experiments:

Figure 6.2 shows the testing circuit used for reading and amplifying the sensor signal. The system consists of the amplifier circuit, a protoboard designed to hold connections, and the Adafruit microcontroller. The entire system was powered by the Adafruit microcontroller due to it being an easy and available power source, as well as providing low amounts of voltage noise. Figure 6.3 shows an EasyEDA drawing of the connection to aid in understanding the circuitry and how to connect it for use. **It is vital to note that the V(Volt) and GND labels have been flipped on the actual amplifier circuit. This means the V(Volt) output on the protoboard must be connected to the ground on the amplifier and vice versa.**



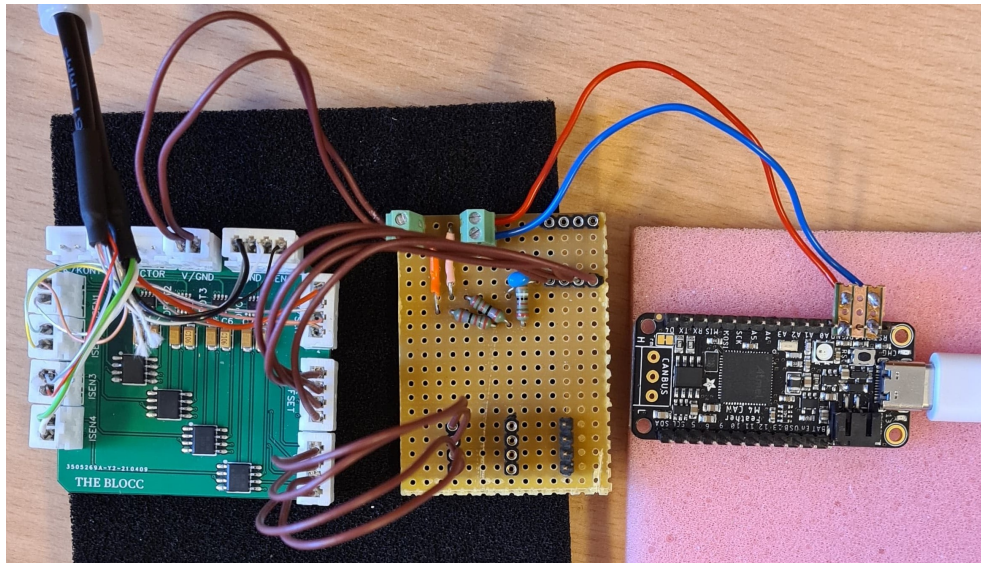


Figure 6.2: Circuitry used during experiments with the sensor. The connections from the Adafruit microcontroller (to the right), are not seen in this picture. The remaining connections can be referenced in Figure 6.3.

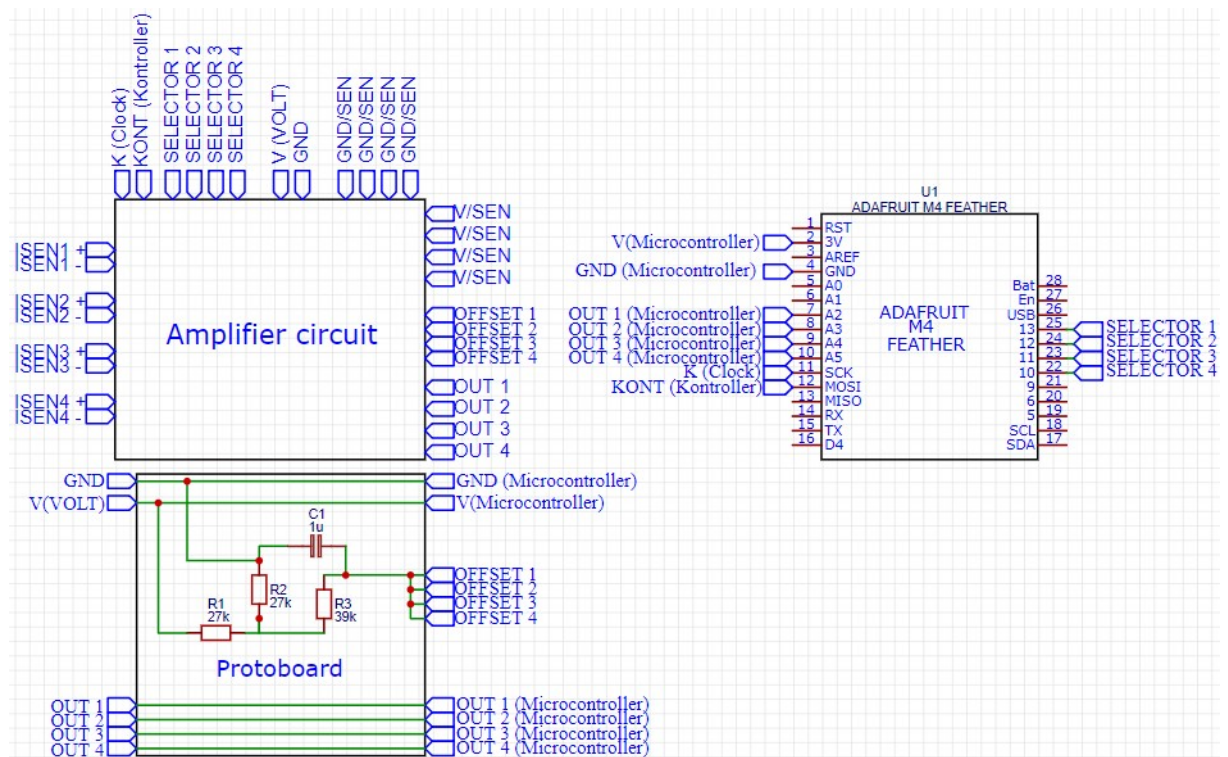


Figure 6.3: Schematic of circuitry used during experiments with the sensor. The  $ISEN_{\pm}$  inputs on the amplifier circuit are the outputs from the force and torque sensors.

**Implementing a moving average filter:**

Due to noise issues by virtue of the protoboard, the project decided to implement a simple averaging filter to be used during testing. The filter consists of an array that records ten values and then averages them to produce a more stable output signal. To ensure stability, the filter also included a 1-millisecond delay. Unfortunately, this means that the system's reaction time was slightly impaired, which may be noticeable in the results.

**Calibrating the F/T sensor system for the experiments:**

The final step before testing could commence was the calibration of the sensors and remapping the signal to display measurements in Newtons (for the force measurements) and Newton millimeters (for the torque measurement). This step was important to make sure the sensors both measured in a linear fashion and produced a signal that corresponded with the applied weights.

To do this, the signal was first remapped from 0 – 4095 to a measurement area of  $\pm 50N$  using the formula shown in 6.3. The formula works by dividing the signal in the measurement area of 0 – 4095, by 4095 and multiplying it with 100. This changes the measurement area from 0 – 4095 to 0 – 100. The formula then subtracts 50 to offset the measurement area to  $\pm 50N$ .

$$Force[N] = \frac{ADC\ value}{ADC\ range} \times F_{range} - F_{offset} = \frac{ADC\ value}{4095} \times 100 - 50 \quad (6.3)$$

Equation 3: Equation used to re-map the input signal from bits to newton.

Since the signal had been remapped, it was then possible to calibrate the system using known weights. The weights were connected to the sensor as shown in figure 6.1a and figure 6.1b. The output was measured by the microcontroller and printed to the serial monitor, along with timestamps using the *millis* function.

To calibrate, the digital potentiometers were used to alter the gain of the amplifier circuit. This was done continuously until the system read as close as possible to the correct value when the weights were applied. Due to the digital potentiometers having a low resolution, as discussed in chapter 4.4.2, it was impossible to fine-tune the gain for exact measurements. Therefore a digital gain was used to correct the signal amplification to an exact amount. Said digital gain can be seen in the equation 6.3 as the 100 that is multiplied with the signal. By tweaking this by  $\pm 1$  it was possible to adjust the gain perfectly. When the weights finally applied the correct amount, the offset was adjusted by changing the  $-50$  at the end of the equation.

By fine-tuning the gain and offset this way, a minor area of the measurements will be lost. However, for testing purposes, the measurement area was more than wide enough. A solution to the digital potentiometer problem, which will unlock the entire signal, can be read about in section 9.3.2.

## 6.2 Experiment 1: Periodically applied force and torque

As the first test, the project decided to test how the system would respond to a periodically changing force/torque applied to the sensors. This would reveal hysteresis and inaccuracies related to a changing force. Moreover, it would reveal any significant delays in response time.

### Method:

The 875g weight was used to provide a periodic force and periodic torque. The weight was periodically lifted, held for 5 seconds, and then released for 5 seconds. It was the same method used by *Veslum* in his assessment of the Mamba sensor system. However, the project used a smaller time interval and applied more weight due to the higher tolerance of the new sensor system. The sensor system was configured as seen in Figure 6.1a. It was dismantled, rotated 90°, and reconfigured to perform the different experiments on each axis in different directions.

### Comments regarding the results:

There is visible inaccuracy in the test results around the 0N/0Nmm mark. This is due to the sensor's high sensitivity and difficulty positioning the weights in the same position when lifted. This would lead to an unpredictable force being applied to the sensor system when holding the weights. The data of interest is the amplitude response, measurement error within the time for force (or torque) being applied, and the general response time.

### 6.2.1 Results: Periodic force experiments on the x-axis

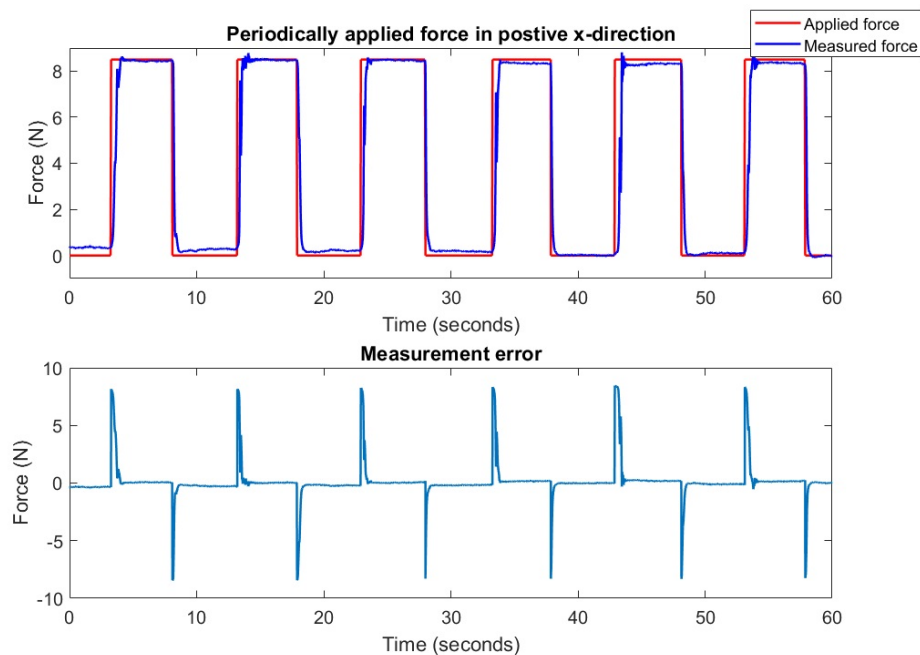


Figure 6.4: Result from the experiment of applying a periodic force in the positive x-direction on the force sensor.



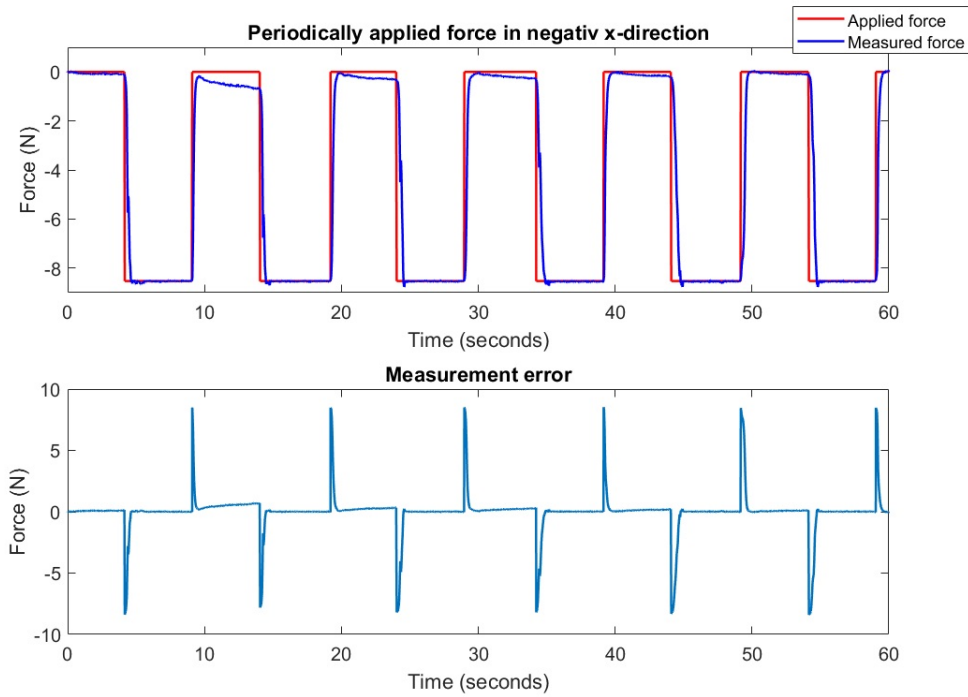


Figure 6.5: Result from the experiment of applying a periodic force in the negative x-direction on the force sensor.

### 6.2.2 Results: Periodic force experiments on the y-axis

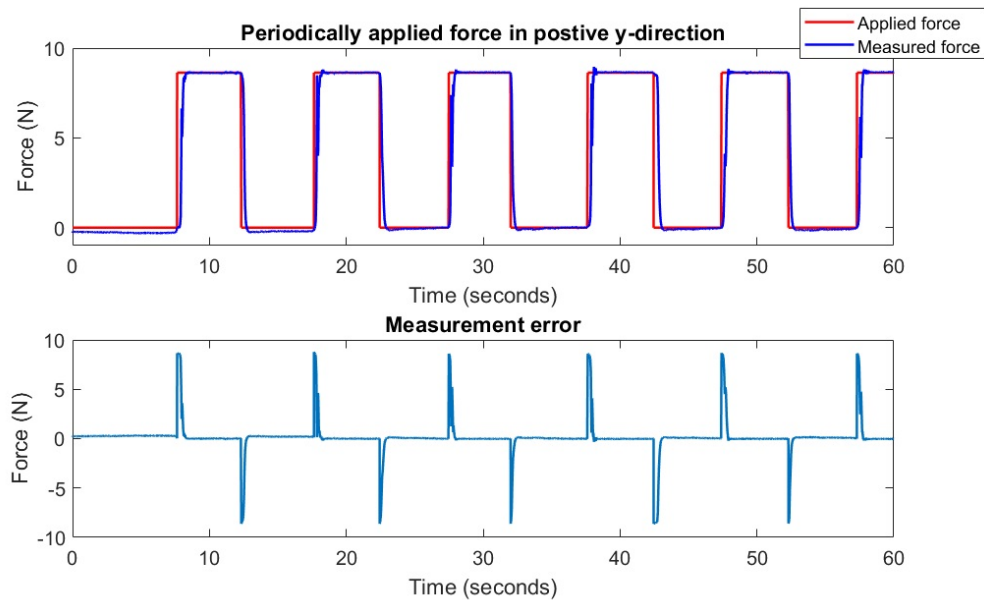


Figure 6.6: Result from the experiment of applying a periodic force in the positive y-direction on the force sensor.

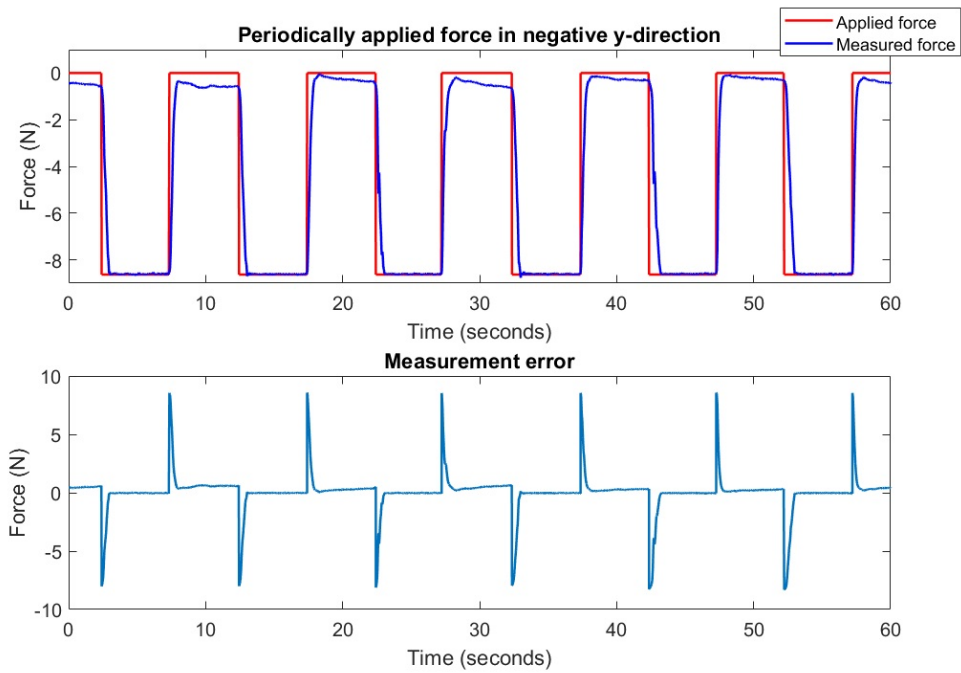


Figure 6.7: Result from the experiment of applying a periodic force in the negative y-direction on the force sensor

### 6.2.3 Result: Periodic torque experiment

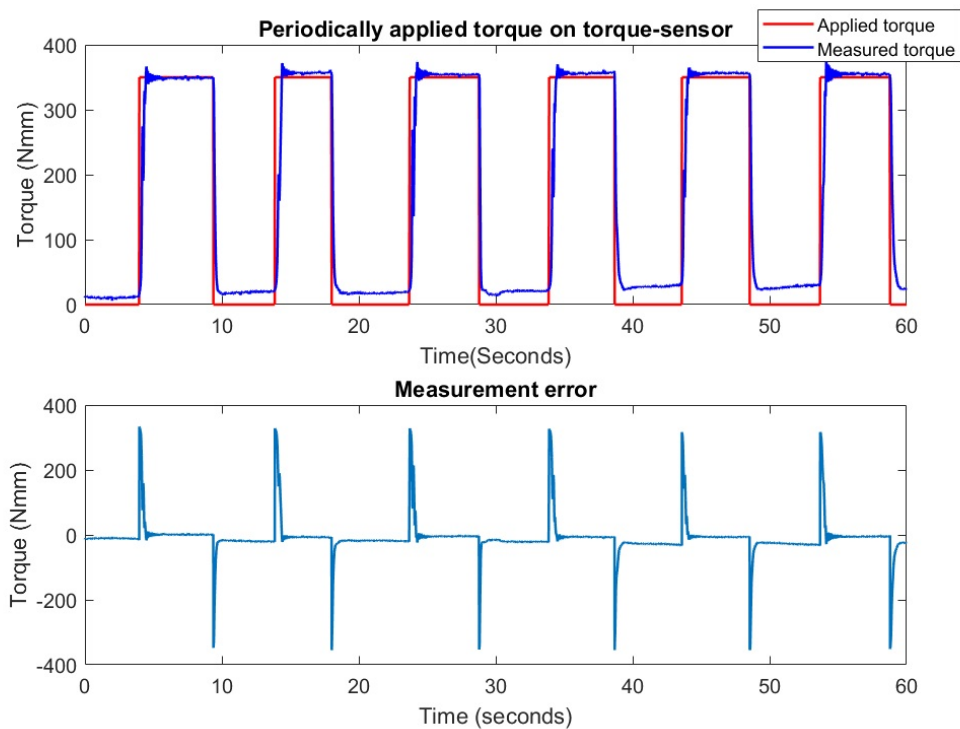


Figure 6.8: Result from the experiment of applying a periodic torque on the torque-sensor

## 6.3 Experiment 2: Crosstalk analysis

Due to the sensors being compiled into what has been dubbed the Sandwich Solution. (see chapter 3.11), the possibility of crosstalk needs to be addressed. While some crosstalk must be expected when combining axial forces as done in the Sandwich Solution, a large amount or a nonlinear amount could be detrimental for its use as a measurement system.

### Method

To test whether or not crosstalk was present in the sensor solution, a statically applied force or torque would be sufficient. Therefore, the tests have been conducted using weights to apply said force/torque to the three different axis ( $M_x$ ,  $F_x$ , and  $F_y$ ). The weights would be connected as shown in figures 6.1a and 6.1b. First, the weights were lifted. Then, the weights were dropped, and the measurement signal on all axis was recorded.

### 6.3.1 Results: Applying torque

The results of the tests are shown in figure 6.9. Figure 6.9 shows the results without the reference force plotted to give a better resolution of the effects on each axis. The applied weight was 875g at a distance of 40 mm, which is approximately equivalent to 343Nmm of torque.

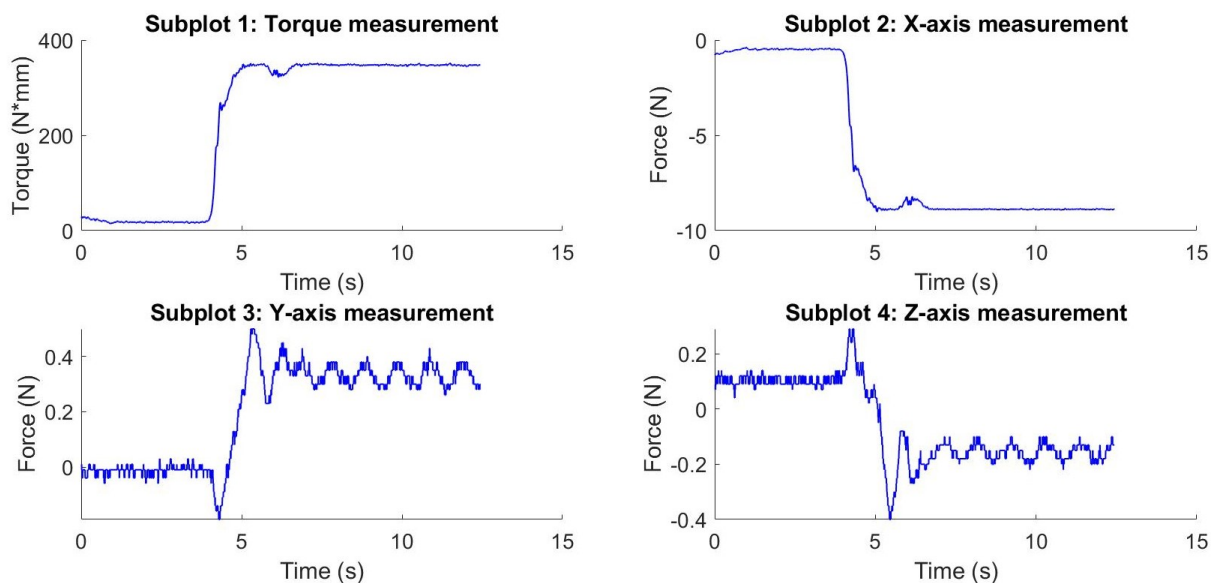


Figure 6.9: Result of applying 343Nmm of torque around the z-axis (with the torque-shaft unsupported, therefore showing  $F_x \approx -8.6N$ ).

### 6.3.2 Results: Applying force (X-axis)

The results of the tests are shown in figure 6.10. Figure 6.10 shows the results without the reference force plotted to give a better resolution of the effects on each axis—the applied weight of  $875g$  which is approximately equivalent to  $8.6N$ .

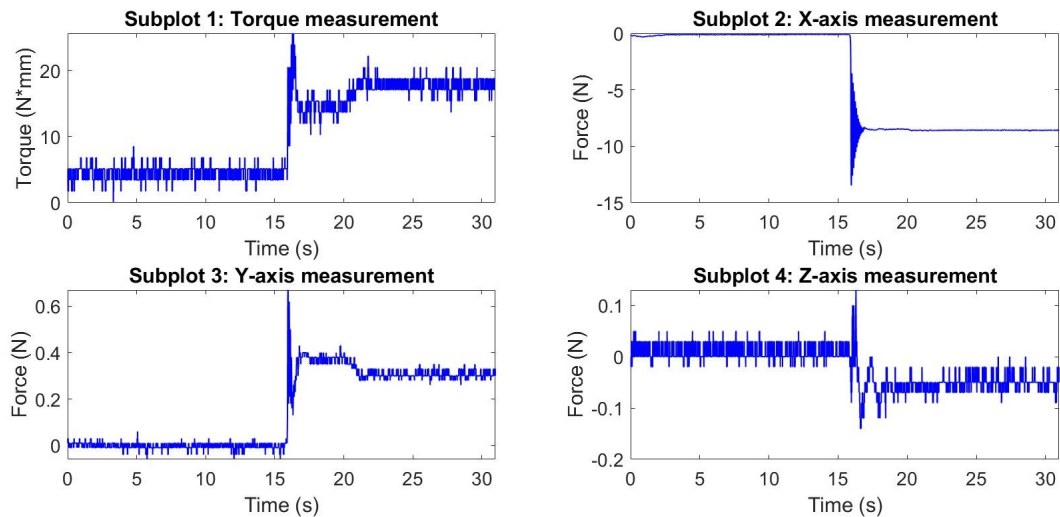


Figure 6.10: Result of applying  $-8.6N$  of force on the x-axis

### 6.3.3 Results: Applying force (Y-axis)

The results of the tests are shown in figure 6.11. Figure 6.11 shows the results without the reference force plotted to give a better resolution of the effects on each axis. The applied weight was 875 grams which is approximately equivalent to  $8.6N$  of force.

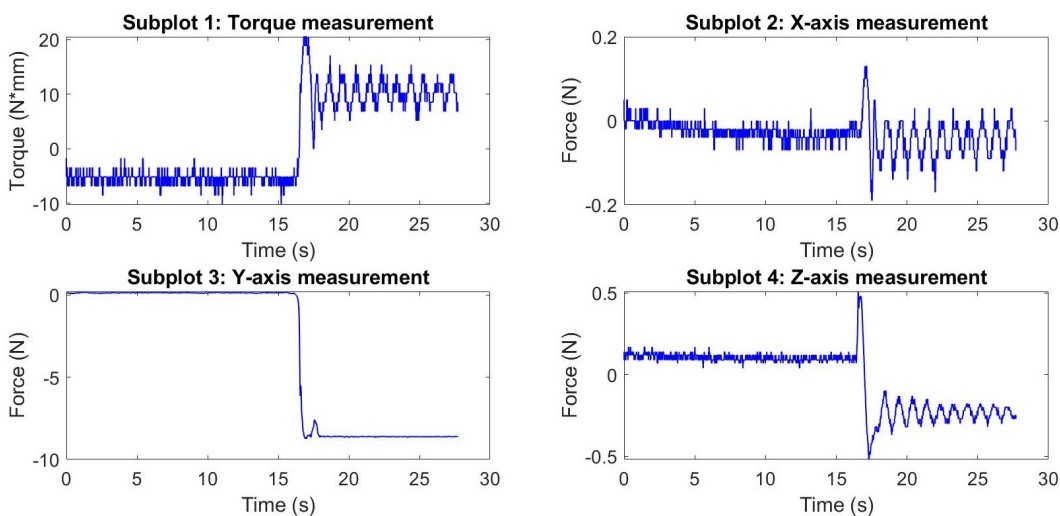


Figure 6.11: Result of applying  $-8.6N$  of force on the y-axis

## 6.4 Experiment 3: Shaking the sensor system

With static tests completed, the project wanted to test how the system would respond to a dynamic load. This experiment intended to test how the system would respond to rapid shaking for a long period of time, to perhaps uncover hysteresis. The end goal was to make it comparable to *Liljebäck's* "voltage drift" experiment on the Mamba snake robot [10] (Figure 2.13a). The rapid shaking is intended to simulate the robot executing rapid, extensive work, putting a load on all sensors in different directions.

It was performed with the sensor system mounted to the test bench that was clamped to a table. The measurement electronics were powered with the microcontroller, and all signals were measured with the microcontroller. The forces were applied by pushing and pulling the force-shaft, mounted to the sensor, in different directions. Before the test, each measurement signal was offset to output roughly zero.

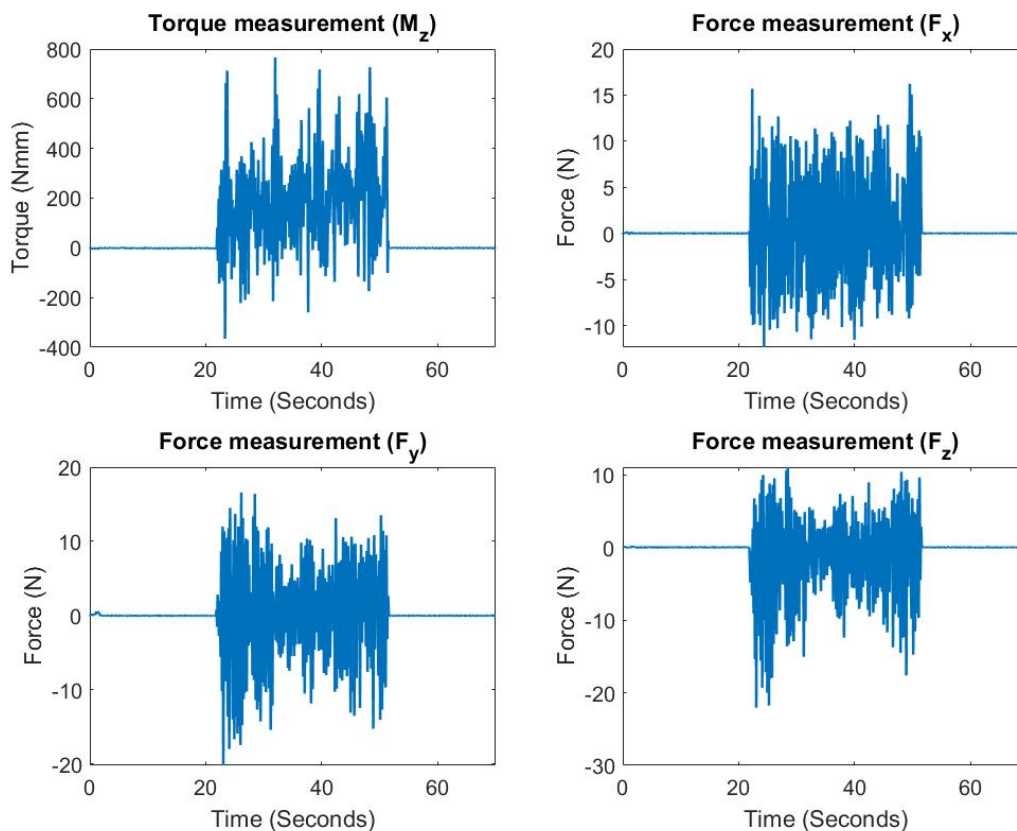


Figure 6.12: Results of shaking the sensor system for a long period of time.

## 6.5 Experiment 4: Heating the sensor system

As covered in section 2.5 regarding the *Mamba* snake robot, the previous joints were prone to reach high temperatures due to a lack of heat exchange with the environment. Therefore, it was of great interest to examine how the selected sensor system would respond to increasing temperatures.

### Method:

The sensor system was mounted to the test bench with the force-shaft attached, however with no weights mounted. All measurement axis was digitally offset to approximately zero before the test began. The sensor system had been left at room temperature through the night, ensuring a start temperature around room temperature (20°C to 25°C). Warm air was applied to the system by using a 2200W hairdryer on a medium temperature setting. The hairdryer was configured with a flat nozzle used to distribute hot air evenly across the sensor system. The heat source was held approximately 20cm away from the sensor system, and its angle changed throughout the test to ensure even heat distributions on all sides of the sensor system.

### Results of the heat experiment

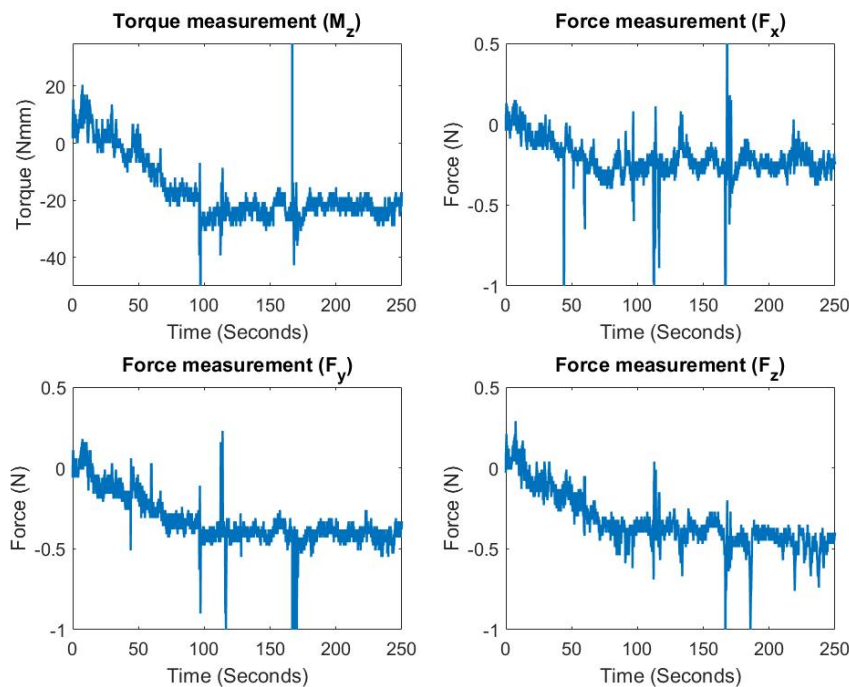


Figure 6.13: Result of the temperature experiment conducted on the sensor system. It shows the measurement value as the sensor system was heated for a period of time

### Comments regarding the results:

The visible spikes in the results are due to one of the project's participants slightly touching the sensor system. The results of interests are the relative drift over time.

## 7 Discussion

This section discusses the results of the experiments conducted on the sensor system in section 6). It also compares the sensor systems performance to the experiments performed on the previous intrinsic force-torque sensor system in the Mamba snake robot ([2] [10]).

### 7.1 Experiment 1: Periodically applied force and torque

This section discusses the results from the periodic force and torque experiments (chapter 6.2). And compares the results to *Veslum's* experiments and assessment of the Mamba sensor system [2].

Firstly, in terms of *accuracy*, the force experiments show that the sensor system performed exceptionally well. The measurement error was near/at zero when a constant force was applied. Moreover, it was stable at the given value. However, in some instances, there is a visible overshoot. This is likely due to the weight being dropped, causing minor spikes and weak oscillations in the force measurements. However, the torque sensor performed differently, as there were some noticeable measurement inaccuracies and unpredictability. Furthermore, the stationary value differs from the different attempts. This is likely somewhat linked to the high sensitivity of the torque sensor and that the experiments were performed at only 6% of the full measurement capacity of the TRT-sensor. Also, the visible inaccuracy and drift are in meier LSB values of torque measurement (7.1). Moreover, during some of the tests, the project experienced issues with obtaining a stable offset voltage, which is notable in the results.

$$LSB_{Mz} = \frac{\tau_{range}}{bit\ range} = \frac{2 \times 5.65 \times 1000[Nmm]}{4095} \approx 2.76 \left[ \frac{Nmm}{Bit} \right] \quad (7.1)$$

$$LSB_F = \frac{F_{range}}{bit\ range} = \frac{2 \times 50 \times 1000[mN]}{4095} \approx 24.4 \left[ \frac{mN}{Bit} \right] \quad (7.2)$$

Secondly, in terms of *time-delay*, (being the time delta between when force was applied until stationary measurement value), it performs relatively well. An estimated total time delay can be assumed by measuring the time-width of the spikes in the "measurement error" plots. For the force measurement experiments, the total time delay ( $\Delta t_{tot}$ ) was estimated to be roughly 0.5 seconds on average. Contributing to the time delay, there are several factors, such as the drop of the weight's time length ( $\Delta t_{drop}$ ), delay caused by the time it takes for metal to bend ( $\Delta t_{metal}$ ), calculation delay caused by the micro-controller ( $\Delta t_{calc}$ ). The drop time varied, as the weight was not dropped from the same height continuously. Moreover, the drop was slightly assisted and held to avoid a pendulum effect. Drop time can be estimated using the formula for a free-falling object, assuming it was dropped from roughly 10cm, it totals at almost 0.14 seconds. Lastly, some inaccuracies were caused by how the experiments were conducted and the way "applied force" or

"applied torque" was graphically assumed. The total time delay in the torque experiment was slightly worse (roughly 0.7 seconds on average), leading the project to believe there is a certain time delay in the straining of metal and plastic components.

$$\begin{aligned}\Delta t_{tot} &= t_{stationary} - t_0 \\ &= \Delta t_{drop} + \Delta t_{metal} + \Delta t_{calc} \pm t_{inaccuracy} \approx 0.5s\end{aligned}\quad (7.3)$$

Thirdly, the experiments showed that the sensor systems performed exceptionally well in terms of *hysteresis*. With a periodically applied force/torque, the sensor system rapidly met the applied force and torque value with great accuracy. The subject was further investigated by calculating the arithmetic mean(average) (7.4) for each iteration within the time period of weight being applied, and the measurement signal had stabilized. The results are shown in Table 7.1. As seen, there are notable inaccuracies in the calibration. To analyze the measurement drift between each iteration, it was chosen to use the average value from the first iteration as reference. The formula is shown in (7.5).

$$\overline{F_{x1}} = \frac{1}{n} \sum_{i=start}^{end} z_i \quad (7.4)$$

Average value when strained

Tests	Iterations					
	1st	2nd	3rd	4th	5th	6th
$\overline{M_z}[Nmm]$	348.7	356.6	354.3	356.4	356.4	355.2
$\overline{F_x}[N]$ (pos. test)	8.440	8.478	8.474	8.348	8.294	8.358
$\overline{F_x}[N]$ (neg. test)	-8.535	-8.539	-8.538	-8.547	-8.546	-8.544
$\overline{F_y}[N]$ (pos. test)	8.623	8.633	8.645	8.653	8.646	8.656
$\overline{F_y}[N]$ (neg. test)	-8.605	-8.609	-8.607	-8.604	-8.600	-8.605

Table 7.1: Average measured value within the time-span of the sensor being strained. Calculated for 6 iteration for the 5 different tests, with the intention of accurately identifying any measurement drift.

$$drift_a(n)[\%] = \frac{\overline{F_a(n)} - \overline{F_a(1)}}{\overline{F_a(1)}} \times 100\% \quad (7.5)$$

The average measurement drift in percent, compared to the first iteration is shown in Figure 7.1 and 7.2. An interesting observation is that the force test on the x-axis in the positive direction had a more significant measurement drift compared to the three other tests. Furthermore, tests performed on the same axis in the negative direction showed a much less significant measurement drift. This leads the project to believe that the drift observed in the  $F_x$  *positive* test is related to noise in the measurement electronics



being more prominent during the experiment. Moreover, it is likely also related to the inaccuracies in the test method and with the previously discussed inaccuracy factors perhaps being more prominent. In other words, it is likely not linked to the sensor itself. Regardless, the measurement drift analysis shows that the sensor system is highly accurate and can reproduce a given measurement value, with a measurement drift in the per thousand range ( $\%$ ).

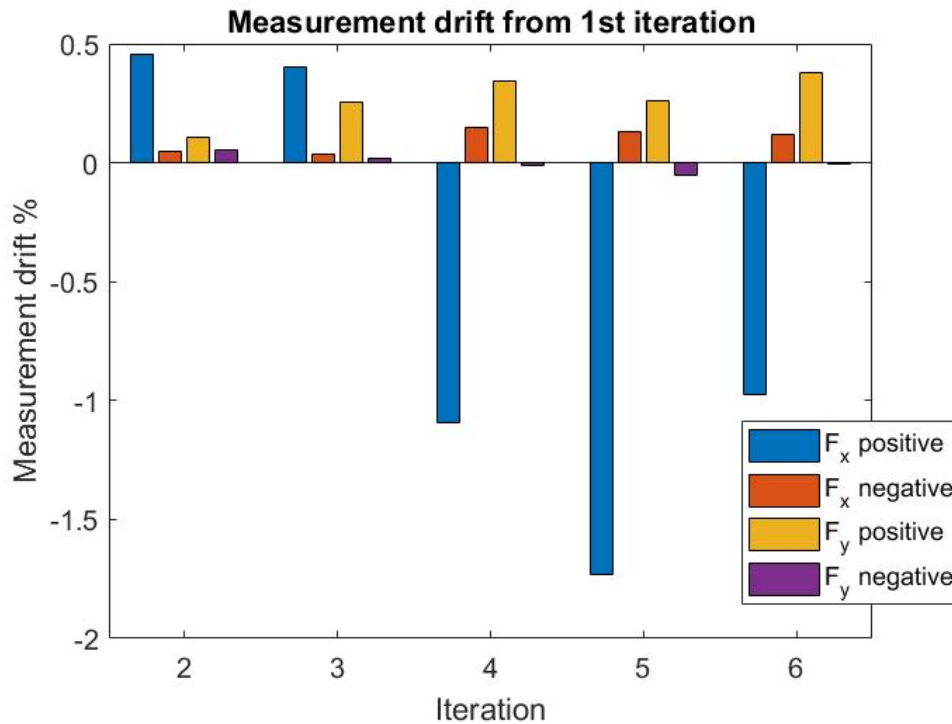


Figure 7.1: Average measurement drift in each iteration (referenced to the first iteration), compared between the 4 different periodic force tests. Formula seen in (7.5)

The results of the torque measurement drift analysis are more inconclusive (Figure 7.2) due to the limited tested range. Compared to the drift in the force-tests, the torque measurement drift seems more prominent. It's important to note that the most prominent measurement error (compared to the rest) in the torque test was in the first iteration. Moreover, the short strain-span of the test performed. Shown in (7.6), the highest drift observed (2.25%) equals a change of roughly 3 LSB on the ADC. Therefore, increasing the chance that the observed drift is mere noise.

$$\begin{aligned}
 drift_{max}[Bits] &= \frac{\tau_{applied}}{\tau_{range}} \times Bit\ range \times drift_{max}[\%] \\
 &= \frac{0.343}{2 \times 5.56} \times 4095 \times 0.025 \approx 3LSB
 \end{aligned} \tag{7.6}$$

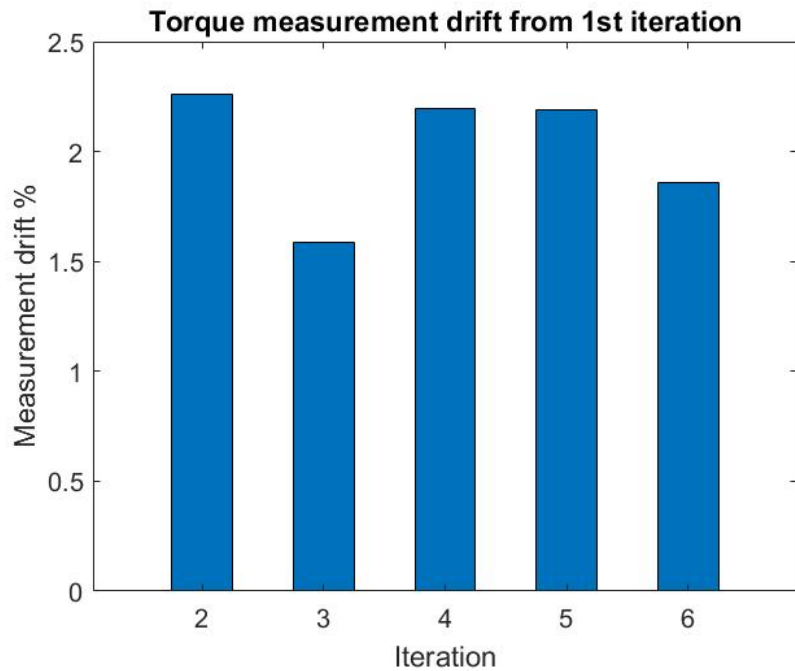


Figure 7.2: Average torque measurement drift in each iteration referenced to the first iteration

Lastly, comparing these test results to *Veslum's* experiments on the Mamba sensor systems shows major improvements in terms of the 3 factors discussed in this section. However, they can't be directly compared due to a few differences regarding the test circumstances. In *Veslum's* experiment, a major inaccuracy factor besides the sensor system itself was deemed linked to vibrations from the servomotor. The project experiments were conducted without a servo-motor present and were mounted to a stable test bench. However, taking that into account, the project's new sensor system performs remarkably better in terms of accuracy and hysteresis. The Mamba sensor system struggled to follow said applied force/torque and had periodic inconsistencies over a period of time and subsequent iterations. However, the Sandwich Solution consistently follows the applied force with great accuracy and reproduces the applied-force signal.

## 7.2 Experiment 2: Crosstalk analysis

This section discusses the results of the crosstalk experiment shown in section 6.3.

As seen in the results of the experiments, the crosstalk between the axis when different forces were applied was minimal. In the torque experiment, both the y and z-axis were almost completely unaffected, and the small changes could be attributed to the design of the testing equipment. The x-axis measurement does show that a force has been applied to it. However, this was caused by the design of the test rig (see figure 6.1b). The x-axis of the system points downward, which means when the torque was applied as shown in the figure, it will also be applied to the x-axis. This was, therefore, an expected measurement.

In the force experiments, the same results of minimal crosstalk can be shown. For example, in the experiment where a force was applied on the x, minimal change appeared in both the torque, y-axis, and z-axis measurements. The same goes for the y-axis measurements.

Based on the results from the crosstalk experiment, a simple tabular has been created, which shows the amount of expected crosstalk between the axis. To calculate crosstalk between the axis, equation (7.7) was used.

$$crosstalk[\%] = \frac{\text{Measured value on non targeted axis}}{\text{Measured value on targeted axis}} \times 100\% \quad (7.7)$$

Affected axis	Estimated Percentage
Crosstalk from x to y	3.5%
Crosstalk from x to z	0.6%
Crosstalk from x to torque	0.6%
Crosstalk from y to x	0.6%
Crosstalk from y to z	3.5%
Crosstalk from y to torque	0.1%

Table 7.2: Measured and calculated crosstalk between axis in percent. (The z-axis is not included due to it not being part of the testing)

It is important to point out that the system was laid on the side when tested for crosstalk, as shown in figure 6.1a. If the system is implemented in a snake robot, the system will most likely stand upright. This means that different axis would receive different amounts of crosstalk than what was perceived during testing on the side.

### 7.3 Experiment 3: Shaking the sensor system

This section discusses the results from the experiment where the system was rapidly shaken for a period of time (Section 6.4). It compares it to *Liljebäcks* voltage drift analysis of the Mamba sensor system [10] (result in figure 2.13a).

Liljebäck's experiments showed a clear drift in the strain-gauge output voltage as a result of shaking the sensor system for a period of time. As seen in figure 6.12, the new sensor system behaves drastically differently. There was little apparent voltage drift (voltage value was calibrated to display force/torque in N/Nmm for all measurement axis) as a result of shaking the sensor system.

Average measurement value	$F_x(N)$	$F_y(N)$	$F_z(N)$	$M_z(Nmm)$
Before shaking ( $t < 21.7s$ )	0.024	0.019	0.025	-1.51
After shaking ( $t > 51.8s$ )	0.019	0.00	0.016	-0.67

Table 7.3: Average measurement values before shaking, and after shaking the sensor system

By analyzing the average force/torque measurement value from before shaking the sensor system until after shaking the sensor system (Table 7.3), shows a very slight change in the average measurement value. This is considered small enough to be a drift in a couple of LSB measures of the ADC. Moreover, after shaking the sensor system, the relative measurement trend is inherently flat around the zero-point, with only minor, highly Gaussian noise oscillations.

In conclusion, the new sensor system, regarding its stiffness and material properties, can zero itself around the zero points after an extensive and rapidly changing load. Moreover, it can do so swiftly and with great accuracy.

### 7.4 Experiment 4: Heating the sensor system

This section discusses the results from the experiment where the system was gradually heated for a period of time (Section 6.5). It compares it to *Liljebäcks* voltage drift analysis of the Mamba sensor system [10] (result in figure 2.13b).

Linear regression (Figure 7.3) shows that the outputted measurement value changed in the negative direction for all axis as the sensor system was heated over a period of time. This means a reduction in the outputted voltage from strain gauges. The exact causation for all axis behaving fairly similarly and moving in the negative direction is unknown. It could be related to uneven heat distribution. Also, the negative trend seems to halt at around 100 seconds. This could be linked to the sensor system reaching the same value as the heat source. The slight measurement oscillations may be related to hot turbulent air from the heat source, causing slight vibrations.

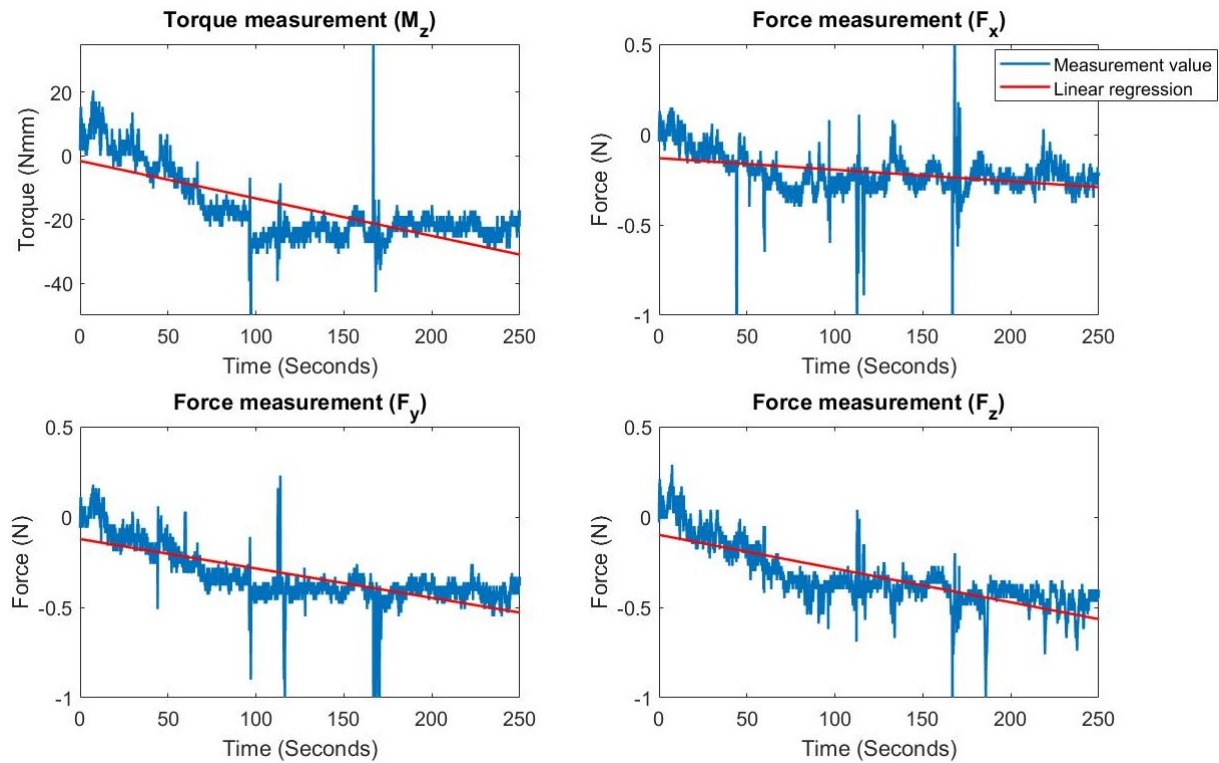


Figure 7.3: Linear regression of each measurement value from experiment 4. Analyzing measurement drift as the sensor system was heated

In conclusion, the project shows that the measured values change slightly as the sensor system is heated. However, the exact amount can not be disclosed without further research on the subject.

## 8 Conclusion

This section contains a summary of the conclusions made in the paper regarding the research process and performance of the selected sensor system.

### 8.1 The market for suitable commercially available force-torque sensors

This paper shows that there are commercially available force-torque sensor solutions suited for a novel snake robot on the market. Satisfactory solutions are presented in section 3. However, regarding the size and weight requirement for an intrinsic solution, such sensors are still highly expensive. This is somewhat linked to the low demand for these sensors. Therefore, production quotas for specific products would, in most cases, have to be reserved. This is one of the factors leading to the high price.

The project identified and designed a cost-effective solution which could be to "sandwich" two cheaper sensor solutions together to in total meet the required measurement axis for the next generation snake robot. The proposed solution was dubbed the Sandwich Solution (Section 3.11) and consists of a 1-axis torque sensor mounted to a 3-axis force sensor through a linking component.

### 8.2 Performance of the selected sensor system

The Sandwich Solution performed beyond the project's expectations. The experiments showed that the sensor system has high accuracy, low level of hysteresis to changing loads, and low time delay. However, the experiments also showed a small presence of crosstalk. Moreover, it found that heating the sensor system would influence the measurement signal. Therefore, the project suggests that the subjects of crosstalk and temperature tolerance related to measurement characteristics should be further examined.

Compared to the Mamba F/T sensor system, the Sandwich Solution performs better in terms of measurement reliability, accuracy, and hysteresis. However, the true performance of the sensor system is still highly reliant on how it is implemented in the final snake robot solution.

## 9 Future work

Although considered a success, there are still numerous changes that needs to be done before the developed system can be utilized. Already mentioned throughout the document, this chapter will reiterate the recommended replacements and discuss the existing problems these will fix.

### 9.1 Linkage, issues, and possible improvements

This section highlights future needed work and testing regarding the linking components needed to connect the two sensors.

During testing, the project found that the ASA 3D-printed linkage component (*LinkageType7*) would suffer from material fatigue after a long testing period. The result of this was that the two linkage components started to move in relation to each other, thus creating slight measurement hysteresis and time delay. The issue at hand is suspected to be related to the locking screw holes in the K3D40-linkage part, in *LinkageType7*, and the small amount of material supporting the screws provide. Moreover, it could also be related to the relatively weak material properties of the ASA-plastic 3D-print. To counteract the issue, the project increased the material thickness around the suspected area by 1mm, making the linkage 1mm taller. Other possible solutions could be to decrease the locking-hole dimensions and use self-drilling screws to lock the sensors together instead of M3-screws. However, the best solution would likely be to produce the linkage parts in solid metal, enabling firm and solid threaded holes.

The machine workshop at ITK CNC cut a linkage prototype in POM-C hard plastic. However, the project could not test it or mount it due to the correct countersunk 10-32 UNF screws never arriving due to issues in customs following Brexit. Therefore, its performance and durability with the sensor system should also be tested and assessed.

Lastly, the project is confident in the design of the linkage. However, there is still room for improvement.

### 9.2 Implementing the Sandwich Solution within a robotic joint

This section covers notes regarding the usage and requirements for future use of the sensor system in a next generation snake robot.

Firstly, to function properly, all relevant strain must be passed through the strain-gauge-based sensor system for the sensors to function properly. Meaning, the bottom (K3D40 sensor) requires a firm and stable mount that is separated from the top (TRT-sensor) where the actively moving components are connected (i.e., a motor and shaft). The motor needs to be suspended by the sensor system. There is also the possibility of

dismantling the Sandwich Solution and configuring the K3D40 sensor elsewhere without the torque-sensor, as long as it can capture the relevant strain.

Secondly, the K3D40-sensor bends slightly (by a few degrees) as it is extruded with force. This would have to be compensated for so that a connected "shaft" does not collide with internal objects or the chassis, causing a cut in the measurement range.

### 9.3 Suggested electronic improvements

The electronics, although providing a respectable testing platform, still contain numerous areas to improve upon. Mostly down to replacing components and noise suppression, this chapter will summarize each area of improvement and discuss a series of recommended solutions.

#### 9.3.1 Switching amplifiers

As discussed in chapter 4.4.1 the original INA122 instrumentation amplifier is at the time of this project over 20 years old. Still retaining excellent characteristics, the technology has advanced to the point where a replacement is almost necessary. Originally chosen for its excellent rail to rail characteristics 4.4.1 in single supply mode, the INA122 suffers from an abysmal slew rate. Although the original documentation, i.e., [2] has no mention of issues regarding the amplifier and the project conducting all its current testing on the same amplifier. The improvements the current generation of in-amps provide are too severe not to capitalize on. Retaining most of the INA122 characteristics, the project strongly recommends the INA849 as a replacement. Better than the INA122 in every aspect, the two most distinguishing features are the perfect rail to rail performance 4.13b and a best-in-the-class slew rate of  $35\text{V}/\mu\text{s}$ . For perspective's sake, the original INA122 had a slew rate of  $0.08\text{--}0.16\text{V}/\mu\text{s}$ , which was the in amps major trade-off for otherwise excellent characteristics. Switching to the INA849 would yield an improved speed of over 250 times the original average, and in a system where speed is key, it is a natural choice.

#### 9.3.2 Replacement of the digital potentiometer

Reliability and repeatability were one of the original project's biggest issues [2]. Caused by the usage of potentiometers that needed to be individually adjusted by hand and would frequently be shaking off course by the snake's movements. As these controlled the snake offset, bridge balance, and amplifier gain, the system needed constant recalibration and tweaking. The project has aimed to solve this by replacing analog potentiometers with digital substitutes. Discussed in 4.4.2, the digital potentiometers are unaffected by physical interference and will retain their values until told otherwise. The result is a dead stable system unaffected by external forces. However, the particular model of digpot utilized brings some issues when setting the gain of the in-amp. Having 256 steps and a total resistance of  $100\text{k}\ \Omega$ , the resistance changes in  $390\ \text{ohm}$  increments. This, combined



with the setting of the gain being nonlinear, creates a system that suffers exponentially reduced precision as the gain increases. The digpot used in this project was the TPL0501 by TI, and when used in conjunction with the INA122, this incrementation limited the gain to 512, with the final two steps being a jump from 251 to 512 times the input. This issue is universal and caused by the voltage dividing method responsible for the adjustable gain on the in-amps. Solving this can be done by two possible solutions, either choosing a digpot with a higher resolution or one with a smaller  $\Omega$  range. However, as different in-amps have different voltage dividing formulas, the appropriate digpot should be chosen after settling on an in-amp.

### 9.3.3 Redesigning the integrated offset

Amplifiers commonly require a dual inverse power supply to portray signals that swing around the zero axis. However, not all circuits are suited to accommodate dual supplies. Therefore, most amps are also able to run in *Single Supply* mode. Discussed in 4.4.1 the single supply mode allows the amp to run off a single supply at the cost of the ability to amplify negative signals. To accommodate this flaw, all modern amplifiers come equipped with an offset pin. As the name implies, any DC voltage applied to the pin will result in a proportional offset applied to the amplified signal. This voltage needs to be stable and preferably the ability to be adjusted to give the system the ability to calibrate. Mentioned in 4.6, the original intention was to control the offset directly from the microcontroller, but due to complications, this idea was scrapped. Time restraints meant that a temporary solution involving a voltage divider and lp-filter were implemented (ref 4.17). This system would not support individual offset adjustments and would prove to produce some noise caused by bad connectors and the board acting as an antenna. Although not sufficient to ruin any measurements, the noise made holding zero almost impossible and calibration a tedious process. As this was a temporary solution only fit for testing, these issues were bearable, but a new solution is required for the final system. Discussed in 4.6 this system should be controlled by a series of voltage dividing digpots intertwined in the existing circuit 9.3.4. Preferably the same as the digpots responsible for setting the gain, these will be able to run off the same timer and bit pin, saving space. The introduction of a digitally controlled offset would also allow for the development of a self-regulating system. By reading the offset and comparing it to a point of reference, the system would be able to increase and decrease the balance on the voltage divider. Crude and flustering with potential issues this is still an example of the possibilities the introduction of a digital voltage regulator can have on the system. The offset needs to provide a stable and adjustable signal, and the introduction of digpot voltage dividers would provide a sufficient platform.

### 9.3.4 Noise reduction improvements

The most defining and reoccurring issue the system faced was interference through noise. Although expected and taken into account when designing the system, the project failed to realize the severity, resulting in inadequate measures. Manifested mainly in external noise

and poor connections 4.5.1, this issue will be resolved by designing a complete integrated circuit and replacing the terminals and headers with non-substitutes. As the current system 6.2 is configured for testing, vast amounts of cable of varying quality and length are connected with no regard for noise suppression. Each cable acts as an antenna and will pick up noise from either other surrounding cables or the environment, which will manifest itself in the circuit. Additionally, the system is separated on different boards with different amounts of noise suppression. Both the power supply and the amplification circuit have copper pours and thin clean traces to prevent noise from leaking between transmission lines. However, the improvised offset circuit 4.6 is constructed using a prototype board and thus lacks these features. This means that the effect of the protection is reduced as any noise rejected by the two PCB will be picked up by the unprotected offset and taint the system regardless. For perspective's sake, the project had to completely recalibrate the entire system mid measurements because a screwdriver was located too close to the test rig. Acting like an antenna and picking up external noise, the screwdriver was moved mid-test and caused the system to lose zero, forcing a re-calibration. Another consistent issue the project faced was poor connections between terminals and headers. Due to the difficulty of producing the terminals 5.4 and the usage of old female jumper wires, the stability of the cable connections were questionable. The aforementioned jumper wires would frequently "wiggle" or disconnect entirely due to the cable not having a proper "grip" in the header. This would constantly change the connectivity of the cables and thus change the signal parameters. The XH-terminals suffered similar issues but for different reasons. As mentioned in 4.5.1 the terminals had an abnormal and difficult manufacturing process. Manufactured by hand, each terminal would yield a different level of quality and connectivity. Further discussed in 9.3.5 this difference in quality led to many of the same connectivity issues as the jumper cables, but were harder to spot and correct as the terminal was protected and hidden by the housing. As previously mentioned, the solution to all the project's noise-related issues is to redesign the entire system into a single PCB and replace the headers. This will, in turn, eliminate most of the shoddy wiring and integrate the troublesome offset circuit into the rest of the system, granting it equal noise-reducing capabilities. As the microcontroller can be soldered directly to the PCB, the only remaining wires will be the connections between the sensor and the circuit. These remaining connections will be secured with the proper headers instead of replacements and thus be manufactured in a way that provides sufficient measurements. This completed system will therefore, in theory, greatly improve noise imperiousness and provided a platform that allows the sensors to function at their full potential.

### **9.3.5 Header and terminal replacement**

Discussed in 5.4 and 9.3.4 the complicated production of the headers produced varying degrees of quality. Unfortunately, this quality variation would lead to a series of issues causing poor reliability and repeatability when the project tried to conduct testing. The three most common issues were the cables detaching from the crimping terminal, the cable not touching the terminal, and the terminal moving in the housing. The two first were caused by poor soldering whilst the latter was caused by cutting off too much terminal "leg", which provide stability inside the housing. These issues all caused poor and unstable connectivity between the terminal and the housing, causing the system to be easily

influenced by physical conditions. As this issue was mainly caused by being forced to utilize a replacement terminal, 4.5, the issues will mainly be solved by utilizing the correct terminal and the correct manufacturing tools. The project has already deemed the JST ZH terminal to be well suited for the project and combined with the correct crimping tool from JST or similar contemporaries, and the header issues should be solved.

## A Appendices

This section includes code and documentation not included in the report.

## Intrinsic Force-Torque Sensor System for a Next Generation Snake Robot

Joel Mörlin, Victor Melhuus and Oscar Mørk  
joeltm@stud.ntnu.no victorme@stud.ntnu.no oscarbm@stud.ntnu.no  
Faculty of Information Technology and Electrical Engineering  
Dept. of Engineering Cybernetics

### Introduction

- ▶ A new snake robot is to be developed at NTNU.
- ▶ The new snake robot will be an indented test-platform for Hybrid Obstacle Aided Locomotion (HOAL).
- ▶ Snakes utilize obstacles in the unstructured environment to locomote. Effective HOAL is an important milestones towards the future goal of fully autonomous snake robotics.

### F/T sensors and HOAL

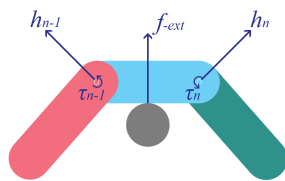


Fig. 1: Forces and torques applied on a 2-jointed 2D-snake pushing up against an object

$$F_R \approx 0$$

$$\Sigma F = ma \quad (1)$$

$$f_{ext} = ma - h_n - h_{n-1} \quad (2)$$

- ▶ Multi-axis force-torque measurement is a central aspect regarding HOAL.
- ▶ By comparing the measured to the force applied on 2 joints ( $h_n$  and  $h_{n-1}$ ) in 2(or 3) dimensions, an external force vector can be estimated (2) [2][3].
- ▶ The sum of all external force vectors would equal a path of locomotion.
- ▶ By regulating the motor torque, using a torque sensor as feedback, the snake would be able to regulate the size and direction of each external force vector. Thereby, the path of locomotion [2][3].

### F/T specifications for a snake robot

#### Specification sheet

Subject	Value	
Height	<40mm	
Diameter	<60 mm	
Weight	As light as possible	
Measurements	$F_x, F_y, F_z$	$M_z$
Capacity	ca. 20N	ca. 3Nm
Safe overload	> 20N	> 3Nm
Oper. temp. range	0C to 60C	
Price	<20 000 NOK	
Delivery time	< 4 weeks	

- ▶ The sensor system must be small enough to be applicable as an intrinsic solution.
- ▶ Needs to measure the relevant strain-axis with high accuracy and little hysteresis.
- ▶ Needs to withstand the highly demanding environment of a snake robot, in terms of temperature and force/torque range.
- ▶ Specifications were determined based on previous research at NTNU, conversations with the HOAL-team, and available solutions on the market.

### Test results

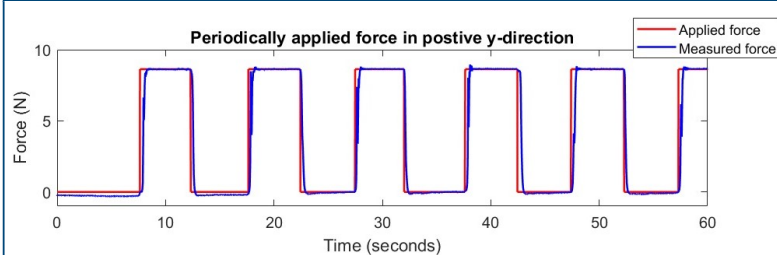


Fig. 2: Results from one of the experiments were a periodic force was applied

### The market

Findings regarding the market for suitable force-torque sensors:

- ▶ 6-axis F/T transducers with acceptable dimensions are highly expensive.
- ▶ The demand for these sensors are low, therefore most sensors must be ordered/produced on a reserved quota.
- ▶ A cost effective solution is to join 2 transducers that together meets the minimum required axis of measurement.

### The Sensor Solution

- ▶ Dubbed the Sandwich Solution.
- ▶ Based on commercially available transducers.
- ▶ Combines a 3-axis force sensor with a 1-axis transmission type torque sensor.
  - ▶ K3D40 3-axis force sensor (bottom Fig. 3) [5].
  - ▶ TRT-50 1-axis torque transducer (top Fig. 3) [4].
- ▶ Measures:  $F_x, F_y, F_z$  and  $M_z$
- ▶ Found to likely be the most cost-effective commercially available solution.

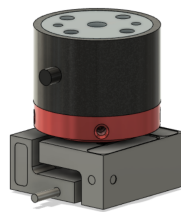


Fig. 3: The Sandwich Solution, 3-axis force and 1-axis torque sensor

#### Sandwich Solution specifications

Subject	Value	
Height	58.4 mm	
Diameter	57mm	
Measurements	$F_x, F_y, F_z$	$M_z$
Capacity	$\pm 50N$	$\pm 5Nm$
Safe overload	$\pm 100N$	$\pm 7.5Nm$
Rated temp. range	15.6C to 60C	
Op. temp. range	-20C to 70C	
Price estimate	20 871 NOK	

### Discussion

Discussing the sensor system's performance

- ▶ High accuracy.
- ▶ Low time-delay.
- ▶ Redundant and reproducible measurement signal with little to no hysteresis.
- ▶ Minor crossfeed between the measurement axis.
- ▶ Increasing temperatures has a minor influence on the measurement signal.

### References

- [1] Pål Liljebäck: *Modelling, development, and control of snake robots* NTNU [https://www.researchgate.net/publication/260095826\\_Snake\\_Robots\\_Modeling\\_Mechatronics\\_and\\_Control](https://www.researchgate.net/publication/260095826_Snake_Robots_Modeling_Mechatronics_and_Control)
- [2] A. A. Transeth and R. I. Leine and C. Glocker and K. Y. Pettersen and P. Liljebäck: *Snake Robot Obstacle-Aided Locomotion: Modeling, Simulations, and Experiments* <https://ieeexplore.ieee.org/document/4456759>
- [3] Christian Holden, Øyvind Stavadahl and Jan Tommy: *Optimal Dynamic Force Mapping for Obstacle-Aided Locomotion in 2D Snake Robots* <http://hdl.handle.net/11250/275548>
- [4] Transducer Techniques: *TRT Series Torque Sensor* <https://www.transducertechniques.com/trt-torque-sensor.aspx>  
Last used: May 19, 2021
- [5] ME-Meßsysteme: *K3D40 3-axis force sensor* <https://www.me-systeme.de/shop/en/sensors/force-sensors/k3d/k3d40>  
Last used: May 19, 2021

## A.2 Sensor research Excel sheet

### Force/Torque multiakse sensorer

Navn	Pris	Måleområde	Temperatur	Tilgængelighed	Dimensioner (Diameter)	Nøjagtighed	Lineærhed	Land og producent	Kommentar	Link
Rotary torque sensor HPS-F1025, hyperflexion	2.160 USD 2.150 Euro	+ 150N Force, +-4Nm Torque + 20 N Force, +- 1Nm Torque	-10 til 55 C -10 til 85 C		21*25 mm 45*77 mm			Kina Tyskland	Kan efterspørge pris uden kvotering	<a href="mailto:direct_email@directindustry.com">direct_email@directindustry.com</a> <a href="mailto:direct_email@directindustry.com">direct_email@directindustry.com</a> <a href="mailto:direct_email@directindustry.com">direct_email@directindustry.com</a>
Naviflex Robotics, NRS-6052-050	Ukjendt	+ 500 N Force, + 10Nm Torque + 200 N Force, + 2,5 Nm Torque	0 til 50 C 0 til 55 C	Beskrivelse	50*75mm			Danmark Frankrig	Sensorselskab fra Danmark med nye biler men er kvoteret. Vælg for opløsning for så meget computerforce må	<a href="http://www.naviflexrobotics.com">http://www.naviflexrobotics.com</a>
Flexi COM132	3.552 Euro	+ 150 N Force, + 2,5 Nm Torque + 15N Force, +-4Nm Torque	5 til 35 C 5 til 35 C	Kvoteret	50*75 mm			USA USA	ME betjener men også bra, best dimensioner. Best overall	<a href="http://www.flexi.com">http://www.flexi.com</a>
3-akset Force/Torque	1.080 Euro	+ 50 N Force, + 1Nm Torque + 50 N Force, + 1Nm Torque	-10 til 70 C -10 til 70 C		64*64mm 72*72mm			Tyskland Tyskland	"billigere" men lyktere enn de andre	<a href="http://www.3axis-force.com">http://www.3-axis-force.com</a>
ATI	Ukjendt	+ 25 N Force, +-4Nm Torque + 250 N Force, +-15Nm Torque	0 til 85 C ca. 0 til 90 C		82*82mm 40*32 mm			USA USA	Funker med multib, kønnet. Utren og lin	<a href="http://www.ati.com/products/force_models.aspx?cat=Mini40">https://www.ati.com/products/force_models.aspx?cat=Mini40</a>
ATI Mini40 S1-50-0.5	6500 dollar	+ 250N Force, +-1.6Nm Torque	Ukjendt	Kvoteret	17*14,5mm			USA		<a href="http://www.ati.com">http://www.ati.com</a>

### 3-akset Force sensor

Navn	Pris	Måleområde	Temperatur	Tilgængelighed	Dimensioner	Nøjagtighed	Lineærhed	Land og producent	Kommentar	Link
K3040 MEME systems	860 Euro + 60 Euro shipping	+ 50 N in Fx,Fy and Fz	-20 til 70 C		46x46x20 mm			Tyskland	Kommer i mange måleområder (+ 20,50,100 N)	<a href="http://www.k3.com">http://www.k3.com</a>
MEME systems	1.080 Euro + 60 Euro shipping	+ 50 N in Fx,Fy and Fz	-10 til 85 C		60x60x25 mm			Tyskland	Kommer i mange måleområder (+ 20,50,100 N)	<a href="http://www.meme-systems.de">http://www.meme-systems.de</a>
3AXX 3-Axis Force Load Cell	4000 \$	+ 20 N in Fx,Fy and Fz	-10 til 85 C		Ukjendt			USA		<a href="http://www.3axis-force.com">http://www.3-axis-force.com</a>

### 1-akset torque sensor

Navn	Pris	Måleområde	Temperatur	Tilgængelighed	Dimensioner	Nøjagtighed	Lineærhed	Land og producent	Kommentar	Link
Mernis, T250	695 + 60 EUR shipping	+ 50Nm	-20 til 70 C		Ø39 x 31mm			Tyskland		<a href="http://www.mernis-systems.de">http://www.mernis-systems.de</a>
TCT Series, low capacity	675 \$ + 171,18\$ shipping	+ 5Nm	-60 til 90 C		Ø42x35x4 mm			USA		<a href="http://www.tct.com">http://www.tct.com</a>

## A.3 Ordering the Sandwich Solution

Written by: Victor Shaw Melhuus ([victorme@stud.ntnu.no](mailto:victorme@stud.ntnu.no))

Date: 09.05.2021

### Ordering the Sandwich Solution

#### Sensors

Name	Comment	Links
K3D40-50N 3-axis force sensor	Select the +- 50N variant.	<a href="https://www.me-systeme.de/shop/en/sensors/force-sensors/k3d/k3d403">https://www.me-systeme.de/shop/en/sensors/force-sensors/k3d/k3d403</a>
TRT series Torque sensor	Select the +-50 lb-in (5.65Nm) variant.  The AMX-4 cable is shipped with it stock. However, the AMX-4 has a straight connector head. <b>It is crucial that the AMX-410-90 with a 90 degree connector head is ordered, due to space consumption. That would have to be negotiated with Transducer Techniquies.</b>	<a href="https://www.transducertechniques.com/trt-torque-sensor.aspx">https://www.transducertechniques.com/trt-torque-sensor.aspx</a>  Cable types: <a href="https://www.transducertechniques.com/mating-assembly-amx.aspx">https://www.transducertechniques.com/mating-assembly-amx.aspx</a>

**Needed screws**

Name	Req. p. sensor	Thread	Length	Links
10-32 UNF A2 Stainless Steel Countersunk Philips Head Machine Screws (For the TRT-sensor)	8	10-32 UNF	1/4" (6.35mm)	<a href="https://www.spaldingfasteners.co.uk/10-32-unf-a2-stainless-steel-countersunk-philips-head-machine-screws/">https://www.spaldingfasteners.co.uk/10-32-unf-a2-stainless-steel-countersunk-philips-head-machine-screws/</a>
M3 Pan Head Machine screws (for K3D40 to linkage connection)	4	M3	10mm	<a href="https://no.rs-online.com/web/p/machine-screws/0198289/">https://no.rs-online.com/web/p/machine-screws/0198289/</a>
M3 Pan Head Machine screws (for locking the linkage)	4	M3	8MM	<a href="https://no.rs-online.com/web/p/socket-screws/3044918/">https://no.rs-online.com/web/p/socket-screws/3044918/</a>
M3 Pan Head Machine screws  (for mounting the K3D40 sensor system) *optional and depends on how the sensor system is implemented in the snake robot*	4	M3	14mm	<a href="https://shop.arvidnilsson.com/nb/bult-mutter-och-bricka/machine-screws/machine-screw-pan-head/mrt-i14583-a4-70-m3x14-t10-115125.html">https://shop.arvidnilsson.com/nb/bult-mutter-och-bricka/machine-screws/machine-screw-pan-head/mrt-i14583-a4-70-m3x14-t10-115125.html</a>



### A.4 Component list with description

#### Power supply circuit

##### 1.1 DC/DC Stepdown converter (36 → 7.4V)

Description:

A DC/DC stepdown converter which is able to reduce a wide array of input voltage levels (7-36 volts) down to a wide array of output voltages (2.5 to 12.6 volts). The DC/DC stepdown converter can in addition deliver up to 6 A worth of power, dependent on the output load in the circuit.

Purpose in circuit:

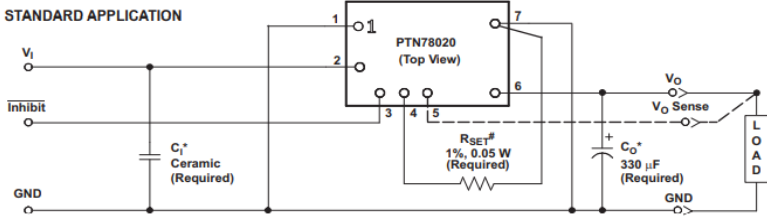
- 1. Reduces the input voltage from 36 volts down to 7.4 volts to accommodate a potential servomotor while being able to deliver enough power to run it (3.5 Ampere).
- 2. Helps with noise reduction by completing the voltage reduction in two steps rather than one.
- 3. NB! The component was chosen due to it being used in the previous iteration and it was therefore easy to implement which saved some time designing a new circuit. It is however rather expensive and could with some redesign to the circuit be swapped out for a cheaper option, if necessary, when the complete robot is to be built.

Producer: Texas Instruments

Supplier: Texas Instruments

Texas instrument item description: TEXAS INSTRUMENTS - PTN78020WAD - IC, ISR 6A ADJ O/P, 78020 Cost: kr 296,-

Hyperlink: [Texas Instruments, PTN78020WAD Step-Down Switching Regulator, 1-Channel 6A 7-Pin, DIP Module | RS Components \(rs-online.com\)](https://www.rs-online.com/product/texas-instruments/PTN78020WAD)



**In addition, the following components are necessary to enable the IC:**

**Resistor:**

- **Purpose:** A resistance is needed to decide the output voltage of the DC/DC converter. This resistance is placed in the position Rset shown in the circuit above. For more information on which resistance values provides which output voltages, check the datasheet for the converter.
- Supplier: LCSC Electronics
- LCSC item description: 7.5kΩ ±1% 1/16W ±100ppm/°C 0402 Chip Resistor - Surface Mount RoHS
- Amount: 1
- Resistance value: 7.5kohm
- Resulting output voltage: 7.405 V

**Ceramic Capacitor:**

- **Purpose:** Decoupling capacitor for input voltage
- Supplier: LCSC Electronics
- LCSC item description: 2.2uF ±10% 50V X7R 1206 Multilayer Ceramic Capacitors MLCC - SMD/SMT RoHS
- Amount: 1
- Capacitance: 2.2 uF

**Electrolyte capacitor:**

- **Purpose:** Decoupling capacitor for output voltage (Chosen for its ability to handle ripple current, needs to at least be able to handle 250 mArms)
- Supplier: LCSC Electronics
- LCSC item description: 330uF ±20% 16V 20mΩ @ 100kHz~300kHz 2.8A @ 100kHz 2.5mm Radial,6.3x8mm Solid Polymer Electrolytic Capacitor RoHS
- Amount: 1
- Capacitance: 330 uF

## **1.2 LDO DC/DC converter, LP38690DT-5.0/NOPB**

Description:

A low dropout DC/DC voltage converter with a fixed output voltage of 5 volts and the ability to deliver 1 ampere of power.

Purpose in circuit:

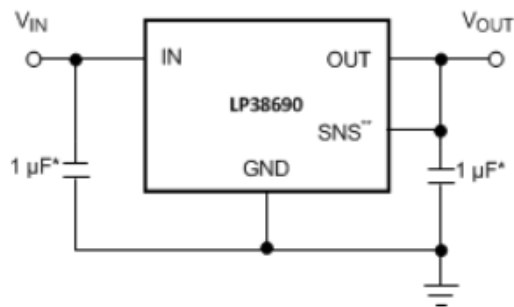
1. Reducing the voltage further from 7.4 volts down to 5 volts to accommodate the sensors excitation voltage as well as the instrument amplifiers gain.
2. Helps reduce noise in the circuit by completing the step down in two steps instead of one (The first DC/DC converter works as step one).

Producer: Texas Instruments

Supplier: Texas Instruments

Texas instruments item description: TEXAS INSTRUMENTS - 1-A, 10-V, low-dropout voltage regulator

Cost: kr 12,-



In addition, the following components are necessary to enable the IC:

#### Ceramic capacitor:

- **Purpose:** Decoupling capacitor for input and output voltage
- Supplier: LCSC Electronics
- LCSC item description: 1uF ±10% 16V X5R 0402 Multilayer Ceramic Capacitors MLCC - SMD/SMT RoHS
- Amount: 2
- Capacitance: 1 uF

## Microcontroller

### 2.1 Adafruit Feather M4 CAN Express with ATSAME51

Description:

A small and compact microcontroller with many digital and analog input/output pins as well as being CAN-buss compatible. Perfect for use in a robot due to its small size.

Purpose in system:

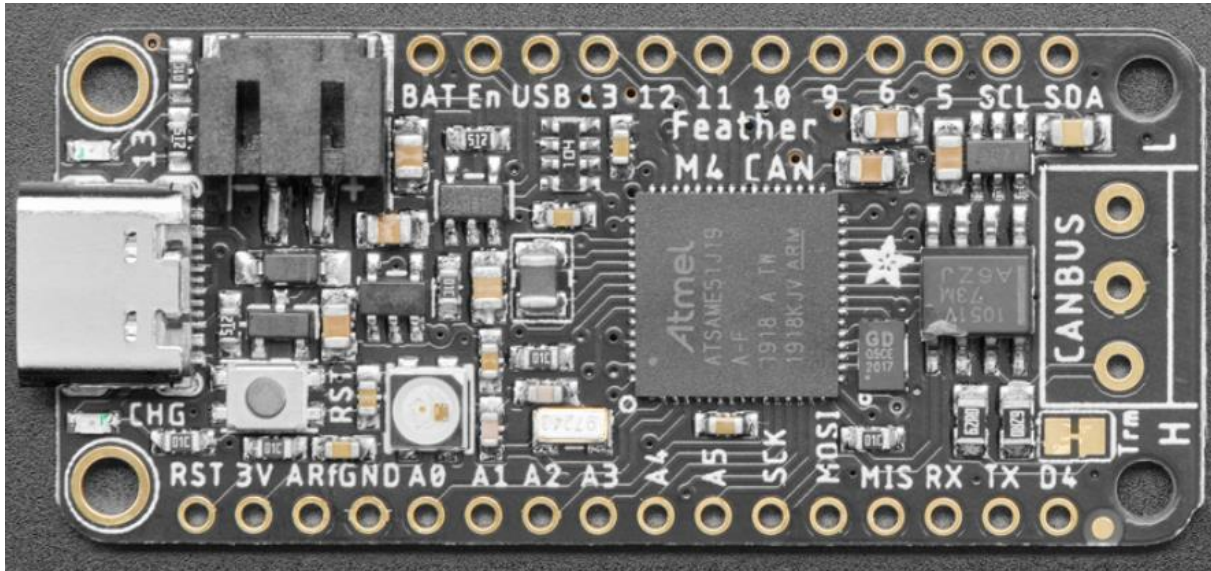
In the system the microcontroller is used for two things, providing analog to digital conversion and running the digital potentiometers. By being able to run the potentiometers from the microcontroller instead of using regular analog potentiometers the system becomes way easier to calibrate.

Producer: Adafruit

Supplier: Adafruit

Adafruit item description: Adafruit Feather M4 CAN Express with ATSAME51, Cost: 25.00 \$

Hyperlink: [Adafruit Feather M4 CAN Express with ATSAME51 : ID 4759 : \\$24.95 : Adafruit Industries, Unique & fun DIY electronics and kits](#)



## Amplifier circuit

### 3.1 INA122UA, Single Supply, Micropower Instrumentation Amplifier

Description:

The INA122 is a precision instrumentation amplifier for accurate, low noise differential signal acquisition. Its two-op-amp design provides excellent performance with very low quiescent current and is ideal for portable instrumentation and data acquisition systems.

Purpose in circuit:

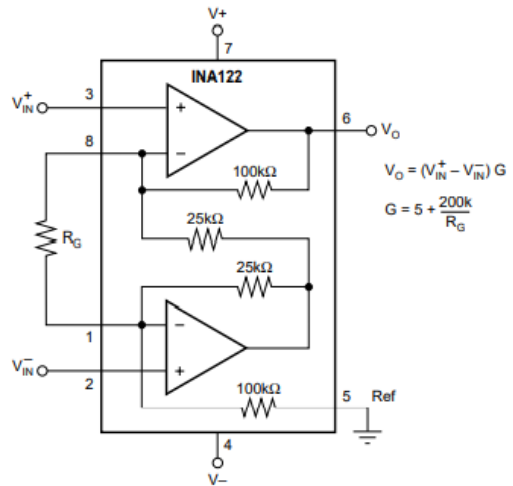
Receive and amplify the signals coming from the sensor and suppress any occurring noise through its CMMR capabilities. Should the system run in single supply mode the INA122 is also tasked with receiving and setting the applied signal offset.

Producer: Texas Instruments

Supplier: LCSC Electronics

Texas instrument item description: TEXAS INSTRUMENTS - INA122UA/2K5 - Cost: kr 33 ,-

Hyperlink: [INA122UA/2K5 | Buy TI parts | TI.com](#)



In addition, the following components are necessary to enable the IC:

**TPL0501:**

- **Purpose:** Connecting to the two gain pins (1 and 8), enabling gain control.
- Supplier: LCSC Electronics
- LCSC item description: SOT-23-8 Digital Potentiometer ICs RoHS
- Amount: 1
- Resistance: 0-100KΩ

**3.2 TPL0501 256-Taps, Single-Channel, Digital Potentiometer with SPI Interface**

Description:

The TPL0501 device is a single-channel, linear-taper, digital potentiometer with 256 wiper positions. This device can be used as a three-terminal potentiometer or as a two-terminal rheostat.

Purpose in circuit:

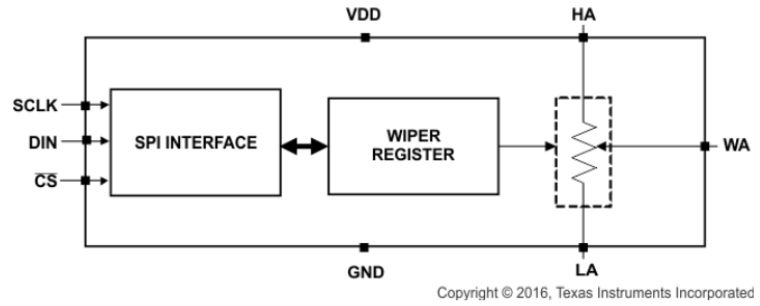
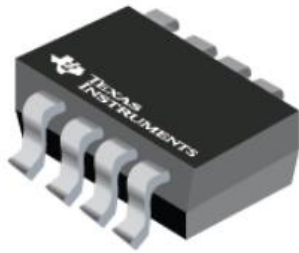
Responsible for setting and controlling the resistance between the two gain pins (1 and 8) on the INA122. Giving the TPL0501 the sole task of regulating the gain on the system.

Producer: Texas Instruments

Supplier: LCSC Electronics

Texas instrument item description: TEXAS INSTRUMENTS - INA122UA/2K5 - Cost: kr 5,1 ,-

Hyperlink: [TPL0501 256-Taps, Single-Channel, Digital Potentiometer With SPI Interface datasheet \(Rev. C\)](#)



In addition, the following components are necessary to enable the IC:

**Adafruit Feather M4:**

- **Purpose:** Allowing control over the digital wiper
- Supplier: Adafruit
- Adafruit item description: Adafruit Feather M4 CAN Express with ATSAME51
- Amount: 1

## A.5 Arduino code

```

1 #include<SPI.h>
2 //The csPin commandlines declares which output ports on the
   adafruit microcontroller the chip select pins on the digipots
   will recieve the signal from.
3 //It is important that it is a digital output port that is chosen,
   but which ones that are chosen are completely up to the user.
4 const int csPin1=10;
5 const int csPin2=11;
6 const int csPin3=12;
7 const int csPin4=13;
8 // Defines which input pins shall recieve signal from the sensors (
   Recommended to use analog pins)
9 // It's important that the name matches the inputsignal so it is
   easy to comprehend the outputdata
10 int Torque=A5;
11 int Xaxis=A4;
12 int Yaxis=A3;
13 int Zaxis=A2;
14 unsigned long time;
15 int counter=0;
16
17
18 const int numReadings = 10;    // the number of readings the
   program uses to average
19 int Torque_value[numReadings]; // the measurement from the torque
   sensor
20 int Xaxis_value[numReadings];  // the measurement from the x axis
   of the force sensor
21 int Yaxis_value[numReadings];  // the measurement from the y axis
   of the force sensor
22 int Zaxis_value[numReadings];  // the measurement from the z axis
   of the force sensor
23 int readIndex = 0;            // the index of the current
   measurement
24 int Torque_total=0; //The total of the measurements from the
   torque sensor
25 int Xaxis_total=0; //The total of the measurements from the x
   axis of the force sensor
26 int Yaxis_total=0; //The total of the measurements from the y
   axis of the force sensor
27 int Zaxis_total=0; //The total of the measurements from the z
   axis of the force sensor
28 int Torque_average=0; //Holds the average of the measurements from
   the torque sensor
29 int Xaxis_average=0; //Holds the average of the measurements from
   the x axis of the force sensor
30 int Yaxis_average=0; //Holds the average of the measurements from
   the y axis of the force sensor
31 int Zaxis_average=0; //Holds the average of the measurements from
   the z axis of the force sensor
32
33 void setup() {
34   Serial.begin(9600);
35   pinMode(csPin1, OUTPUT);
36   pinMode(csPin2, OUTPUT);
37   pinMode(csPin3, OUTPUT);
38   pinMode(csPin4, OUTPUT);

```

```

39  pinMode(Torque, INPUT_PULLUP);
40  pinMode(Xaxis, INPUT_PULLUP);
41  pinMode(Yaxis, INPUT_PULLUP);
42  pinMode(Zaxis, INPUT_PULLUP);
43  analogReadResolution(12);
44  //SPI.begin initialises SPI communication with the digipots.
45  SPI.begin();
46  SPI.setBitOrder(MSBFIRST);
47  SPI.setDataMode(SPI_MODE0);
48  //Resets the the measurements registers before running the program
49  for (int thisReading = 0; thisReading < numReadings; thisReading
      ++){
50      Torque_value[thisReading] = 0;
51      Xaxis_value[thisReading] = 0;
52      Yaxis_value[thisReading] = 0;
53      Zaxis_value[thisReading] = 0;
54  }
55  while(!Serial);
56 }
57
58 void loop() {
59     //Sets the resistance value for the digipots by changing the
        wiper position based on the middle inputvalue
60     //To find which wiper position gives which resistancevalue, take
        the total potmeter value and divide it by 255.
61     //PS! To calculate which gain requires which resistance value, it
        is possible to use the formula Resistance=200000/(Gain-5)
62     DigitalPotWrite(0x00, 1, csPin1);
63     DigitalPotWrite(0x00, 1, csPin2);
64     DigitalPotWrite(0x00, 1, csPin3);
65     DigitalPotWrite(0x00, 1, csPin4);
66
67     // subtract the last reading from the arrays after it has been
        filled once
68     if (counter >= 10){
69         Torque_total = Torque_total - Torque_value[readIndex];
70         Xaxis_total = Xaxis_total - Xaxis_value[readIndex];
71         Yaxis_total = Yaxis_total - Yaxis_value[readIndex];
72         Zaxis_total = Zaxis_total - Zaxis_value[readIndex];
73     }
74     // Read from the sensors:
75     Torque_value[readIndex] = analogRead(Torque);
76     Xaxis_value[readIndex] = analogRead(Xaxis);
77     Yaxis_value[readIndex] = analogRead(Yaxis);
78     Zaxis_value[readIndex] = analogRead(Zaxis);
79     // Add the readings to the totals:
80     Torque_total = Torque_total + Torque_value[readIndex];
81     Xaxis_total = Xaxis_total + Xaxis_value[readIndex];
82     Yaxis_total = Yaxis_total + Yaxis_value[readIndex];
83     Zaxis_total = Zaxis_total + Zaxis_value[readIndex];
84     // Advance to the next position in the array:
85     readIndex = readIndex + 1;
86     // Resets the readIndex when at the end of the array:
87     if (readIndex >= numReadings) {
88         readIndex = 0;
89     }
90     // calculates the averages:

```



```

91 Torque_average = Torque_total / numReadings;
92 Xaxis_average = Xaxis_total / numReadings;
93 Yaxis_average = Yaxis_total / numReadings;
94 Zaxis_average = Zaxis_total / numReadings;
95 // Changes the average value from an int to a float
96 float Torque_float=float(Torque_average);
97 float Xaxis_float=float(Xaxis_average);
98 float Yaxis_float=float(Yaxis_average);
99 float Zaxis_float=float(Zaxis_average);
100 // Remaps the signal from 0-4095 to +-50 newton or newton
    millimeters.
101 float Torque_new_average=(Torque_float/4095.00)*10000.00-5000.00;
102 float Xaxis_new_average=(Xaxis_float/4095.00)*100.00-50;
103 float Yaxis_new_average=(Yaxis_float/4095.00)*100.00-50;
104 float Zaxis_new_average=(Zaxis_float/4095.00)*100.00-50;
105 //sends the averages to the computer to be plotted:
106 time=millis();
107 Serial.print(time);
108 Serial.print(" ");
109 Serial.print(Torque_new_average);
110 Serial.print(" ");
111 Serial.print(Xaxis_new_average);
112 Serial.print(" ");
113 Serial.print(Yaxis_new_average);
114 Serial.print(" ");
115 Serial.println(Zaxis_new_average);
116 // delay in between reads for stability
117 delay(1);
118 // Counts upwards to ten to start the value subtraction loop at
    the top
119 if (counter<=10){
120 counter=counter+1;
121 }
122 }
123 //Code that uses SPI to send a positionvalue from 0-255 to the
    digipots.
124 void DigitalPotWrite(int cmd, int val, int CS_PIN)
125 {
126 // constrain input value within 0 - 255
127 val = constrain(val, 0, 255);
128 // set the CS pin to low to select the chip and allow transfer:
129 digitalWrite(CS_PIN, LOW);
130 // send the command and value via SPI:
131 SPI.transfer(cmd);
132 SPI.transfer(val);
133 // Set the CS pin high to execute the command:
134 digitalWrite(CS_PIN, HIGH);
135 }

```

## A.6 Matlab code: Plotting periodic experiment

### Function to calculate a time vector from Arduino millis

```
1 function vec = timeVec(data)
2 timestamps = data(:,1)';
3 vec = (timestamps - timestamps(1))./1000;
4 end
```

### Plotting Fy

```
1 clc
2 clear
3
4 data_raw = load('data_yneg_periodisk.txt'); %Loading data file
5 data = data_raw(40000:end,:); %Trimming the data file
6 y_akse = data(:,2)'; %Assigning the y-axis
7 time = timeVec(data); %Using the timeVec function to generate ...
   the time-array
8
9 apf = zeros(1,length(time)); %Preamble of applied force array.
10
11 for i = 1:length(time)-1 %Inserted the estimated time for when ...
   force was applied
12     if time(i) >= 2.41 && time(i) <= 7.35
13         apf(i) = -8.63;
14     end
15     if time(i) >= 12.44 && time(i) <= 17.41
16         apf(i) = -8.63;
17     end
18     if time(i) >= 22.42 && time(i) <= 27.23
19         apf(i) = -8.63;
20     end
21     if time(i) >= 32.36 && time(i) <= 37.37
22         apf(i) = -8.63;
23     end
24     if time(i) >= 42.37 && time(i) <= 47.27
25         apf(i) = -8.63;
26     end
27     if time(i) >= 52.23 && time(i) <= 57.21
28         apf(i) = -8.63;
29     end
30     if time(i) >= 67.29 && time(i) <= 72.28
31         apf(i) = -8.63;
32     end
33     if time(i) >= 77.58 && time(i) <= 82.16
34         apf(i) = -8.63;
35     end
36 end
37
38 subplot(2,1,1)
39 plot(time,apf,'r','LineWidth',1.5); %plotting applied force
40
41 hold on
42 plot(time,y_akse,'b','LineWidth',1.5); %plotting y-axis force ...
   measurement
43
```

```
44 %Setting labels and setting graph limits
45 ylabel('Force (N)')
46 xlabel('Time (seconds)')
47 title('Periodically applied force in negative y-direction')
48 xlim([0 60])
49 ylim([-9 1])
50 legend('Applied force','Measured force')
51
52 subplot(2,1,2);
53 error = apf- y_akse; %Calculating the error graph
54 plot(time,error,'LineWidth',1.5)
55
56 %Adding labels and limits
57 ylabel('Force (N)')
58 xlabel('Time (seconds)')
59 title('Measurement error')
60 ylim([-10 10])
61 xlim([0 60])
```

Same process repeated for each periodic force test.

## Calculating average value when strain is applied

```
1 %preamble
2 clc
3 clear
4
5 %Force in positive y direction
6 data = load('data.ypos.perdioidisk.txt');
7 y_akse_data = data(:,2)';
8 y_akse = y_akse_data(1:end);
9 time = timeVec(data); %Sets start time to 0, and converts to seconds
10
11
12 y_akse_apf = zeros(6,length(time));
13 c = ones(1,6); %Array with counters
14 for i = 1:length(time)-1 %Inserted the estimated time for when ...
    force was applied
15     if time(i) ≥ 8.4 && time(i) ≤ 12.33
16         y_akse_apf(1,c(1)) = y_akse(i);
17         c(1) = c(1) + 1;
18     end
19     if time(i) ≥ 18.4 && time(i) ≤ 22.44
20         y_akse_apf(2,c(2)) = y_akse(i);
21         c(2) = c(2) + 1;
22     end
23     if time(i) ≥ 28.2 && time(i) ≤ 32.01
24         y_akse_apf(3,c(3)) = y_akse(i);
25         c(3) = c(3) + 1;
26     end
27     if time(i) ≥ 38.3 && time(i) ≤ 42.45
28         y_akse_apf(4,c(4)) = y_akse(i);
29         c(4) = c(4) + 1;
30     end
31     if time(i) ≥ 48.2 && time(i) ≤ 52.3
32         y_akse_apf(5,c(5)) = y_akse(i);
33         c(5) = c(5) + 1;
34     end
35     if time(i) ≥ 58.2 && time(i) ≤ 62.24
36         y_akse_apf(6,c(6)) = y_akse(i);
37         c(6) = c(6) + 1;
38     end
39 end
40 y_akse_apf_s = y_akse_apf(:,1:2576); %trimming the data
41
42 avg = zeros(6,1);
43
44 for k=1:6
45     avg(k) = sum(y_akse_apf_s(k,:))/length(y_akse_apf_s(k,:));
46 end
```

Same process repeated for each test

## Plotting measurement drift from 1st iteration

```
1     clc; clear;
2
3     %Average iteration data
4     torque = [348.7248 356.6058 354.2615 356.3847 356.3594 355.2107];
5     f_x_pos = [8.4398 8.4784 8.4738 8.3475 8.2939 8.3575];
6     f_x_neg = [-8.5345 -8.5387 -8.5378 -8.5471 -8.5456 -8.5444];
7     f_y_pos = [8.6233 8.6326 8.6452 8.6531 8.6459 8.6562];
8     f_y_neg = [-8.6050 -8.6094 -8.6065 -8.6041 -8.6004 -8.6047];
9
10    %Calculating deviation in percent of 1st iteration.
11    t_error_perc = ((torque - torque(1))./torque(1))*100;
12    fxp_error_perc = ((f_x_pos - f_x_pos(1))./f_x_pos(1))*100;
13    fxn_error_perc = ((f_x_neg - f_x_neg(1))./f_x_neg(1))*100;
14    fyp_error_perc = ((f_y_pos - f_y_pos(1))./f_y_pos(1))*100;
15    fyn_error_perc = ((f_y_neg - f_y_neg(1))./f_y_neg(1))*100;
16
17    %Plotting
18    b_graph = [fxp_error_perc(2:end) fxn_error_perc(2:end) ...
19              fyp_error_perc(2:end) fyn_error_perc(2:end)];
19    bar(b_graph)
20    %bar(t_error_perc,'BarWidth',0.5)
21    title('Measurement drift from 1st iteration')
22    ylabel('Measurement drift %')
23    xlabel('Iteration')
24    xticklabels(2:6)
25    legend('F_x positive','F_x negative','F_y positive','F_y negative')
26    %xlim([1.1 6.9])
```

## A.7 Matlab code: Crossfeed analysis

### Plotting the crossfeed test

```
1      %preamble
2      clc
3      clear
4
5      %Force in negative y direction
6      data = load('Sensorlogdata_Crossfeed_maling_1.Yaxis_Negativ.txt');
7      Torque_akse_data = data(:,2)';
8      x_akse_data = data(:,3)';
9      y_akse_data = data(:,4)';
10     z_akse_data = data(:,5)';
11     Torque_akse = Torque_akse_data(1:end);
12     x_akse = x_akse_data(1:end);
13     y_akse = y_akse_data(1:end);
14     z_akse = z_akse_data(1:end);
15
16     time = timeVec(data); %Sets start time to 0, and converts to seconds
17
18     %Plotting Torque
19     subplot(2,2,1)
20     plot(time,Torque_akse,'b','LineWidth',1.0);
21     title('Subplot 1: Torque measurement')
22     xlabel('Time (s)');
23     ylabel('Torque (N*mm)');
24     %Plotting X
25     subplot(2,2,2)
26     plot(time,x_akse,'b','LineWidth',1.0);
27     title('Subplot 2: X-axis measurement')
28     xlabel('Time (s)');
29     ylabel('Force (N)');
30     %Plotting Y
31     subplot(2,2,3)
32     plot(time,y_akse,'b','LineWidth',1.0);
33     title('Subplot 3: Y-axis measurement')
34     xlabel('Time (s)');
35     ylabel('Force (N)');
36     %Plotting Z
37     subplot(2,2,4)
38     plot(time,z_akse,'b','LineWidth',1.0);
39     title('Subplot 4: Z-axis measurement')
40     xlabel('Time (s)');
41     ylabel('Force (N)');
```

## A.8 Matlab code: Plotting shaketest

### Plotting the results from the shaketest

```
1     clc
2     clear
3
4     data = load('Sensorlogdata-Riste.maling-1.Alle-Akser.txt');
5
6     time = timeVec(data);
7
8     torque = data(:,2)';
9     x_axis = data(:,3)';
10    y_axis = data(:,4)';
11    z_axis = data(:,5)';
12
13    subplot(2,2,1)
14    plot(time, torque,'LineWidth',1.5)
15    xlabel('Time (Seconds)')
16    ylabel('Torque (Nmm)')
17    title('Torque measurement (M.z)')
18    xlim([0 70])
19
20    subplot(2,2,2)
21    plot(time, x_axis,'LineWidth',1.5)
22    xlabel('Time (Seconds)')
23    ylabel('Force (N)')
24    title('Force measurement (F.x)')
25    xlim([0 70])
26
27    subplot(2,2,3)
28    plot(time, y_axis,'LineWidth',1.5)
29    xlabel('Time (Seconds)')
30    ylabel('Force (N)')
31    title('Force measurement (F.y)')
32    xlim([0 70])
33
34    subplot(2,2,4);
35    plot(time, z_axis,'LineWidth',1.5)
36    xlabel('Time (Seconds)')
37    ylabel('Force (N)')
38    title('Force measurement (F.z)')
39    xlim([0 70])
```

## A.9 Matlab code: Plotting temperature experiment

### Plotting the results from the temperature experiment

```

1     clc
2     clear
3
4     data = load('Sensorlogdata.temperatur.maling-1.Alle.akser.txt'); ...
        %Loading data
5
6     time = timeVec(data); %Calculatime time vector from millis
7     torque = data(:,2)'; %Seperating measurement data
8     x_axis = data(:,3)';
9     y_axis = data(:,4)';
10    z_axis = data(:,5)';
11
12    subplot(2,2,1) %Plotting torque
13    plot(time, torque,'LineWidth',1.5)
14    xlabel('Time (Seconds)')
15    ylabel('Torque (Nmm)')
16    title('Torque measurement (M.z)')
17    ylim([-50 35])
18    xlim([0 250])
19    hold on
20    m_reg = polyfit(time,torque,1); %Linear regression
21    torque_reg = polyval(m_reg,time);
22    plot(time, torque_reg,'r','LineWidth',1.5) %Plotting lr
23
24    subplot(2,2,2)
25    plot(time, x_axis,'LineWidth',1.5)
26    xlabel('Time (Seconds)')
27    ylabel('Force (N)')
28    title('Force measurement (F.x)')
29    ylim([-1 0.5])
30    xlim([0 250])
31    hold on
32    fx_reg = polyfit(time,x_axis,1);
33    fx_reg_vals = polyval(fx_reg,time);
34    plot(time, fx_reg_vals,'r','LineWidth',1.5)
35
36    legend('Measurement value','Linear regression')
37
38    subplot(2,2,3)
39    plot(time, y_axis,'LineWidth',1.5)
40    xlabel('Time (Seconds)')
41    ylabel('Force (N)')
42    title('Force measurement (F.y)')
43    ylim([-1 0.5])
44    xlim([0 250])
45    hold on
46    fy_reg = polyfit(time,y_axis,1);
47    fy_reg_vals = polyval(fy_reg,time);
48    plot(time, fy_reg_vals,'r','LineWidth',1.5)
49
50    subplot(2,2,4);
51    plot(time, z_axis,'LineWidth',1.5)
52    xlabel('Time (Seconds)')
53    ylabel('Force (N)')

```



```
54 title('Force measurement (F.z)')
55 ylim([-1 0.5])
56 xlim([0 250])
57 hold on
58 fz_reg = polyfit(time,z_axis,1);
59 fz_reg_vals = polyval(fz_reg,time);
60 plot(time, fz_reg_vals,'r','LineWidth',1.5)
```

## References

- [1] P. Liljebäck, *Modelling, development, and control of snake robots*, ser. Doktoravhandling ved NTNU (trykt utg.) Norwegian University of Science, Technology, Faculty of Information Technology, Mathematics, and Electrical Engineering, Department of Engineering Cybernetics, 2011, vol. 2011:70, ISBN: 9788247126677.
- [2] F. Veslum, “Assessment of the mamba snake robot sensor system,” 2020.
- [3] L. R. Grace Pryor David Hu and J. Polk. (2009). “The secret of a snake’s slither,” [Online]. Available: [https://www.nsf.gov/news/news\\_summ.jsp?cntn\\_id=114941](https://www.nsf.gov/news/news_summ.jsp?cntn_id=114941) (visited on 03/17/2021).
- [4] A. A. Transeth, R. I. Leine, C. Glocker, K. Y. Pettersen, and P. Liljebäck, “Snake robot obstacle-aided locomotion: Modeling, simulations, and experiments,” *IEEE Transactions on Robotics*, vol. 24, no. 1, pp. 88–104, 2008. DOI: 10.1109/TR0.2007.914849.
- [5] F. Sanfilippo, J. Azpiazu, G. Marafioti, A. Transeth, Ø. Stavadahl, and P. Liljebäck, “Perception-driven obstacle-aided locomotion for snake robots: The state of the art, challenges and possibilities,” *Applied Sciences*, vol. 7, p. 336, Mar. 2017. DOI: 10.3390/app7040336.
- [6] C. Holden, Ø. Stavadahl, and J. T. Gravdahl, “Optimal dynamic force mapping for obstacle-aided locomotion in 2d snake robots,” eng, 2014, ISSN: 2153-0858. [Online]. Available: <http://hdl.handle.net/11250/275548>.
- [7] A. A. Circuits. (). “Torque conversion calculator (image used),” [Online]. Available: <https://www.allaboutcircuits.com/tools/torque-conversion-calculator/> (visited on 03/24/2021).
- [8] A. K. Ghosh, *Introduction to Measurement and Instrumentation, Forth Edition*. PHI Learning, 2012, pp. 330–371.
- [9] P. Liljebäck. (). “Kulko - a snake robot with tactile sensors,” [Online]. Available: <https://robotnor.no/research/kulko-a-snake-robot-with-tactile-sensors/> (visited on 03/17/2021).
- [10] —, “Analysis of force sensor drift,” 2012.
- [11] T. Techniques. (). “Low capacity (in-lb) general purpose reaction torque sensor,” [Online]. Available: <https://www.transducertechniques.com/trt-torque-sensor.aspx> (visited on 03/17/2021).
- [12] Futek. (). “Torque measurement,” [Online]. Available: <https://www.futek.com/torque-measurement> (visited on 03/17/2021).
- [13] A. Owen-Hill and R. Inc. (). “A brief history of robotic force torque sensors,” [Online]. Available: <https://robohub.org/robotic-force-torque-sensors-a-brief-history/> (visited on 03/17/2021).
- [14] K. Group. (). “Wind tunnel testing,” [Online]. Available: <https://www.kistler.com/en/solutions/research-and-development-testing/aviation-testing/wind-tunnel-testing/> (visited on 03/17/2021).

- [15] K. O. Hill, Y. Fujii, D. C. Johnson, and B. S. Kawasaki, "Photosensitivity in optical fiber waveguides: Application to reflection filter fabrication," *Applied Physics Letters*, vol. 32, no. 10, pp. 647–649, 1978. DOI: 10.1063/1.89881. eprint: <https://doi.org/10.1063/1.89881>. [Online]. Available: <https://doi.org/10.1063/1.89881>.
- [16] FBGS. (). "Fbg principle," [Online]. Available: <https://fbgs.com/technology/fbg-principle/> (visited on 03/17/2021).
- [17] —, (). "Strain gauge sg-01," [Online]. Available: <https://fbgs.com/components/strain-sensor-sg-01/> (visited on 03/17/2021).
- [18] X. He. (). "A sub-millimetric 3-dof force sensing instrument with integrated fiber bragg grating for retinal microsurgery," [Online]. Available: <https://www.ncbi.nlm.nih.gov/pmc/articles/PMC3965652/> (visited on 03/17/2021).
- [19] S. R. Taal, H. Yamada, and S. Hirose, "3 axial force sensor for a semi-autonomous snake robot," pp. 4057–4062, 2009. DOI: 10.1109/ROBOT.2009.5152366.
- [20] N. Hendrich, F. Wasserfall, and J. Zhang, "3d printed low-cost force-torque sensors," *IEEE Access*, vol. 8, pp. 140 569–140 585, 2020. DOI: 10.1109/ACCESS.2020.3007565.
- [21] Futek. (). "Futek home page, about," [Online]. Available: <https://www.futek.com/aboutus> (visited on 03/17/2021).
- [22] L. I. S. AB. (). "Norwegian representative of futek," [Online]. Available: <https://1isab.no/> (visited on 03/17/2021).
- [23] Futek. (). "Qma142," [Online]. Available: <https://www.futek.com/store/multi-axis-sensors/QMA/custom-6-axis-sensor-QMA142/QSH01919> (visited on 03/17/2021).
- [24] Thomasnet. (). "Mini 40-e transducer," [Online]. Available: <https://www.thomasnet.com/catalogs/item/1060453-13586-1009-1080/ati-industrial-automation/mini40-e-transducer/> (visited on 04/24/2021).
- [25] A. I. Automation. (). "F/t sensor: Mini40," [Online]. Available: [https://www.atia.com/products/ft/ft\\_models.aspx?id=Mini40](https://www.atia.com/products/ft/ft_models.aspx?id=Mini40) (visited on 04/23/2021).
- [26] —, *Manual: F/t can bus and serial bus network interface for oem*. [Online]. Available: [https://www.atia.com/app\\_content/documents/9610-05-1030.pdf](https://www.atia.com/app_content/documents/9610-05-1030.pdf) (visited on 04/24/2021).
- [27] Me-Meßsysteme. (). "About page," [Online]. Available: <https://www.me-systeme.de/en/about-us> (visited on 03/17/2021).
- [28] —, (). "K6d40 6-axis force/torque sensor," [Online]. Available: <https://www.me-systeme.de/shop/en/sensors/force-sensors/k6d/k6d402> (visited on 03/17/2021).
- [29] —, (). "K3d40," [Online]. Available: <https://www.me-systeme.de/shop/en/sensors/force-sensors/k3d/k3d404> (visited on 03/17/2021).
- [30] —, (). "K3d40-10n datasheet," [Online]. Available: [https://www.me-systeme.de/product-pdf?product\\_id=1661&lang=en](https://www.me-systeme.de/product-pdf?product_id=1661&lang=en) (visited on 03/17/2021).
- [31] T. Techniques. (). "Mating assembly (amx)," [Online]. Available: <https://www.transducertechniques.com/mating-assembly-amx.aspx> (visited on 03/17/2021).

- [32] Me-Meßsysteme. (). “Mounting instructions for 3-axis sensors,” [Online]. Available: <https://www.me-systeme.de/produkte/sensoren/kxd/k3d/allgemeine-anleitungen/ba-k3d-mounting-en.pdf> (visited on 03/30/2021).
- [33] B. B. Corporation. (). “Single supply, micropower instrumentation amplifier (input common-mode voltage vs output voltage),” [Online]. Available: <https://www.ti.com/product/INA122> (visited on 04/13/2021).
- [34] —, (). “Inax126 micropower instrumentation amplifier single and dual versions (figure 4. negative power supply rejection vs frequency),” [Online]. Available: <https://www.ti.com/product/INA126> (visited on 04/13/2021).
- [35] —, (). “Ina849 ultra-low-noise, high-bandwidth, instrumentation amplifier (pin configuration),” [Online]. Available: <https://www.ti.com/product/INA849> (visited on 04/20/2021).
- [36] —, (). “Single supply, micropower instrumentation amplifier (figure 1. basic connections.),” [Online]. Available: <https://www.ti.com/product/INA122> (visited on 04/20/2021).
- [37] —, (). “Ina849 ultra-low-noise, high-bandwidth, instrumentation amplifier (table 8-1. commonly used gains and resistor values),” [Online]. Available: <https://www.ti.com/product/INA849> (visited on 04/13/2021).
- [38] —, (). “Single supply, micropower instrumentation amplifier (figure 1. basic connections.),” [Online]. Available: <https://www.ti.com/product/INA122> (visited on 05/11/2021).
- [39] T. I. Incorporated. (). “PI0501 256-taps, single-channel, digital potentiometer with spi interface (figure 20. example layout for dcn package),” [Online]. Available: <https://www.ti.com/product/TPL0501-100> (visited on 05/11/2021).
- [40] A. Barela. (). “Adafruit m4 express pinout display,” [Online]. Available: <https://learn.adafruit.com/assets/78439> (visited on 04/30/2021).
- [41] R. PRO. (). “Rs pro, m3 pan head, 10mm steel pozidriv bright zinc plated,” [Online]. Available: <https://no.rs-online.com/web/p/machine-screws/0198289/> (visited on 05/09/2021).
- [42] A. Nilsson. (). “I14583-a4-70 m3x14 ph t10 ma.skr.,” [Online]. Available: <https://shop.arvidnilsson.com/nb/bult-mutter-och-bricka/machine-screws/machine-screw-pan-head/mrt-i14583-a4-70-m3x14-t10-115123.html> (visited on 04/27/2021).
- [43] R. PRO. (). “Rs pro m3 x 8mm hex socket countersunk screw plain stainless steel,” [Online]. Available: [https://no.rs-online.com/web/p/socket-screws/3044918/?cm\\_mmc=NO-PLA-DS3A--google--CSS\\_NO\\_NO\\_Fasteners\\_%5C%26\\_Fixings\\_Whoop--\(NO:Whoop!\)+Socket+Screws--3044918&matchtype=&aud-772940708119:pla-339757525811&gclid=CjwKCAjw7J6EBhBDEiwA5UUM2p0spvcdgclyr9fiR2tStSi1bHqtX5TA1fSyR0Vg7dq2nY-fbcMivxoCCfYQAvD\\_BwE&gclsrc=aw.ds](https://no.rs-online.com/web/p/socket-screws/3044918/?cm_mmc=NO-PLA-DS3A--google--CSS_NO_NO_Fasteners_%5C%26_Fixings_Whoop--(NO:Whoop!)+Socket+Screws--3044918&matchtype=&aud-772940708119:pla-339757525811&gclid=CjwKCAjw7J6EBhBDEiwA5UUM2p0spvcdgclyr9fiR2tStSi1bHqtX5TA1fSyR0Vg7dq2nY-fbcMivxoCCfYQAvD_BwE&gclsrc=aw.ds) (visited on 04/27/2021).

- [44] S. Fasteners. (). “Rs pro, m3 pan head, 10mm steel pozidriv bright zinc plated,” [Online]. Available: <https://www.spaldingfasteners.co.uk/10-32-unf-a2-stainless-steel-countersunk-philips-head-machine-screws/> (visited on 05/09/2021).

